NASA Contractor Report 195427/VOL1

High Pressure, Earth-Storable Rocket Technology

Volume 1

D.M. Jassowski
Aerojet, Sacramento, California

Prepared under Contract NAS3–27003

National Aeronautics and
Space Administration

Lewis Research Center

October 1997

The NASA STI Program Office ... in Profile

Since its founding, NASA has been dedicated to the advancement of aeronautics and space science. The NASA Scientific and Technical Information (STI) Program Office plays a key part in helping NASA maintain this important role.

The NASA STI Program Office is operated by Langley Research Center, the lead center for NASA's scientific and technical information. The NASA STI Program Office provides access to the NASA STI Database, the largest collection of aeronautical and space science STI in the world. The Program Office is also NASA's institutional mechanism for disseminating the results of its research and development activities. These results are published by NASA in the NASA STI Report Series, which includes the following report types:

- TECHNICAL PUBLICATION. Reports of completed research or a major significant phase of research that present the results of NASA programs and include extensive data or theoretical analysis. Includes compilations of significant scientific and technical data and information deemed to be of continuing reference value. NASA counter-part of peer reviewed formal professional papers, but having less stringent limitations on manuscript length and extent of graphic presentations.

- TECHNICAL MEMORANDUM. Scientific and technical findings that are preliminary or of specialized interest, e.g., quick release reports, working papers, and bibliographies that contain minimal annotation. Does not contain extensive analysis.

- CONTRACTOR REPORT. Scientific and technical findings by NASA-sponsored contractors and grantees.

- CONFERENCE PUBLICATION. Collected papers from scientific and technical conferences, symposia, seminars, or other meetings sponsored or co-sponsored by NASA.

- SPECIAL PUBLICATION. Scientific, technical, or historical information from NASA programs, projects, and missions, often concerned with subjects having substantial public interest.

- TECHNICAL TRANSLATION. English-language translations of foreign scientific and technical material pertinent to NASA's mission.

Specialized services that help round out the STI Program Office's diverse offerings include creating custom thesauri, building customized databases, organizing and publishing research results ... even providing videos.

For more information about the NASA STI Program Office, you can:

- Access the NASA STI Program Home Page at http://www.sti.nasa.gov/STI-homepage.html

- E-mail your question via the Internet to help@sti.nasa.gov

- Fax your question to the NASA Access Help Desk at (301) 621-0134

- Phone the NASA Access Help Desk at (301) 621-0390

- Write to:
  NASA Access Help Desk
  NASA Center for AeroSpace Information
  800 Elkridge Landing Road
  Linthicum Heights, MD 21090-2934

NASA Contractor Report 195427/VOL1

High Pressure, Earth-Storable Rocket Technology
Volume 1

D.M. Jassowski
Aerojet, Sacramento, California

October 1997

Available from

NASA Center for Aerospace Information
800 Elkridge Landing Road
Linthicum Heights, MD 21090-2934
Price Code: A06

National Technical Information Service
5287 Port Royal Road
Springfield, VA 22100
Price Code: A06

TABLE OF CONTENTS

APPENDICES

LIST OF TABLES

LIST OF FIGURES

LIST OF FIGURES (cont.)

NOMENCLATURE

C*	Characteristic Exhaust Velocity, feet/sec
CVD	Chemical Vapor Deposition
ETH	Electrothermal Heated
FFC	Fuel Film Cooled
FFT	Fast Fourier Transform
HIPC	High Chamber Pressure
Is	Specific Impulse
LEO	Low Earth Orbit
MEO	Medium Earth Orbit
MR	Mixture Ratio, Mass Flow Oxidizer-to-Mass Flow Fuel
NPR	Prandtl Number
NST	Stanton Number
NTO	Nitrogen Tetroxide
ODE	One Dimensional Equilibrium
ODK	One Dimensional Kinetic
PSD	Power Spectral Density
Pc	Chamber Pressure, psia
RCS	Reaction Control System
Re	Reynolds Number Based on Local Diameter
Re dt	Reynolds Number Based on Throat Diameter
TDK	Two Dimensional Kinetic
Tr	Recovert Temperature, °F
hg	Heat Transfer Coefficient, Btu/in.^2-sec°F
qcw	Cold Wall Heat Flux, Btu/in.^2-sec
qhg	Hot Wall Heat Flux, Btu/in.^2-sec
grad	External Radiation Hat Flux, Btu/in.^2-sec

1.0 SUMMARY

This report describes the activities of the Basic Program of NASA Contract NAS 3-27003, High Pressure, Earth-Storable Rocket Technology. The objectives of the Basic Program are to (1) determine spacecraft applications which could benefit from high-pressure thruster operation, (2) determine the appropriate propellants, operating conditions and chamber materials, (3) fabricate testbed hardware, and (4) fire the testbed hardware to obtain data on the effect of pressure on combustion efficiency and heat transfer.

Technical activity from August 1993 through October 1994 is described, including results of 70 firings of testbed hardware. The overall program, which has three subsequent Options, will culminate with the design, fabrication and testing of two high pressure flight thrusters.

The program investigated the effect of increasing the chamber pressure of nitrogen tetroxide/hydrazine spacecraft axial engines at the 100 lbf thrust level from the conventional value of about 100 psia to 500 psia. Performance improvements from 327 sec at 100 Pc to 333 sec at 250 Pc were demonstrated, corresponding to a 2% increase in overall Isp efficiency, from 94% to 96%. Reliable performance data were not obtained at 500 psia.

Heat transfer was shown to have predictable correlation with operating conditions, and to give acceptable equilibrium chamber temperatures at least to 250 psia. Extrapolated data for operation at 500 Pc indicate that chamber temperatures may reach or exceed those presently demonstrated for Ir-Re.

Thruster front end thermal management, injector operation, and stability were directly demonstrated at 100, 250 and 500 psia: chamber equilibrium thermal operation was demonstrated at 100 and 250 psia.

2.0 INTRODUCTION

The overall program objective is to incorporate the advantages of higher chamber pressure operation into high performance thrusters for spacecraft. This is to be accomplished in a Basic program followed by three Optional programs.

The Basic program, reported here, was divided into four major tasks which were conducted over a 15-month period beginning mid August, 1993, as shown in Figure 1. The program activity consisted of Task 1, System Parameter Selection, Task 2, Rocket Testbed Design, Task 3, Rocket Testbed Fabrication, and Task 4, Rocket Testbed Testing.

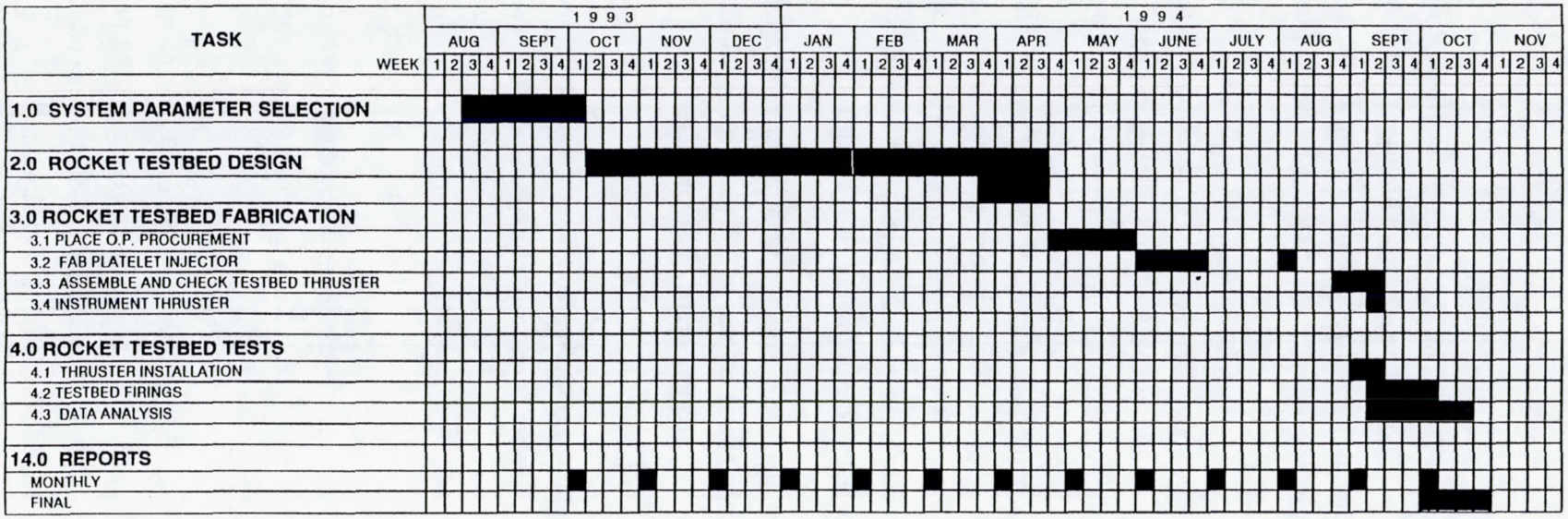

Figure 1. Basic Program Schedule

2.1 PROGRAM APPROACH

The initial program activity was to determine the most suitable application, propellants, range of operating conditions, and potential practical chamber materials. This was completed in the first month, and utilized the results of a industry-wide survey. The results of this task are presented in Appendix A.

During Task 2 the design for the testbed hardware was developed. Hot fire testing was conducted to guide the design and verify its adequacy. This task produced a testbed design package which incorporated existing hardware and new or modified components required to meet the requirements for operation at high pressure. The design package, including the test data and substantiating analyses, is presented in Appendix B.

In Task 3, Fabrication, a high temperature rhenium chamber was fabricated by the CVD process, a high pressure, film-cooled platelet injector was fabricated by the etch and bond process, and, as a parallel activity separate from the contract, Glen Malone of Electroformed Nickel provided a electrodeposited iridium coating on an existing rhenium chamber for test in Task 4.

In Task 4, the testbed hardware, instrumented to provide heat transfer, combustion efficiency, performance, thermal management, compatibility and stability data, was hot fire tested. The resulting test data have been collected, analyzed, correlated and are presented in this report.

2.1.1 Applications

By survey of spacecraft primes and other data sources, it was determined in the first month of the program that the applications which had the most likelihood of using high performance, high-pressure rocket technology were those that had high total impulse requirements, where the performance advantage can provide a significant propellant mass savings. In addition, the size reduction provided by higher Pc favored retrofitting into ongoing spacecraft bus designs, such as Hughes 601, Martin 7000 series, or LMSD Bus-1.

Reassessment of the market 15 months later shows a potential growth in lower total impulse applications. These are represented by small (100 to 800 kg) satellites which are part of low and medium earth-orbit constellations for mass telecommunications and other

commercial services delivery. Table 1 lists some of these constellations and their characteristics. In the cases where the spacecraft is a new design, potential for mass and cost savings exists by use of 0.5 to 5 lbf-class NTO/hydrazine bipropellant thrusters to replace hydrazine monopropellant thrusters.

2.1.2 Operating Conditions

Most applications dictate the choice of propellants: nitrogen tetroxide/hydrazine, to support dual mode operation (bipropellant axial engine and monopropellant RCS). Standard operating pressure for spacecraft thrusters is in the range of 100 psia chamber pressure, with thruster inlet pressures of about 220 to 235 psia. We show that existing spacecraft tankage can support thruster operation at 250 psia chamber pressure with no modification. Thruster operation to chamber pressures of 500 psia is practical using electrically-driven pumps powered by solar power which can be made available during the geotransfer phase. Very small high speed pumps for similar applications are now under development.

2.1.3 Thruster Materials and Design

Heat transfer and performance considerations show that radiation-cooled chambers operating at thermal equilibrium with the combustion as are required to give maximum performance. The only material systems known to be capable of long life under these conditions are based on iridium-protected rhenium. Our testing has shown that a moderate amount of fuel film cooling for front end thermal management, coupled with a trip to provide mixing, is a satisfactory approach for these propellants.

2.1.4 Effect of High-Pressure Operation

The effect of increasing chamber pressure at constant mass flow (thrust level) was to make predictable increases in combustion efficiency and therefore performance. Flight thruster specific impulse was determined from measured altitude thrust measurements to be in excess of 330 sec at 250 psia chamber pressure. Equilibrium chamber temperatures of 3500°F at 100 Pc and 3800F at 250 Pc were directly measured and are well within the 4000°F long life limit for Ir-Re.

Table 1. Small Satellite Applications Potential Constellations

HIPC424
11-2-94

SYSTEM	COMPANY	LOCATION	TYPE	ORBIT QUANTITY	ORBIT LOCATION	ON-ORBIT PROPULSION?	SYSTEM COST
AIRES			MOBILE TELEPHONE	48	LEO		
COSCON				73			
dbX		ST.LOUIS					
ELLIPSO	ELLIPSO CORP.	WASHINGTON, D.C.	MOBILE TELEPHONE	21	MEO/LEO	HYDRAZINE MONO	$650x10^6
FINAL ANALYSIS INC		GREENBELT MD		24	LEO		
GEONETS	SMOLLSAT ASSOCIATION	MOSCOW, RUSSIA	COMMUNICATION SATELLITES	6	MEO		
GLOBALSTAR	LORAL QUALCOMM SERVICES, INC.	PALO ALTO, CA	MOBILE TELEPHONE	48	LEO	HYDRAZINE MONO	$3.5x10^9
INTERFEROMETRICS INC.		VIENNA, VA					
IRIDIUM	IRIDIUM, INC.	WASHINGTON, D.C.	MOBILE TELEPHONE	66	POLAR	HYDRAZINE ETH	$3.37x10^9
LEO ONE				56			
LEOSAT		WASHINGTON					
ODYSSEY	TRW, INC.	CLEVELAND, OH	MOBILE TELEPHONE	12	LEO		$2.5x10^9
ORBCOMM	ORBITAL COMMUNICATIONS CORP.	FAIRFAX, VA	MOBILE TELEPHONE	26	LEO		$225,000/UNIT
SIGNAL	NPO ENERGIA	KALINGRAD, RUSSIA	MOBILE TELEPHONE	48			
SMALLSATS	NASA/TRW, OTHERS		TRW, OTHERS	TBD			$1x10^6/UNIT
SPACEWAY	HUGHES			9			$3.2x10^9
STARSYS	STARSYS GLOBAL POSITIONING, IN	LANHAM, MD	DIGITAL MESSAGING AND POSITIONING	24	LEO	COLD GN2	
TAOS				10			
TELEDESIC	GATES, McCaw	KIRKLAND, WA		840	LEO	TEFLON EP	$9x10^9
VOLUNTEERS IN TECH AS		ARLINGTON, VA					

2.2 RESULTS AND CONCLUSIONS

The program results are summarized in this Section, along with the conclusions drawn from them. Detailed discussion of the design, analyses, testing and data correlations which developed these results are provided in Section 3.0 and the Appendices.

Combustion Efficiency

There was an increase of 2% in Isp efficiency, defined as (delivered specific impulse)/(One Dimensional Equilibrium specific impulse) as pressure was increased from 100 to 250 psia. Direct efficiency data were not obtained in Task 4 at 500 psia because of leakage; however, further increase is expected. Flight specific impulse increased significantly from 326 sec at 100 psia to 333 (-2δ) sec at 250 psia; again, further increase is expected in going to 500 psia. Basic technologies for further reducing combustion losses have been identified, including application of combustion catalysts to reduce kinetic losses and surface tailoring to reduce boundary layer losses, both of which are still significant.

Heat Transfer

Good chamber thermal data were obtained at radiation equilibrium chamber conditions for 100 and 250 psia chamber pressure. Steady state maximum chamber outer wall temperatures were 3500°F and 3800°F respectively, at similar operating conditions. Extrapolating the maximum chamber temperature to 500 psia will result in temperatures above 4000°F if the thruster is operated at the optimum MR. This can be accommodated by either increasing chamber emissivity, reducing MR, decreasing trip height or increasing film cooling to provide lower local gas temperatures, or by demonstrating long life for the Ir-Re system at the higher temperature. Thermal response data provided derivation of the local heat transfer coefficient and local gas temperature, which in turn gives a measure of the extent of mixing introduced by the trip. The data indicate the mixing is good but not perfect; potential for improvement exists.

Injector, front end and trip heat transfer were acceptable, even at 500 psia. Local overheating of a small portion of the Haynes 25 sleeve used to hold the Pt-10% Rh trip did occur; the Haynes alloy was used to accommodate the combination of three trip lengths and three trip heights to permit trip optimization. Subsequent designs will use all Pt-Rr or Pt-Ir alloy, which has thermal margin.

2.2, Results and Conclusions (cont.)

The predicted increase in specific impulse with chamber pressure was obtained. The 300:1 vacuum performance is projected to be 327 sec at 100 psia and 333 sec at 250 psia.

Compatibility

Initial material compatibility measurements indicate the Ir-Re chamber life should be as long as previously demonstrated for NTO/MMH propellants (>6 hr at 100 lbf without failure and >15 hr at 5 lbf).

Stability

The thruster was stable at all operating conditions, even when tested at injector pressure drops as low as 10 to 20% of Pc.

Spacecraft Integration

The low inlet pressures required for the 250 psia chamber pressure make operation from existing flight qualified tanks practical with some modification in spacecraft operating philosophy.

2.3 RECOMMENDATIONS

Significant payoff, both in performance and reduced size result from increased chamber pressure, justifying further development in the Option program. Emphasis should be in the pressure range up to 250 psia, since higher pressures will require extensive spacecraft changes (e.g., electrically driven pumps).

To obtain better thermal management and life data, the Option testing should emphasize early tests with potential material systems (e.g., Ir-Re, manufactured by various processes), in flight-like configurations. Test times of the order of hundreds of seconds are necessary for accurate thermal management demonstration and of thousands of seconds for realistic life projections for typical applications which require hours of life.

Because of changes in spacecraft design/planning during the last 15 months, much more need for high performance thrusters is evident in the 0.5 to 5 lbf thrust class. We recommend Option I testing be conducted at this thrust level. This will have the following programmatic advantages:

2.3, Recommendations (cont.)

- Significantly reduced material cost for chambers
- Enables long duration firings to be cost effective because of the greatly reduced propellant costs.
- Will result in a thruster which fills a present void in the technology (high performance NTO/hydrazine in the 0.5-5 lbf). Such a thruster will enable a major reduction in spacecraft mass by replacing the present workhorse hydrazine monoprops (at 230 sec or less) with an all bipropellant thruster system with Is greater than 300 sec, without a need for large amounts of electrical power, consistent with the capabilities of most small satellites.

3.0 TECHNICAL DISCUSSION

The technical aspects of the program are described here. The technical approach was to determine the best set of operating conditions to meet NASA program requirements, to design a set of testbed hardware consistent with these conditions, and then to build and test the hardware to determine the effect of increased pressure on thruster operation.

3.1 SYSTEM PARAMETER SELECTION

This one-month task had as its output the selection of application and operating conditions to be used in the remainder of the Basic program. Applications, typified by recent launches, are listed in Table 2. Thrusters available or planned for spacecraft application and their characteristics are shown in Table 3. A user survey was conducted to determine future trends and propulsion needs. The results of this survey, Table 4, were used to guide choice of application and operating condition. The values of the selected parameters and the basis for their choice are given in Table 5.

To guide the subsequent portions of the program, target high pressure flight thruster concept designs were prepared. These thruster designs are illustrated in Figure 2 and described in Table 6. The predicted performance for these engines is detailed in Table 7.

Further details of the Task 1 process and its results are given in Appendix A.

HIPC52

8-2-93

Table 2. Typical Applications for High-Pressure, Earth-Storable Propulsion Systems Based on 1992 Launches

SPACECRAFT MANUFACTURER	1992 LAUNCH DATE	SPACECRAFT	LAUNCH VEHICLE	SPACE-CRAFT WEIGHT, Kg	APPLICATION
AEROSPATIALE	2-26	ARABSAT	ARIANE 44L	1310	COMMUNICATIONS SATELLITE
AEROSPATIALE	7-9	EUTELSAT 2 F4	ARIANE 44L	1877	COMMUNICATIONS SATELLITE
ALENIA ESPAZIO	10-23	LAEGOS II	STS-52	405	GEODYNAMICS SATELLITE
BRITISH AEROSPACE	4-15	INMARSAT 2 F4	ARIANE 44L	1310	COMMUNICATION SAT.
DEUTSCHE AEROSPACE	10-12	DFS 3 KOPERNICUS	DELTA 2	1398	COMMUNICATION SAT.
FAIRCHILD SPACE	6-7	EUVE	DELTA 2	3275	SCIENCE SAT.
FAIRCHILD SPACE	8-10	TOPEX/POSEIDON	ARIANE 42P	2402	OCEAN SENSING
HUGHES	3-14	GALAXY 5	ATLAS CENTAUR	1412	HS-376 COMMUNICATION
HUGHES	5-14	PALAPA B4	DELTA 2	1254	COMMUNICATION SAT.
HUGHES	8-13	OPTUS B1	LONG MARCH	7650	COMMUNICATION SAT.
HUGHES	12-21	OPTUS B1	LONG MARCH	7650	COMMUNICATION SAT.
HUGHES	10-28	GALAXY VII	ARIANE 42P	2968	COMMUNICATION SAT.
INDIAN SPACE RESEARCH ORGANIZATION	5-20	SROSS	ASLV	106	SCIENCE SAT.
INDIAN SPACE RESEARCH ORGANIZATION	7-9	INSAT 2A	ARIANE 44L	1906	COMM./WEATHER/SEARCH SAT.
MARTIN [GE ASTRO-SPACE]	6-10	INTELSAT K	ATLAS 2A	2928	COMMUNICATIONS SAT.
MARTIN [GE ASTRO-SPACE]	8-31	SATCOM C4	DELTA 2	1375	COMMUNICATIONS SAT.
MARTIN [GE ASTRO-SPACE]	9-10	SATCOM C3	ARIANE 44LP	1375	COMMUNICATIONS SAT.
MARTIN [GE ASTRO-SPACE]	9-25	MARS OBSERVER	TITAN III	2573	SPACECRAFT
MATRA MARCONI SPACE	4-15	TELECOM 2B	ARIANE 44L	2275	COMMUNICATIONS SATELLITE
MATRA MARCONI SPACE	9-10	S80/T	ARIANE 42P	50	COMMUNICATIONS SATELLITE
MATRA MARCONI SPACE	9-10	HISPASAT 1A	ARIANE 44LP	2194	COMMUNICATIONS SATELLITE
MITSUBISHI ELECTRIC	2/11	JERS 1	H-1	1340	RESOURCES SATELLITE
NIPPON ELECTRIC	7-24	GEOTAIL	DELTA 2	1008	SCIENCE SAT.
PEOPLE'S REPUBLIC OF CHINA	8-9	FSW-2	CZ-2D	2400	SCIENCE SAT.
PEOPLE'S REPUBLIC OF CHINA	10-6	FSW-1	CZ-2C	2100	SCIENCE SAT.
ROCKWELL SPACE SYSTEMS	2-23	GPS 12	DELTA 2	1665	GLOBAL POSITION
ROCKWELL SPACE SYSTEMS	4-10	GPS 13	DELTA 2	1665	GLOBAL POSITION
ROCKWELL SPACE SYSTEMS	7-7	GPS 14	DELTA 2	1665	GLOBAL POSITION
ROCKWELL SPACE SYSTEMS	9-9	GPS 15	DELTA 2	1665	GLOBAL POSITION
ROCKWELL SPACE SYSTEMS	11-22	GPS 16	DELTA 2	1665	GLOBAL POSITION
ROCKWELL SPACE SYSTEMS	12-18	GPS 17	DELTA 2	1665	GLOBAL POSITION
SOUTH KOREAN AIST/U. SURREY	9-10	KITSAT-A	ARIANE 42P	52	COMMUNICATIONS SAT.
SPACE SYSTEMS/LORAL	2-26	SUPERBIRD B1	ARIANE 44L	2560	COMMUNICATIONS SAT.
SPACE SYSTEMS/LORAL	12-1	SUPERBIRD A1	ARIANE 42P	2780	COMMUNICATIONS SAT.
SWEDISH SPACE CORP.	10-6	FREJA	CZ-2C	259	SCIENCE SAT.

DATA FROM "TRW SPACE LOG, 1992", TRW SPACE AND ELECTRONICS GROUP Avg. weight= 2005 Kg

Table 3. Small Earth-Storable Liquid Rocket Engines for Satellite and Space Vehicles

HIPC74

8-11-93

SUPPLIER	MODEL	THRUST	PROPELLANTS	CHAMBER MATERIAL	BURN TIME	Pc	MR	Is	AREA RATIO	MASS	DATA SOURCE
AEROJET		2.00N	NTO/MMH				1.65	265	150		INTER. SPACE. DIR/90-91
AEROJET		21.35N	NTO/MMH				1.65	285	150		INTER. SPACE. DIR/90-91
AEROJET		445N	NTO/MMH				1.65	309	150		INTER. SPACE. DIR/90-91
ATLANTIC RSEARCH		22-4500N FAMILY		COLUMBIU							INTER. SPACE. DIR/90-91
DEUTSCHE AEROSPACE		4N	NTO/MMH	Pt-Rh	>40 HRS	7 BAR	1.64	285	187	270 gm	AIAA 93-2120
DEUTSCHE AEROSPACE		10N	NTO/MMH	Pt/Rh	>40 HRS	9 BAR	1.65	290	150	300gm	AIAA 93-2120
DEUTSCHE AEROSPACE		400N				10 BAR	1.643	317	220	3117kg[elc	AIAA 93-2120
MARQUARDT	R-1E	110N	NTO/MMH	Cb	82000		1.65	280	100		INTER. SPACE. DIR/90-91
MARQUARDT	R-40A	3870N	NTO/MMH	Cb	500 MAX/15,319	10.5 ATM	1.6	281/306	20/120	10.25KG	INTER. SPACE. DIR/90-91
MARQUARDT	R-4D	490N	NTO/MMH or AH	Cb	UP TO 1 HR	6.84 ATM	1.65	312		3.63 KG	INTER. SPACE. DIR/90-91
MARQUARDT	R-42SR	140-300LBF	NTO/MMH		>3E6LBF-SEC	350-150		303	164		AIAA 93-2118
MARQUARDT	R-6C	22N	NTO/MMH	Cb	UNLIMITED		1.6+-.1	290	100	0.66 KG	
MARQUARDT	R-6C-2.2	10N									INTER. SPACE. DIR/90-91
MARQUARDT	R4-D	490N									AIAA-93-2517
ROCKET RESEARCH CO.	MR-50, -103, -104,		]-HYDRAZINE MONO.								INTER. SPACE. DIR/90-91
ROCKET RESEARCH CO.	-107, -111, -501		-501 IS ELEC. AUG.					280-304(EP)			INTER. SPACE. DIR/90-91
ROYAL ORDNANCE	LEROS-1	105LBF	NTO/HYDRAZINE	Cb,Ti INJ	22.8Ksec(1990)	80-100	0.7-1.0	318(320 '93)	200		PRESENT. AT APD, 5-28-93
ROYAL ORDNANCE	LEROS-2	125LBF	NTO/MMH					311			PRESENT. AT APD, 5-28-93
ROYAL ORDNANCE	LEROS-2A		NTO/MMH	*ADV. MATL				320('93)	300		PRESENT. AT APD, 5-28-93
ROYAL ORDNANCE	LEROS-20	5LBF	NTO/MMH	Cb				295			PRESENT. AT APD, 5-28-93
ROYAL ORDNANCE	LEROS-20A	5LBF	NTO/MMH	*NEW MATL				295('92)310('			PRESENT. AT APD, 5-28-93
ROYAL ORDNANCE	LEROS-20H	NTO/HYDRAZINE	NTO/HYDRAZINE					TARGET 300(			PRESENT. AT APD, 5-28-93
ROYAL ORDNANCE	LEROS-20HA[?]	5LBF	NTO/HYDRAZINE	ADV. MATL				TARGET 313			INTER. SPACE. DIR/90-91
TRW	DUAL-MODE		NTO/HYDRAZINE								INTER. SPACE. DIR/90-91
TRW	ERIS										INTER. SPACE. DIR/90-91
TRW	MRE-0.1,-1, -4		]-HYDRAZINE MONO.								INTER. SPACE. DIR/90-91
TRW	-R/GRO, -15/OMV, -50		]								INTER. SPACE. DIR/90-91
TRW	OMV	VARI.: 57.8-578N	NTO/MMH	Cb ALLOY		0.75-6.8 AT	1.64	280-308	125	6.8 kg	INTER. SPACE. DIR/90-91
UNITED TECH/HAM STD	REA 10, 17-6,	]-.89-26.7N	]-HYDRAZINE MONO.								INTER. SPACE. DIR/90-91
UNITED TECH/HAM STD	17-12, -16, 39-2	]	]								

Table 4. Mission Data Survey Results

Mission Data

1. What are your required satellite propulsion system on-station operability times:

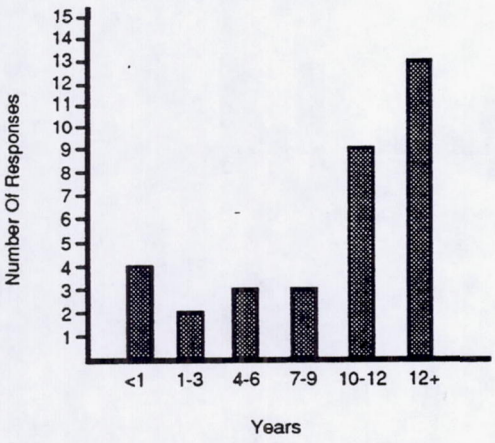

If you integrate apogee delta V into your satellite, how would you accomplish GTO transfer and GEO circularization:

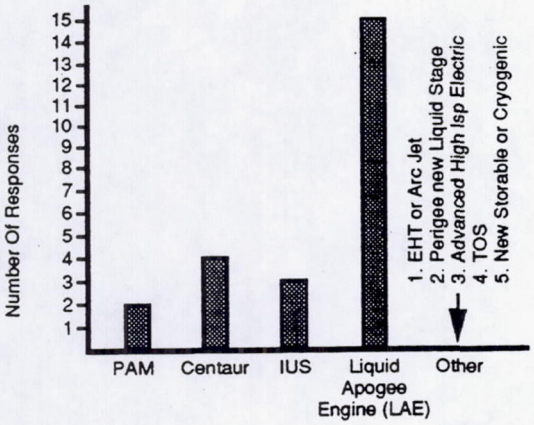

3. Please rank the total impulse per satellite requirement you anticipate in the near future:

note: the question was ambiguous and results therefore inconclusive

4. Please rank in order of unsatisfied need for desired engines (1-4, 4 = most desired)

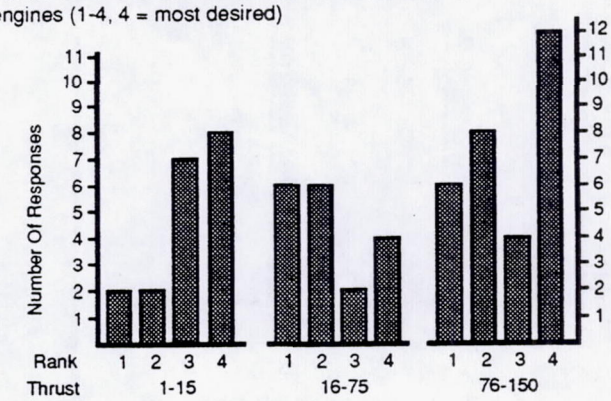

What is your preferred thrust level

Axial Engine: 90 - 110 (1)
100 - 110 (7)
100 - 200 (4)
1000+ (1)

Reaction Control Thrusters: ≤1 (6)
2-5 (9)
>5 (2)

What is your maximum acceptable satellite g level:
≤.1 (9) .2 - 1 (4) >1 (4)

5. Is throttlability of interest:

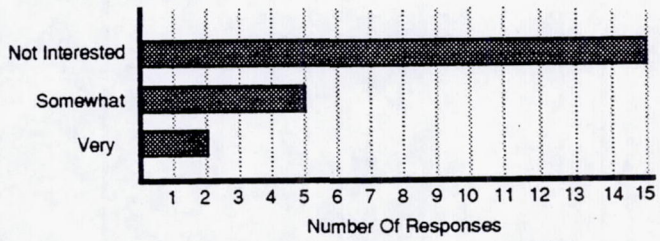

6. What is your minimum impulse bit (lbF-sec):

< .03 (4) .03 - .05 (6) >.05 (2)

7. Which is preferred:

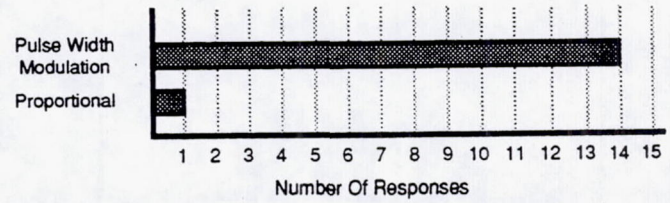

Table 4. Mission Data Survey Results (cont.)

Mission Data (cont.)

8. What is your preferred propellant combination:

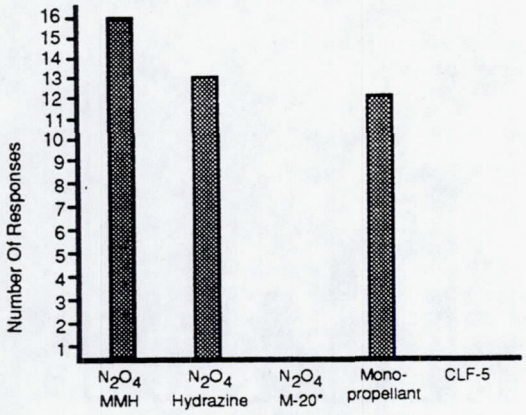

* M-20 = 80% Hydrazine + 20% MMH

(Note: H_2O_2 / RP-1 of interest to 1 respondent)

9. Please provide a weighting factor (1-10, 10 = most important) for the following propellant parameters:

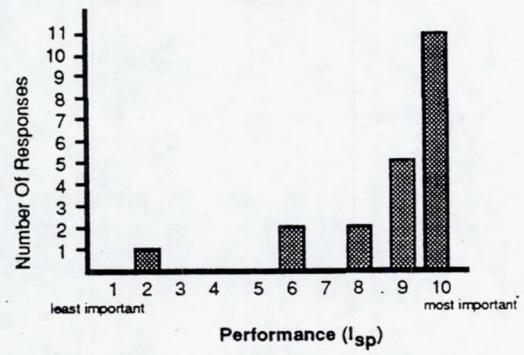

Performance (I_{sp})

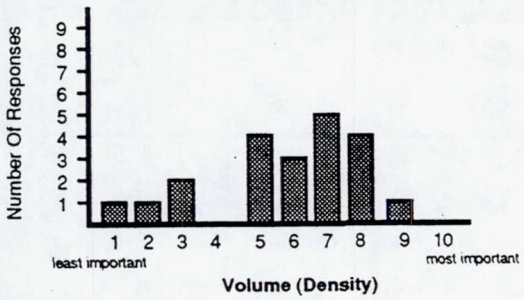

Volume (Density)

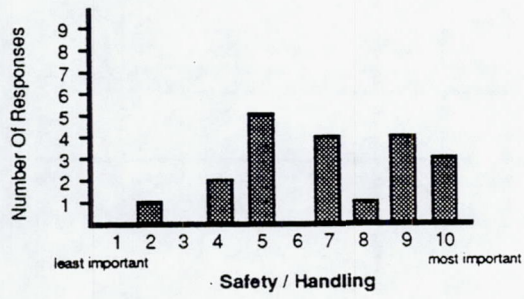

Safety / Handling

(9. cont.) Please provide a weighting factor (1-10, 10 = most important) for the following propellant parameters:

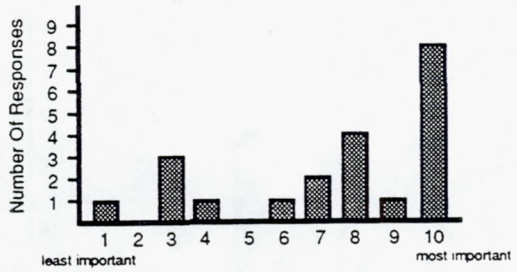

Cost

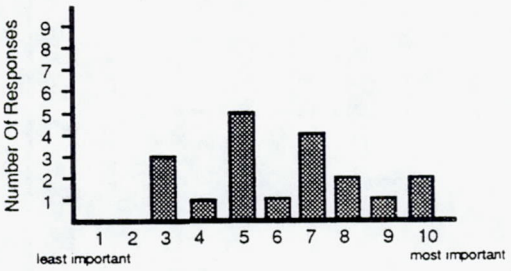

Storage Difficulty

Table 5. HIPC Parameter Space Bases for Parameter Selection

HIPC33

7-8-93

UPDATE 9-9-93

PARAMETER	SELECTION	BASIS
COST	LOW COST DESIGN APPROACH [TO BE DETERMINED]	SHORT TIME FRAME FOR INVESTMENT PAY-BACK FORCES LOW UP-FRONT COSTS AND LOW UNIT COSTS: POTENTIAL SAVINGS OF LONGER SATELLITE OPERATING LIFE OCCUR TOO LATE [A DECADE OR MORE AFTER LAUNCH]; MUST COMPETE ON COST TO BE A VIABLE APPLICATION
PROPELLANTS	N204/N2H4	INCREASED PERFORMANCE OVER NTO/MMH USER TREND IS TOWARDS NTO/AH SURVEY SHOWS NEARLY EQUAL WEIGHT FOR MMH & AH (16 vs. 13) PERMITS DUAL MODE OPERATION NEXT GENERATION; CONSISTANT WITH PROGRAM TIME SCALE PROVIDES TRANSITION TO ELECTRIC PROPULSION PROVIDES MARKETABLE NEW TECHNOLOGY FOR APD NO USERS SURVEYED EXPRESSED INTEREST IN CIF5 ONLY POTENTIAL CIF5 APPLICATIONS HAVE SMALL EXPECTED FREQUENCY OF OCCURENCE INFRASTRUCTURE FOR CIF5 NOT CONSISTENT WITH PROGRAM REQUIREMENTS
THRUST LEVEL	100LBF-CLASS	AXIAL ENGINE HAS BIGGEST PAYOFF THRU PROPELLANT SAVINGS TYPICALLY 80% OR MORE OF PROPELLANT MASS DIVERT OR ATTITUDE CONTROL PROPULSION SPECIFICALLY EXCLUDED IN CONTRACT TREND IS DOWNWARDS IN THRUST (e.g. FROM 200 TO 100LBF) SURVEY SHOWS 8/5 OR BETTER FOR 90-110 LBF CLASS
Is GOAL	335 SEC	REQUIRED TO BE COMPETETIVE
TOTAL IMPULSE	3,000,000LBF-SEC MINIMUM	EQUIVALENT TO 8+ HOURS OF FIRING TIME AT 100 LBF
MATERIALS	Ir-Re	BASE-LINE MATERIAL SYSTEM; OTHERS WILL BE INVESTIGATED IN TASK 4 AND BEYOND NO OTHER MATERIAL SYSTEM HAS DEMONSTRATED REQUIRED LIFE AT HIGH PERFORMANCE

Table 5. HIPC Parameter Space Bases for Parameter Selection (cont.)

PARAMETER	SELECTION	BASIS
CHAMBER PRESS.	APPROX. 250 PSIA APPROX 500 PSIA	HIGHEST THAT CAN BE OBTAINED WITH EXISTING TANK PRESSURES HIGHEST THAT CAN BE PUMP-FED WITH POWER CONSTRAINTS TEST PROGRAM WILL COVER WIDER RANGE; WILL BE STRUCTURED SO THAT FLIGHT-TYPE ENGINE CAN BE EITHER HIGH OR MEDIUM Pc
MIXTURE RATIO	TBD	OPTIMUM FROM TESTING/ANALYSIS
VALVE	TEST STAND FLIGHT	TO PERMIT HIGH INLET PRESSURE OPERATION REQ'D FOR OPTION 3 FLIGHT TYPE ENGINE; MAY NEED FOR OPTION 2
INJECTOR	S/N LM-2 S/N 7 S/N 8	FOR TASK 2 TESTS USE EXISTING LASER-MACHINED (UNFIRED) INJECTOR DESIGN/FAB NEW INJECTOR FOR TASK 4 NEW DESIGN MAY BE REQUIRED AS ITERATION FOR OPTION 1 AND FOR FLIGHT-TYPE ENGINE BRILLIANT PEBBLES OR LDI EXISTING OPTIONS FOR 500 Pc ENGINE
FRONT END	FUEL-COOLED REGEN	APD HAS LARGE DATA BASE FOR 100LBF CLASS RUN INITIAL TESTS WITH WATER COOLING THERMAL BARRIER COATING WILL PROVIDE GOOD THERMAL MARGIN FOR N2H4
FLIGHT PRESSURIZATION SYSTEM	PRESSURE-FED PUMP-FED	FOR NEAR-TERM/REPLACEMENT AND GROWTH APPLICATIONS FOR LONG-TERM, HIGHEST PRESSURE APPLICATIONS ELECTRIC MOTOR DRIVE MONOPROP GG DRIVE
OTHER PARAMETERS	ENVELOPE, MASS, ETC.	TO BE FINALIZED AS PROGRAM PROGRESSES: USE COMPOSIT OF HUGHES/LMSC/GE/JPL/LORAL/ESA SPECIFICATIONS FOR INITIAL WORK

Reference - AJ10-221 Ir-Re NTO/MMH

Pc = 114 psia
F = 110 lbf
ε = 286:1
Is = 321.8 sec

Concept 1A - NTO/Hydrazine

Pc = 250 psia
F = 100 lbf
ε = 300:1
Is = 330 sec

Concept 2A - NTO/Hydrazine

Pc = 500 psia
F = 100 lbf
ε = 300:1
Is = 335 sec

Figure 2. Comparison of Flight Engine High Pc Concepts to Reference

Table 6. Basis for Conceptual Designs

FLIGHT TYPE CONCEPT DESIGN=	AJ10-221 [REFERENCE]	#1A	#2A
CHAMBER PRESSURE SELECTION CRITERIA	JPL SPEC	~MAX. Pc WITH EXISTING TANKS[1]	~MAX. Pc PUMP-FED[2]
DESIGN Pc, PSIA	115	250	500
THRUST, LBF	110	100	100
PROPELLANTS	NTO/MMH	NTO/HYDRAZINE	NTO/HYDRAZINE
DESIGN BASIS	JPL SPEC	AJ10-221	BRILLANT PEBBLES
Is, SEC	321.8	330	335
C*, FT/SEC	5500	5650	5720
NORMALIZED Is PERFORMANCE [AJ10-221=1.0]	1	1.025	1.041
THRUSTER EFFICIENCY [3]	0.91	.93	.94
NORMALIZED CHAMBER HEAT FLUX [AJ10-221=1.0]	1	0.93	6.8
NORMALIZED THROAT HEAT FLUX [AJ10-221=1.0]	1	1.55	2.36
CHAMBER TEMPERATURE, oF	3380	3790	3950
ENVELOPE, MAX DIA., IN	13.8	9.2	6.5
ENVELOPE, MAX LENGTH	30	20.7	15
MAX WEIGHT, LBM	10	TBD	TBD
VALVE	MOOG TORQUEMOTOR	LOW COST	LOW COST
AREA RATIO	286	300	300
DESIGN LIFE, HOURS	>6	>12	>12
FRONT END DESIGN	FUEL-REGEN S.S.	FUEL-REGEN S.S.+THER. BARR. COATING	FILM-COOLED PLATINUM-Rh TRIP
INJECTOR	S/N6-2	RE-BALANCE AJ10-221 FOR HYDRAZINE	USE BRILLIANT PEBBLES TI INJ.
CONTRACTION RATIO	4	11	2.4
L', IN	4.2	4.2	2.1
THROAT DIA, IN	0.804	0.521	0.368
CHAMBER DIA, IN	1.71	1.71	0.57
MINIMUM INJECTOR DELTA P, PSI [STAB. LIMIT]	35 (CALC)	75	150
CHAMBER MATERIAL	Ir-Re	LOW-COST Ir-Re	LOW-COST Ir-Re

[1] TYPICAL MAX. PRESSURE FOR EXISTING TANKS IS ~400 PSIA.
[2] POWER LIMITED AT ABOUT 3 KW.
[3] RELATIVE TO ODE AT DESIGN MR

Table 7. Predicted Performance for High-Pressure Earth-Storable Thruster Concepts

HIPC105

9-11-93

PARAMETER	VALUES		COMMENTS
CASE	1A	2A	Concept designs
CHAMBER PRESSURE, PSIA	250	500	Operating chamber pressure
MR, O/F	1.15	1.15	Mixture ratio (optimum to be determined in Tasks 2 and 4)
AREA RATIO, Ae/At	300	300	Nozzle area ratio; can be modified to meet specific envelope/performance needs
Rthroat, INCHES	0.26	0.185	Throat radius
Lnozzle, INCHES	13.2	9.4	Nozzle length, throat to exit
% BELL	83.4	83.4	Percent of length of 30 deg conical nozzle to same exit diameter
Isp ODE, LBF-SEC/LBM	357.3	357.5	Theoretical performance based on 1-dim. equilibrium composition
Isp ODK, LBF-SEC/LBM	349.6	352.3	Theoretical performance based on 1-dim. kinetics-limited composition
Isp TDE, LBF-SEC/LBM	353.0	353.1	Theoretical performance based on 2-dim. equilibrium composition
Isp bl, LBF-SEC/LBM	7.4	6.2	Performance loss due to boundary layer
eta kinetics, %	97.8	98.6	Kinetics efficiency
eta divergence, %	98.8	98.8	Divergence efficiency
Isp, PI, LBF-SEC/LBM	337.9	341.8	Performance of a perfect injector
ERE, %	98	.98	Combustor energy release efficiency
Isp del, LBF-SEC/LBM	331	335	Predicted delivered performance
THRUSTER EFFICIENCY, %	92.6	93.7	Overall thruster efficiency, based on ODE theoretical performance

3.2 ROCKET TESTBED DESIGN

Modifications to existing testbed hardware required for increased chamber pressure operation were designed in Task 2. To verify the designs, hot fire testing was conducted. Failure of the regeneratively cooled trip occurred, caused by improper test design (post test purge, causing overheating of stagnant hydrazine, which detonated). This showed that inadequate design margin existed with regenerative cooling, necessitating use of a backup fuel film cooled design, which was tested and provided the basis for the testbed design.

The 46 design verification tests are summarized in Table 8. Figure 3 is a drawing of the regeneratively cooled testbed hardware used in the first 16 tests; Figures 4 and 5 are photographs of the hardware. The extrapolation performance of this thruster is shown in Figure 6. The film cooled trip assembly used in subsequent tests is shown in Figure 7; its performance is summarized in Figure 8.

The testbed rocket engine assembly design which was an output of Task 2 is shown in Figure 9. The trip, holder and rhenium chamber design are shown in Figures 10, 11, and 12, respectively.

Further details on the Task 2 activity are given in Appendix B.

3.3 ROCKET TESTBED FABRICATION

The hardware necessary for the Task 4 testing was fabricated in Task 3. A new 250 psi rhenium chamber was fabricated by the CVD process. To conserve funds, it was decided to use an existing 100 Pc Ir-Re chamber. The Ir coating on this chamber had been intentionally damaged in plume signature tests on another program where the chamber was operated with film cooling, without a trip. This permitted evaluation of a different forming process, electrodeposition of Ir, which was used to repair the coating.

Since thermal analysis showed that, under the constraints necessitated by the testbed hardware, the front end heating would limit the 500 psia tests to short duration, it was decided to save the cost of a Re chamber and use the Task 2 copper chamber.

Table 8. Summary of Testing Task 2 Testbeds

TEST GROUP	HARDWARE TRIP	HARDWARE COOLING	THROAT	CHAMB. EXT.	OPERATING CONDITIONS Pc	OPERATING CONDITIONS MR	DATA MEASUREMENTS PERFORM.	DATA MEASUREMENTS THERMAL	DATA MEASUREMENTS STABIL.	PLUME EMISS.
-101 to -113	regen	water	-1, -2, -3	--	100, 250, 500	0.94 TO 1.22	yes	--	yes	yes
-114 to -118	regen	fuel	-3	--	100	0.77 TO 1.03	yes	--	yes	yes
-119 to -127	FFC	FC	-2,-3	--	100, 250	0.92 TO 1.24	yes	yes	yes	--
-128 to -131	FFC	FC	-3	--	100	0.9 TO 1.27	yes	yes	yes	--
-132 to -142	FFC	FC	-1, -2, -3	--	100, 250, 500	0.73 TO 1.29	yes	yes	yes	--
-143 to -146	FFC	FC	-2	yes	250	0.84 TO 1.35	yes	yes	yes	--

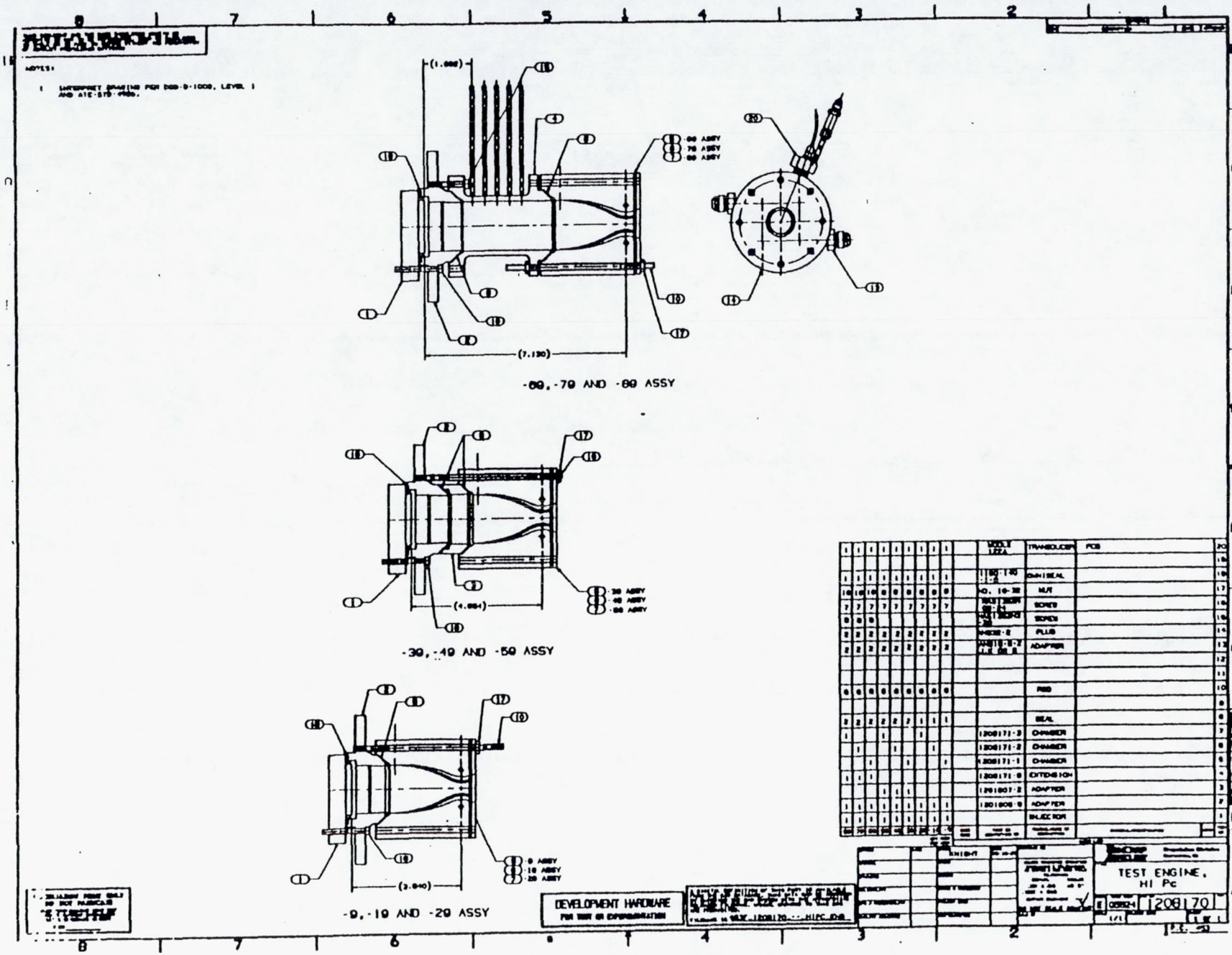

Figure 3. Regen Cooled Testbed

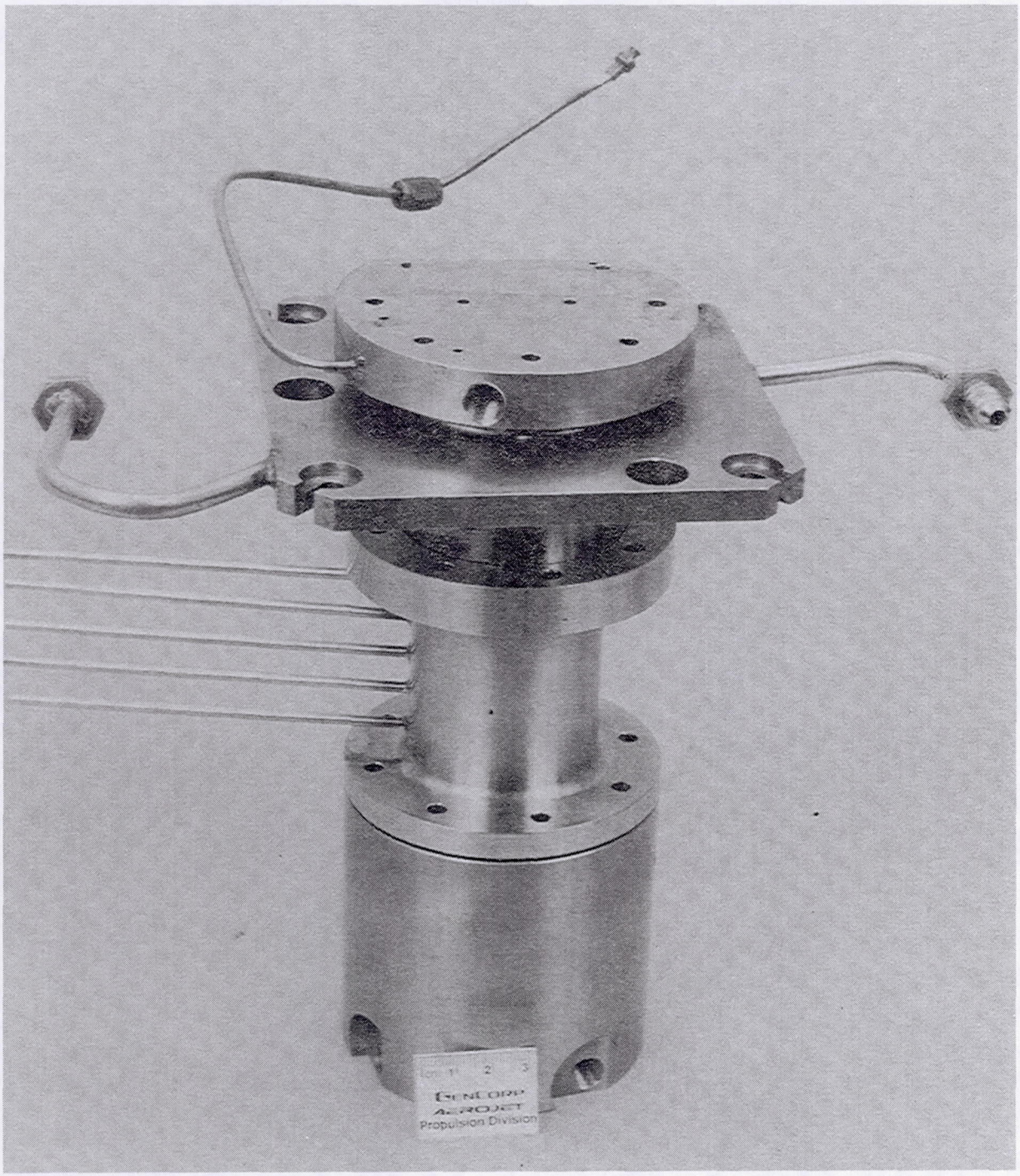

C1293 5275

Figure 4. Task 2 Testbed Assembly

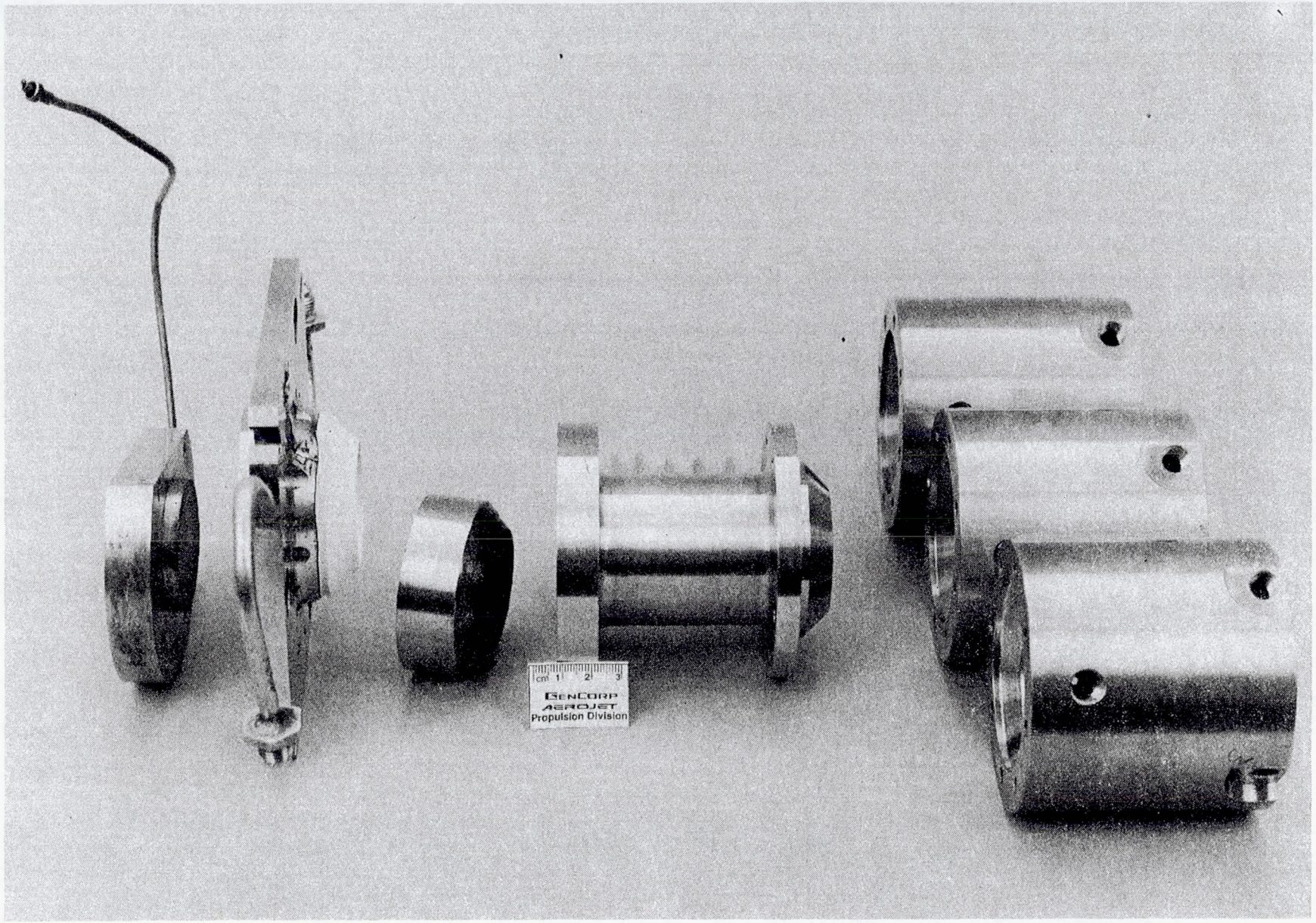

C1293 5276

Figure 5. Task 2 Testbed Components

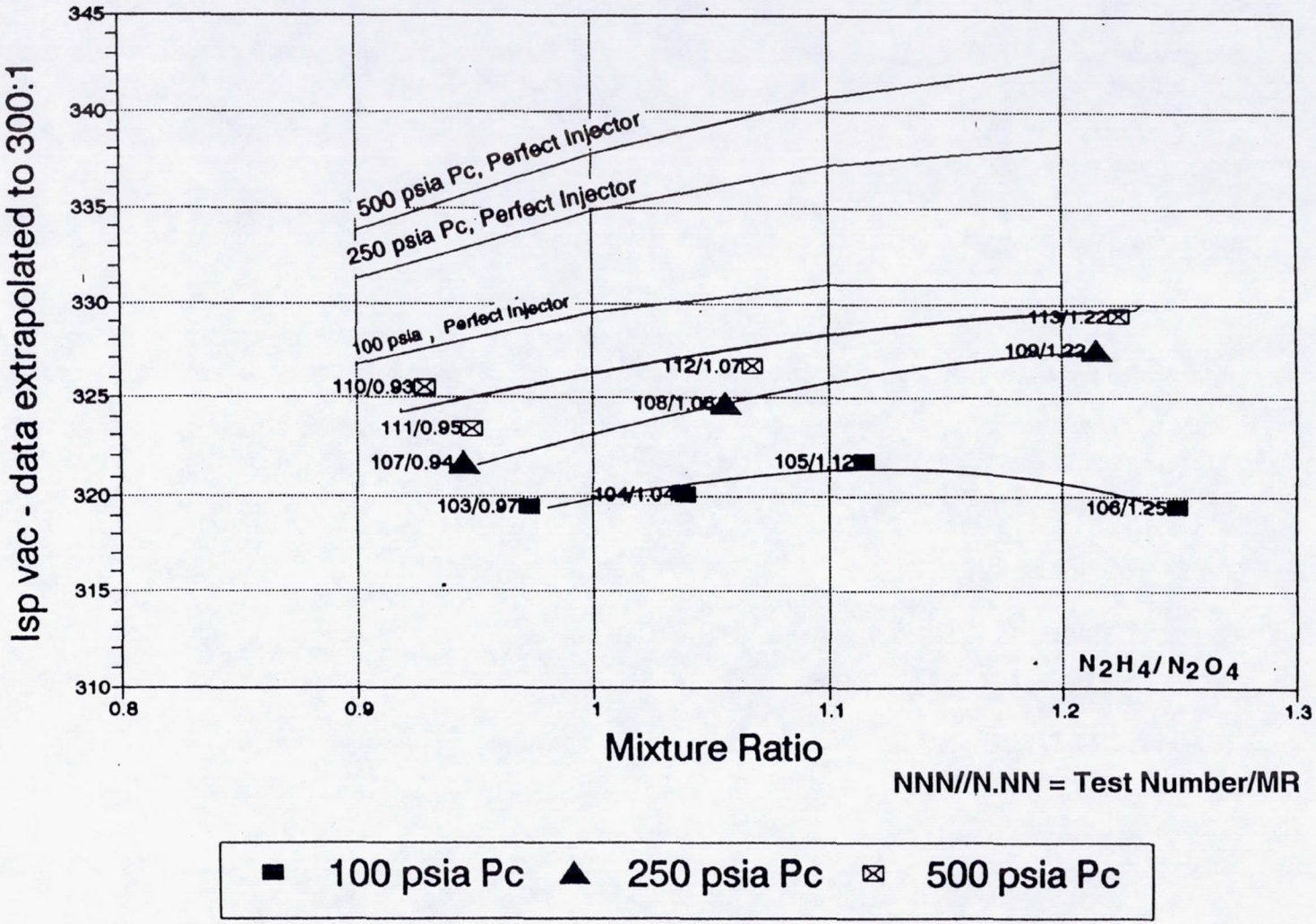

Figure 6. Extrapolated Performance for 300:1 Nozzle

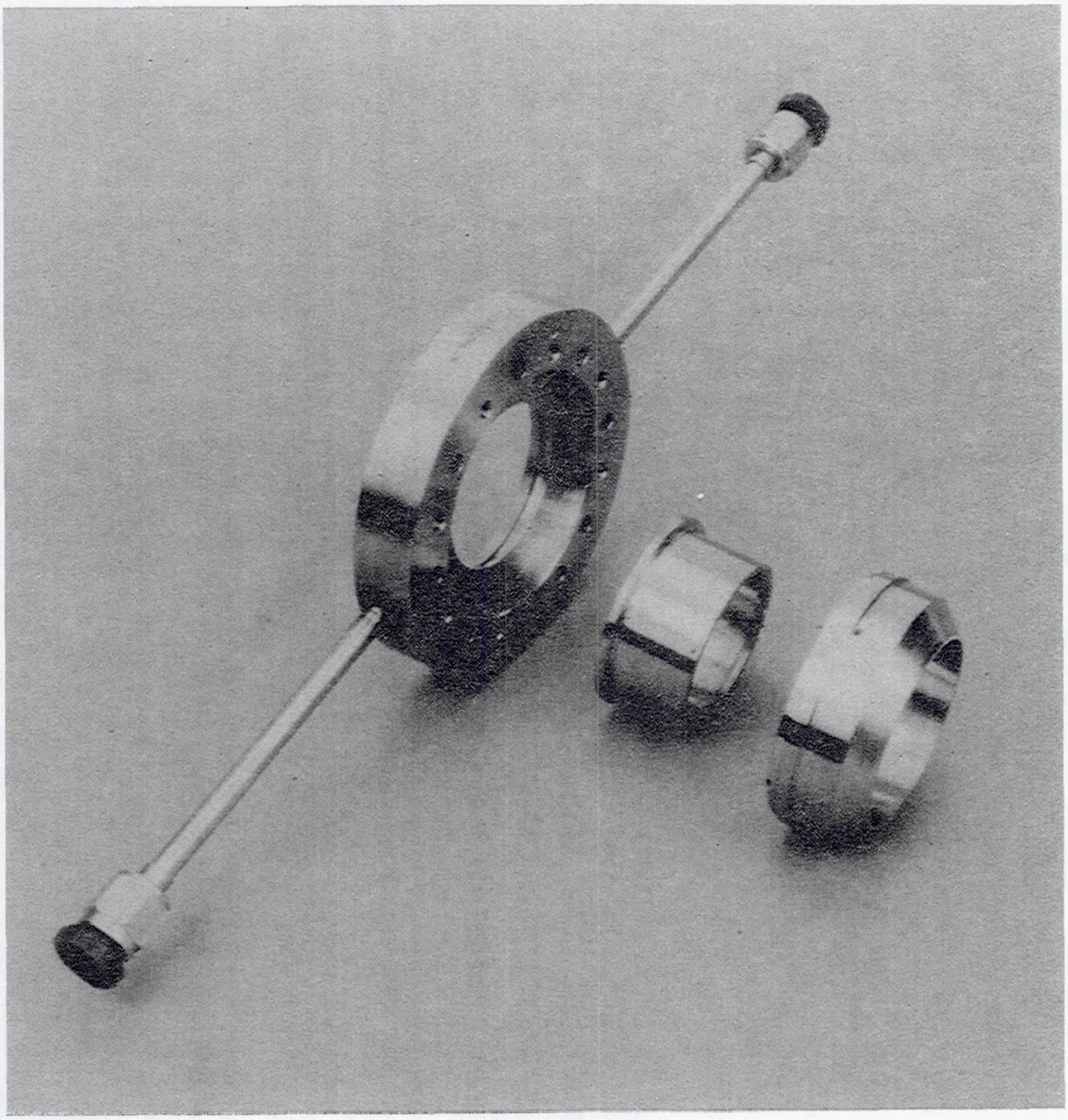

C1192 6987

Figure 7. Trip Section Prior to Installation of Thermocouples

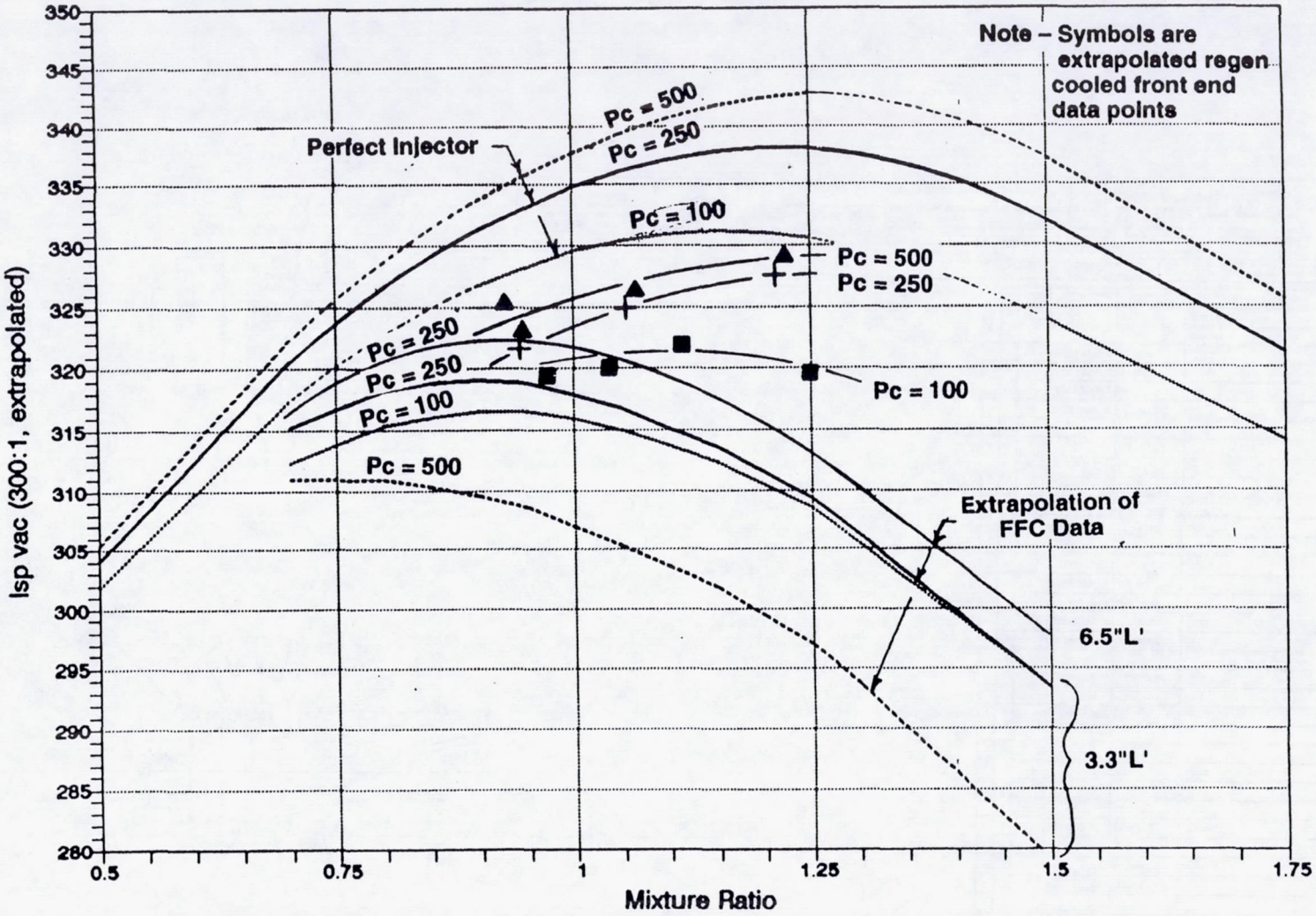

Figure 8. 300:1 Extrapolation of Regen Cooled Front End and FFC Data

NOTES:

1. INTERPRET DRAWING PER ATC-STD-4926.

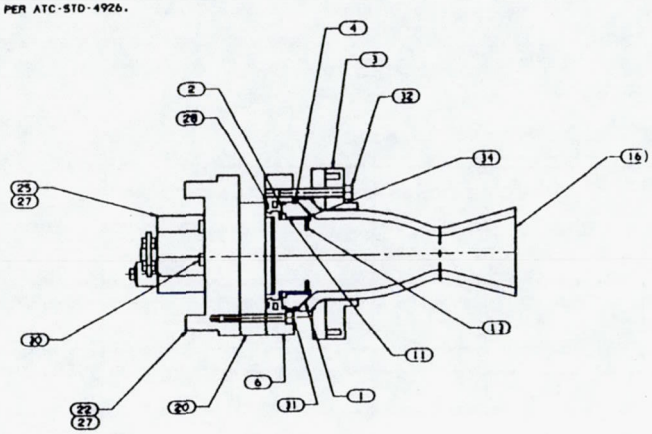

-9 ASSY

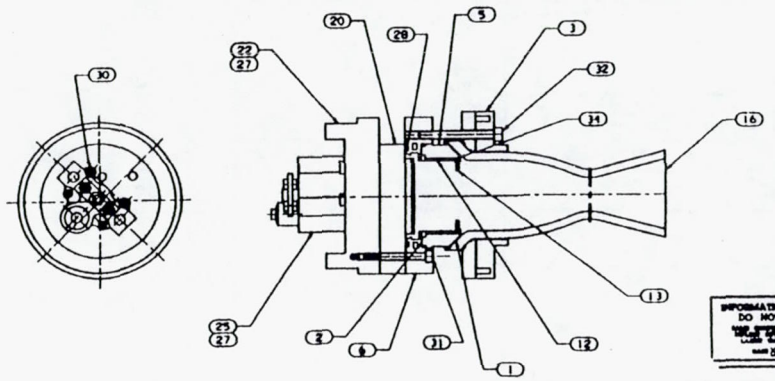

-19 ASSY

3	3		28700-90F -1	SCREW		14
8	-		20097-1F -28	SCREW		13
	8		20097-1F -24	SCREW		12
7	7		20097-08C -22	SCREW		11
4	4		20097-04C -A	SCREW		10
						29
1	1		2-140	SEAL	PARKER	28
4	4		AR10304 -012A0	SEAL		27
						26
1	1			VALVE	MOOG	25
						24
						23
1	1		A-5364-030	ADAPTER, VALVE		22
						21
1	1		1208178-9	INJECTOR		20
						19
			1208177-3	CHAMBER		18
1	1		1208177-2	CHAMBER		17
			1208177-1	CHAMBER		16
			1208176-3	TRIP		15
1	1		1208176-2	TRIP		14
			1208176-1	TRIP		13
1			1208174-3	HOUSING, TRIP		12
	1		1208174-2	HOUSING, TRIP		11
			1208174-1	HOUSING, TRIP		10
						9
						8
						7
1	1		1207296-9	ADAPTER		6
1			1207294-2	RING		5
	1		1207294-1	RING		4
1	1		1199065-9	CLAMP		3
1	1		-2	SEAL	GRAFOIL	2
2	2		-1	SEAL	GRAFOIL	1
QTY -19	QTY -9	ZONE	PART OR IDENTIFYING NO.	NOMENCLATURE OR DESCRIPTION	MATERIAL	ITEM

DEVELOPMENT HARDWARE
FOR TEST OR EXPERIMENTATION

INFORMATION PRINT ONLY
DO NOT FABRICATE

KNIGHT

ENGINE, HIPC

E 05824 1208175

1208175

Figure 9. HIPC Engine

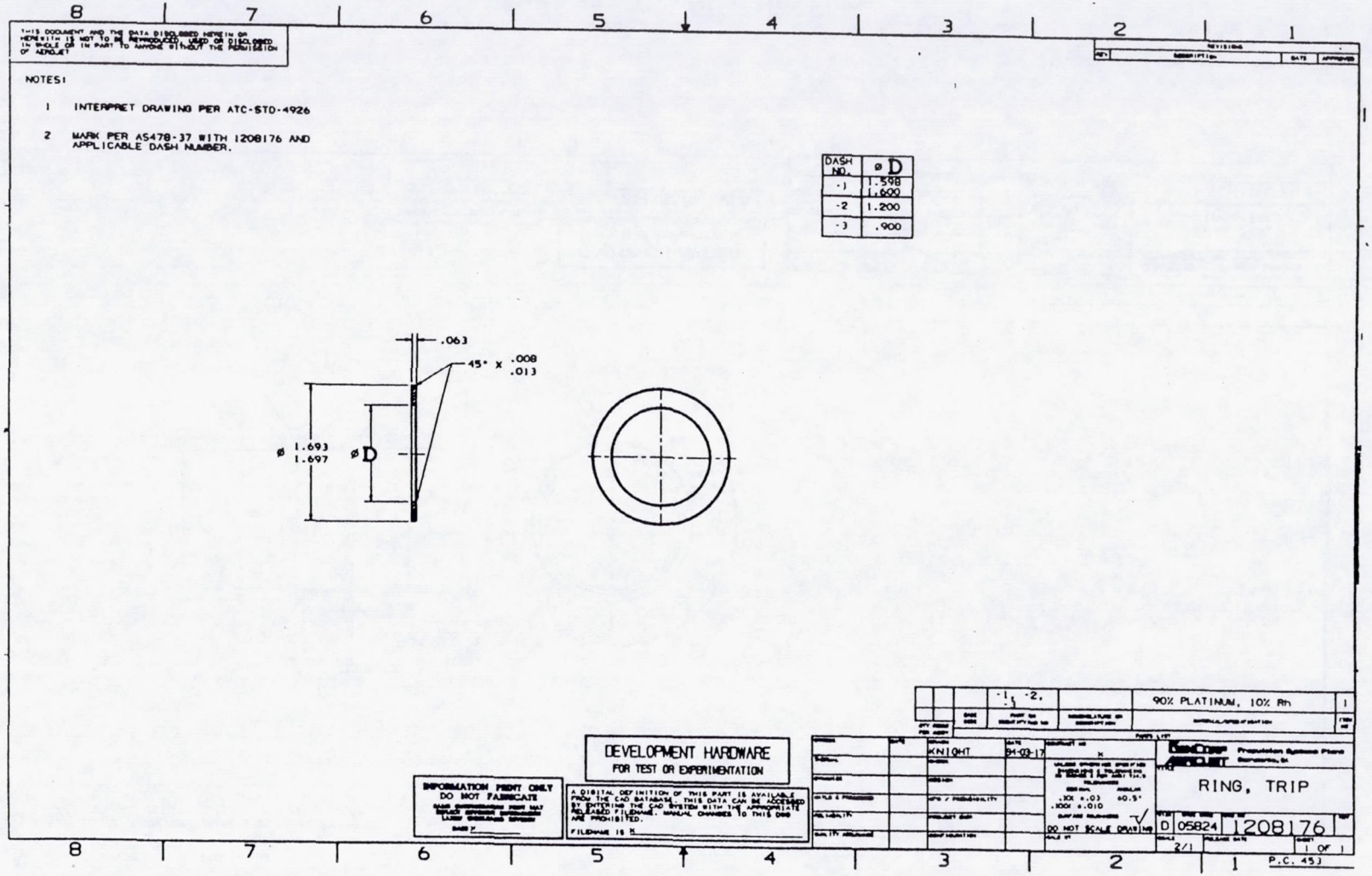

Figure 10. Trip Ring

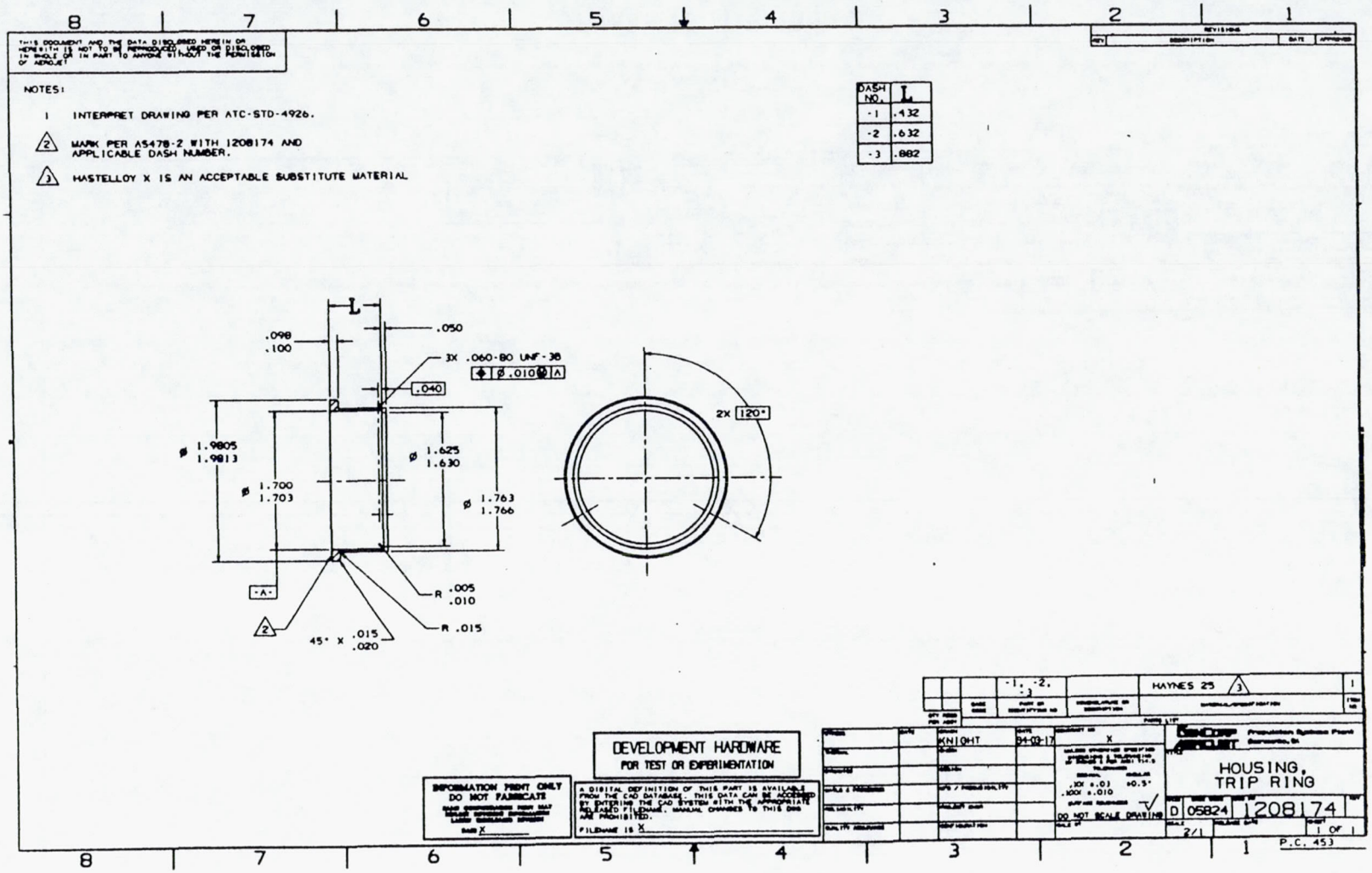

Figure 11. Trip Ring Housing

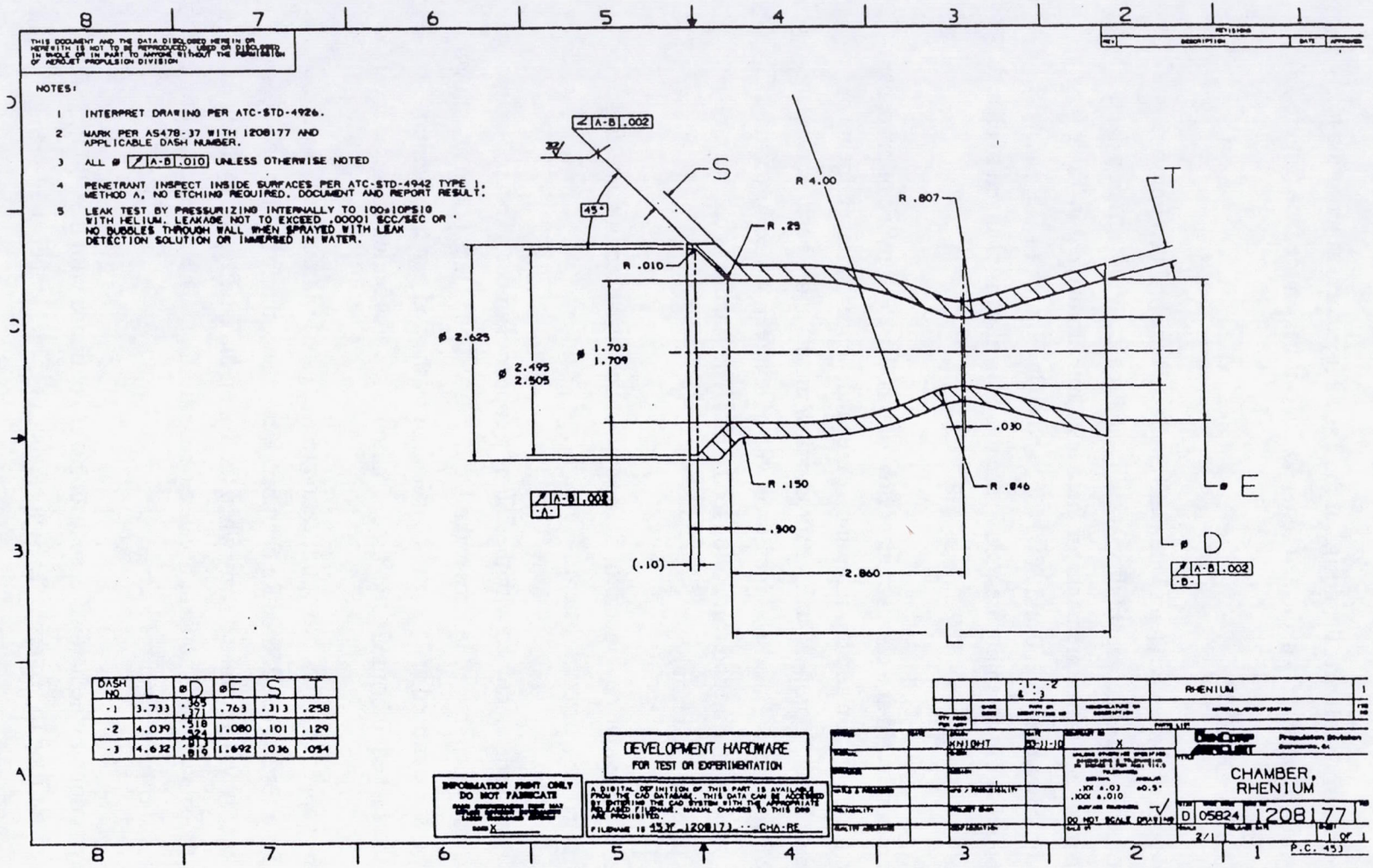

DASH NO	L	ØD	ØE	S	T
-1	3.733	.505 .371	.763	.313	.258
-2	4.039	.518 .524	1.080	.101	.129
-3	4.632	.813 .819	1.692	.036	.054

Figure 12. Rhenium Chamber

3.3, Rocket Testbed Fabrication (cont.)

In addition to the trip hardware, the design of the Task 2 injector was modified to make a 20% FFC platelet injector with 24 dedicated film cooling orifices on the face (Figure 13).

3.4 ROCKET TESTBED TESTS

A total of 24 tests of the testbed hardware were conducted to obtain combustion efficiency, heat transfer, performance, compatibility, stability and spacecraft integration data. The configuration and performance measurements for these tests are summarized in Table 9. The three sets of testbed hardware, 100, 250 and 500 Pc are shown in Figures 14, 15, and 16. The same injector, adapter and trip assembly are used in each; the chamber is changed to change the operating pressure.

The tests were conducted at a constant mass flow of $0.300 \pm 2\%$ lbm/sec of propellant while varying hardware configuration and mixture ratio. Three independent measurements of propellant flow were made for each propellant: two turbine flow meters and a positive displacement flow meter (PDFM) in series. Thrust was measured with a flexure mounted force stand using redundant strain gage measuring and calibration load cells. The stand was calibrated by direct force application prior to each firing.

A small, fast-acting valve developed for SDIO application was used in the testing. This valve is shown mounted on a divert thruster in Figure 17.

The first 12 tests were conducted with the 250 psia copper chamber. Their objective was to optimize trip geometry (height and length) and mixture ratio. The values tested are shown in Table 9. Test time was standardized at 15 sec since calculations showed that the rhenium chambers would reach thermal equilibrium in this time. These tests were conducted at sea level.

Following the copper chamber trip optimization tests, Tests 113 through 124 were conducted at vacuum. Four tests of the 250 Pc Re chamber, were made, the first 3 for 15 sec and the last planned for 60 sec. It was terminated early when the 1/8 in. dia facility line to the fuel inlet manifold pressure transducer (PFJ) popped, because of overheating. The appearance of the chamber at equilibrium is shown in Figure 18.

No damage was done to the hardware, so testing was continued with the 100 Pc Ir-Re chamber, which was fired for four 15-sec tests. The appearance of this chamber at 14 sec is

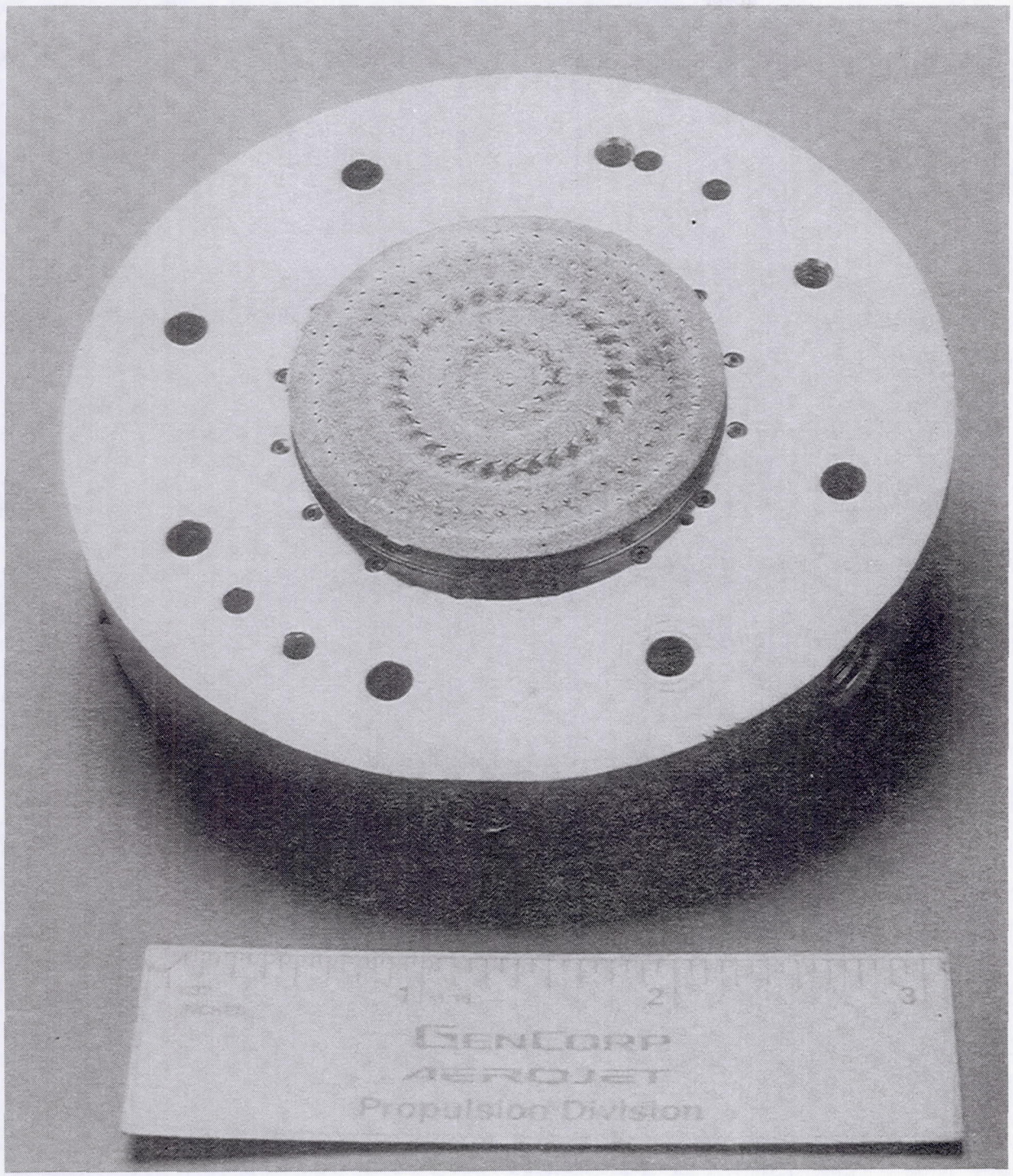

C1094 3515

Figure 13. Injector S/N 007, Post Test-124

Table 9. Our Actual Test Program

HIPC289 FINAL TEST DATA

9-27-94 HIGH Pc TASK 4 TESTING

UPDATE 10-27-94

TESTBED DATA: CONFIGURATION AND PERFORMANCE MEASUREMENTS

C* CORRECTED FOR TOTAL PRESSURE AND HOT THROAT DIAMETER

TEST No.	TESTBED CONFIGURATION Ht in.	Lt in.	Matl.	COLD Dt IN.	AREA RATIO, e Ae/At	FIRING TIME sec	DATA TIME sec	MR O/F	PC-1 psia	Pt psia	Wt lbm/sec	TESTED NOZZLE Is vac sec	AEROJET PROJECTED AT TEST MR (95% Bell, 140F fuel) (e=300:1) Is vac sec	AEROJET PROJECTED AT OPTIM. MR (e=300:1) Is vac sec	AEROJET PROJECTED AT TEST MR COMBUST. EFFIC.	C* ft/sec	TESTED NOZZLE Cf vac –	COMMENT
101	0.25	0.75	Cu	0.519	1.68	0.5												
102	0.25	0.75	Cu	0.519	1.68	15.0	14.4	0.84	248	246	0.298	241	329	333	0.959	5656	1.371	Corr. for F offset at FS-2
103	0.25	0.75	Cu	0.519	1.68	14.8	14.3	0.79	245	243	0.298	241	327	333	0.963	5593	1.385	
104	0.25	0.75	Cu	0.519	1.68	15.0	14.4	0.91	247	245	0.300	241	330	332	0.952	5604	1.383	
105	0.25	0.75	Cu	0.519	1.68	15.0	14.4	0.72	246	244	0.302	238	322	332	0.961	5547	1.382	
106	0.25	0.75	Cu	0.519	1.68	15.0	14.4	1.00	249	246	0.300	241	332	333	0.946	5631	1.378	
107	0.40	0.75	Cu	0.520	1.67	15.0	14.4	0.80	247	245	0.297	239	324	330	0.954	5613	1.367	
108	0.40	0.75	Cu	0.520	1.67	15.0	14.4	0.90	250	248	0.301	241	330	333	0.954	5678	1.365	Valve leak: ignition pop
109	0.40	0.75	Cu	0.521	1.66	15.0	14.4	0.71	247	244	0.302	237	320	331	0.958	5594	1.364	
110	0.40	0.75	Cu	0.521	1.66	15.0	14.4	0.77	247	245	0.300	238	323	330	0.955	5636	1.359	
111	0.25	0.30	Cu	0.521	1.66	15.0	14.4	0.81	248	246	0.303	239	325	330	0.953	5616	1.367	
112	0.25	0.30	Cu	0.521	1.66	15.0	14.4	0.97	248	246	0.299	241	331	332	0.946	5668	1.366	
113	0.25	0.75	Re	0.521	3.11	15.0	14.4	0.72	242	240	0.301	266	323	333	0.964	5626	1.521	
114	0.25	0.75	Re	0.522	3.10	15.0	14.4	0.83	247	244	0.304	269	329	333	0.960	5707	1.514	
115	0.25	0.75	Re	0.522	3.10	15.0	14.4	0.87	242	240	0.299	268	328	332	0.953	5691	1.515	
116	0.25	0.75	Re	0.522	3.10	46.8	14.5	0.85	245	242	0.302	268	328	332	0.956	5694	1.515	F offset, POJ leak, PFJ line break
117	0.25	0.75	Ir-Re	0.833	18.3	15.0	14.4	0.70	97.0	90.5	0.291	290	318	327	0.953	5594	1.669	Miniskit chamber
118	0.25	0.75	Ir-Re	0.833	18.3	15.0	14.4	0.87	100	93.7	0.299	295	324	326	0.942	5649	1.677	
119	0.25	0.75	Ir-Re	0.833	18.3	15.0	14.4	0.97	101	93.8	0.298	296	326	327	0.933	5677	1.676	
120	0.25	0.75	Ir-Re	0.833	18.3	15.0	14.4	1.08	100	93.6	0.300	295	326	327	0.921	5643	1.680	
121	0.25	0.75	Cu	0.367	1.68	0.5												
122	0.25	0.75	Cu	0.367	1.68	15.0	14.4	0.76	505	504	0.304							Not corrected for leakage
123	0.25	0.75	Cu	0.367	1.68	15.0	14.4	0.84	501	500	0.302							Not corrected for leakage
124	0.25	0.75	Cu	0.367	1.68	15.0	14.4	1.01	509	508	0.304							Not corrected for leakage

TOTAL FIRING TIME= 363 sec

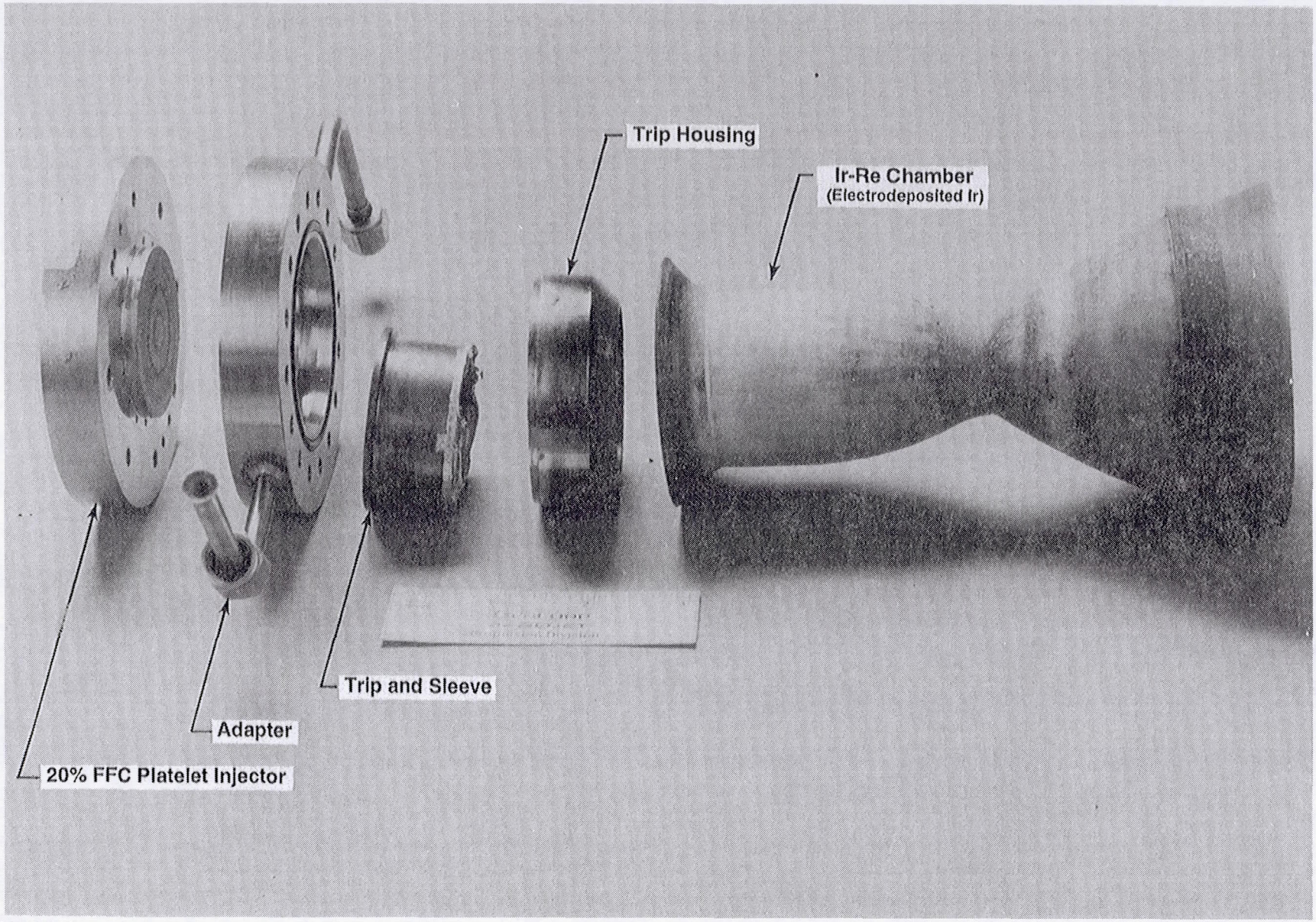

C1094 3519

Figure 14. 100 psia Chamber Pressure Testbed

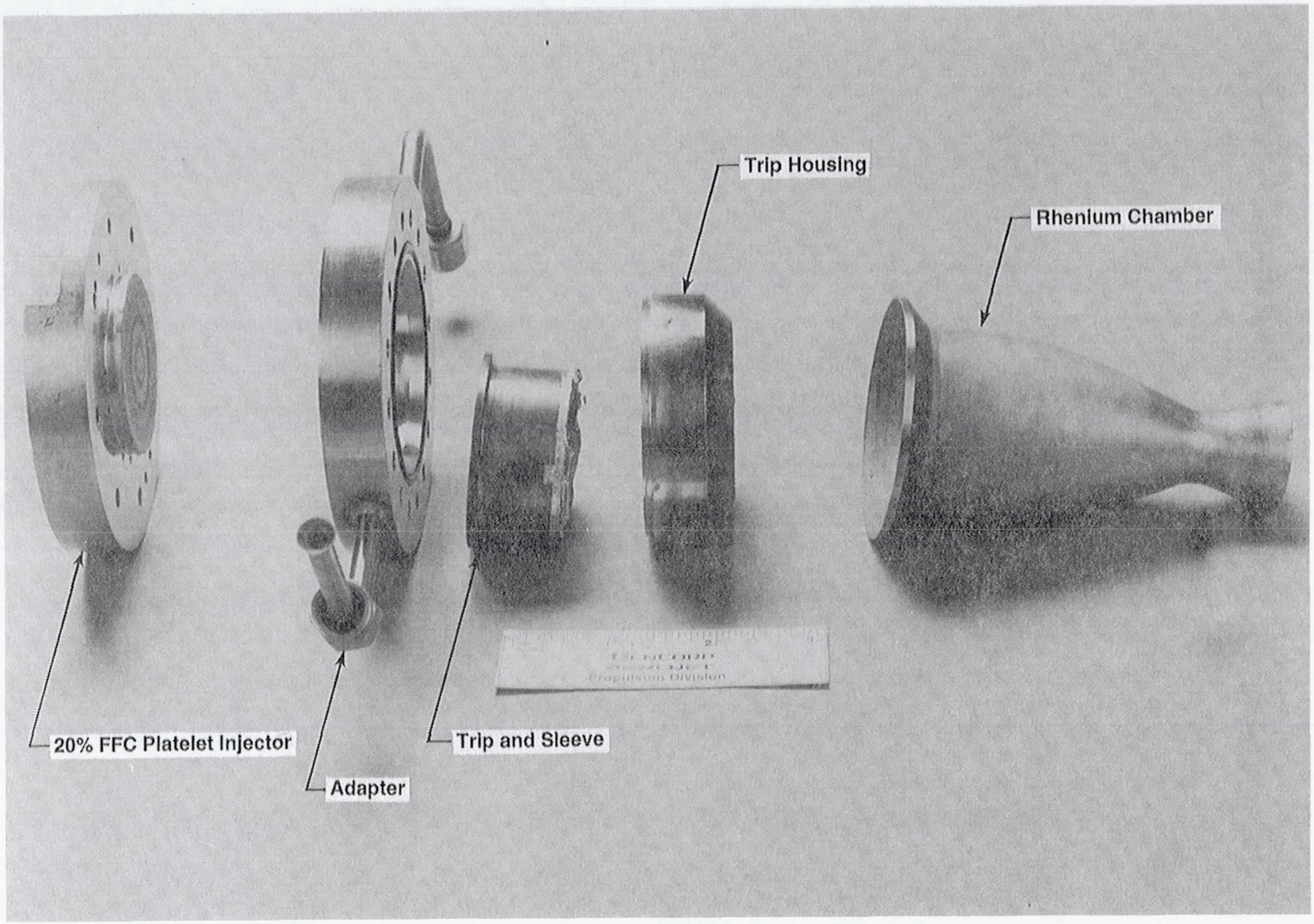

C1094 3520

Figure 15. 250 psia Chamber Pressure Testbed

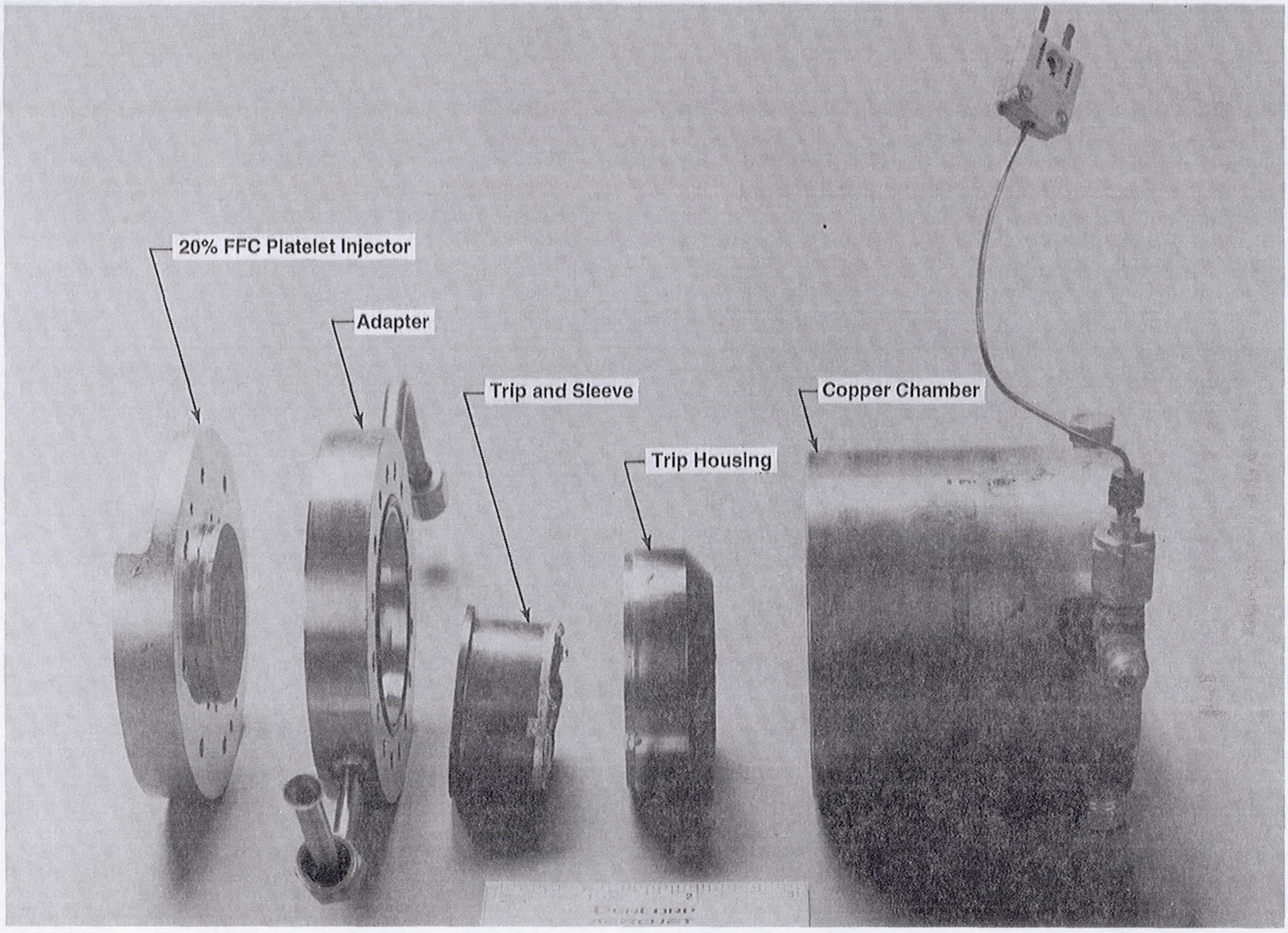

C1094 3518

Figure 16. 500 psia Testbed

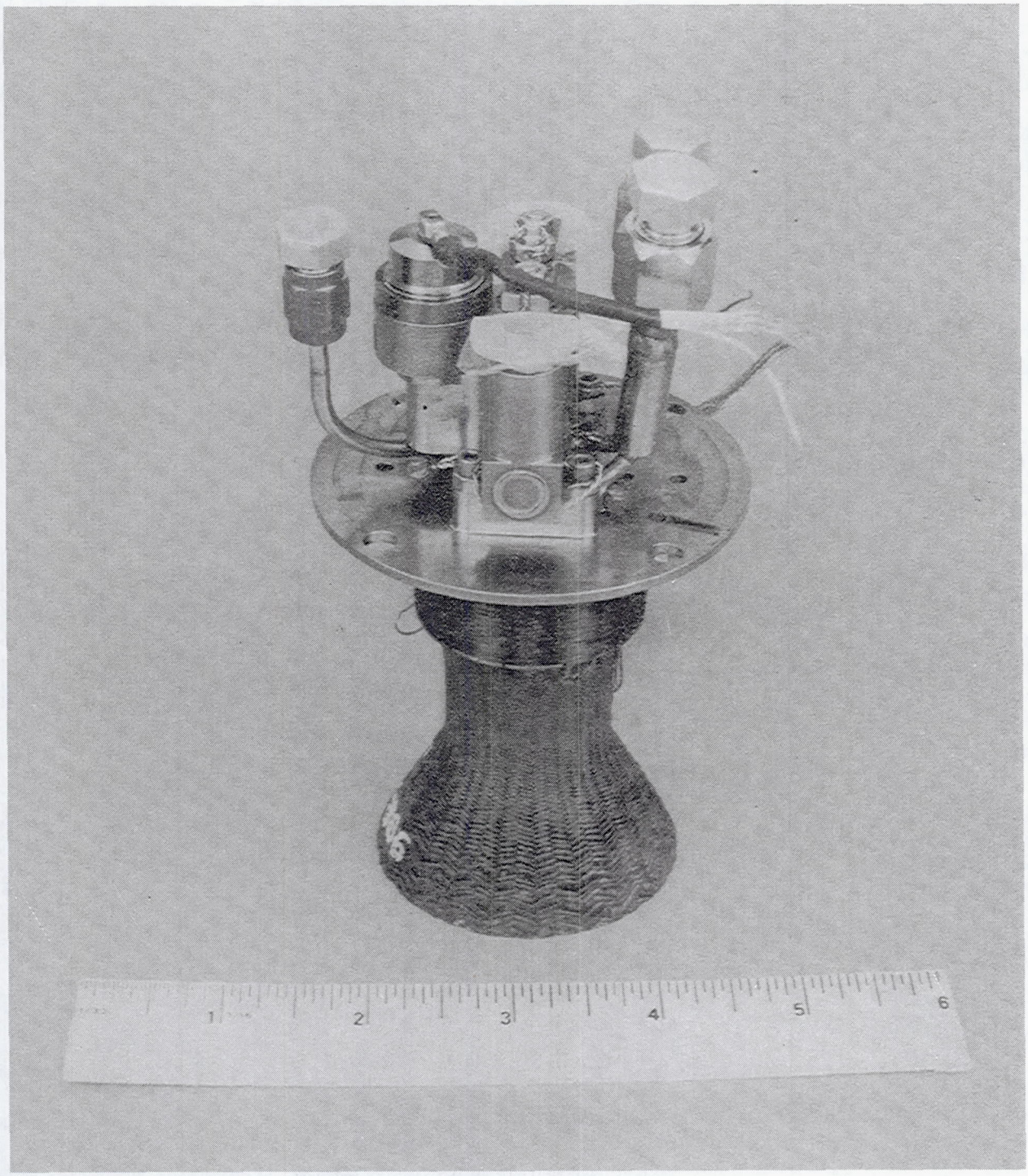

C0492 2106

Figure 17. Light Weight SDI Pilot Operated Bipropellant Valve Was Used in Task 2 and Task 4 Testing

C1094 3389

Figure 18. 250 psia Testbed at 24 sec – Test-116

shown in Figure 19. These tests were followed by four tests at 500 psia of the copper chamber. Leakage at Grafoil seals on the 500 psi chamber invalidated the performance data for these tests.

The Pt-Rh trip was intact but badly worn at the end of the test series. To reduce cost, the trip was made in two pieces, a Pt-Rh "washer" and a Haynes 25 sleeve with a downstream step to retain the washer. The step overheated and gradually reacted with the platinum, forming a low melting point alloy. In subsequent hardware the trip assembly will be a single piece of Pt-Rh.

3.4.2 Test Data

The measurement types made during the testing and the form of data presentation are shown in Table 10. The instrumentation used in the test program are listed in Table 11. The data were output in several forms. Immediately after each test an oscillograph record of time varying data was reviewed for anomalies (all of these data were also recorded on FM tape for later review at higher resolution). Digital data taken at 30,000 channels/sec were available in quick-look tabulations which gave direct instantaneous measurements of engineering units (EU) data and time-averaged values of directly measured and calculated parameters (performance summaries). These data were reviewed after each firing. The digital data were also transmitted to central data analysis where final EU, performance summaries and analog plots were prepared. In addition, abbreviated sets of PC-compatible EU and performance summary data were transmitted to the project to use in further analysis and correlation. Table 12 is a detailed description of the data presented in the performance summary.

The abbreviated EU and the performance summary data listings are presented in Appendix C and are available on floppy discs. The analog plots of the data are included in Appendix C as well. Video coverage of each firing is also available.

The high frequency test data indicated in Table 13 were analyzed by playing the FM tape through a FFT analyzer to obtain spectral density plots. These provide amplitude/frequency measurements and would clearly indicate if unstable operation is occurring. None was observed. The spectral plots are given in Appendix C.

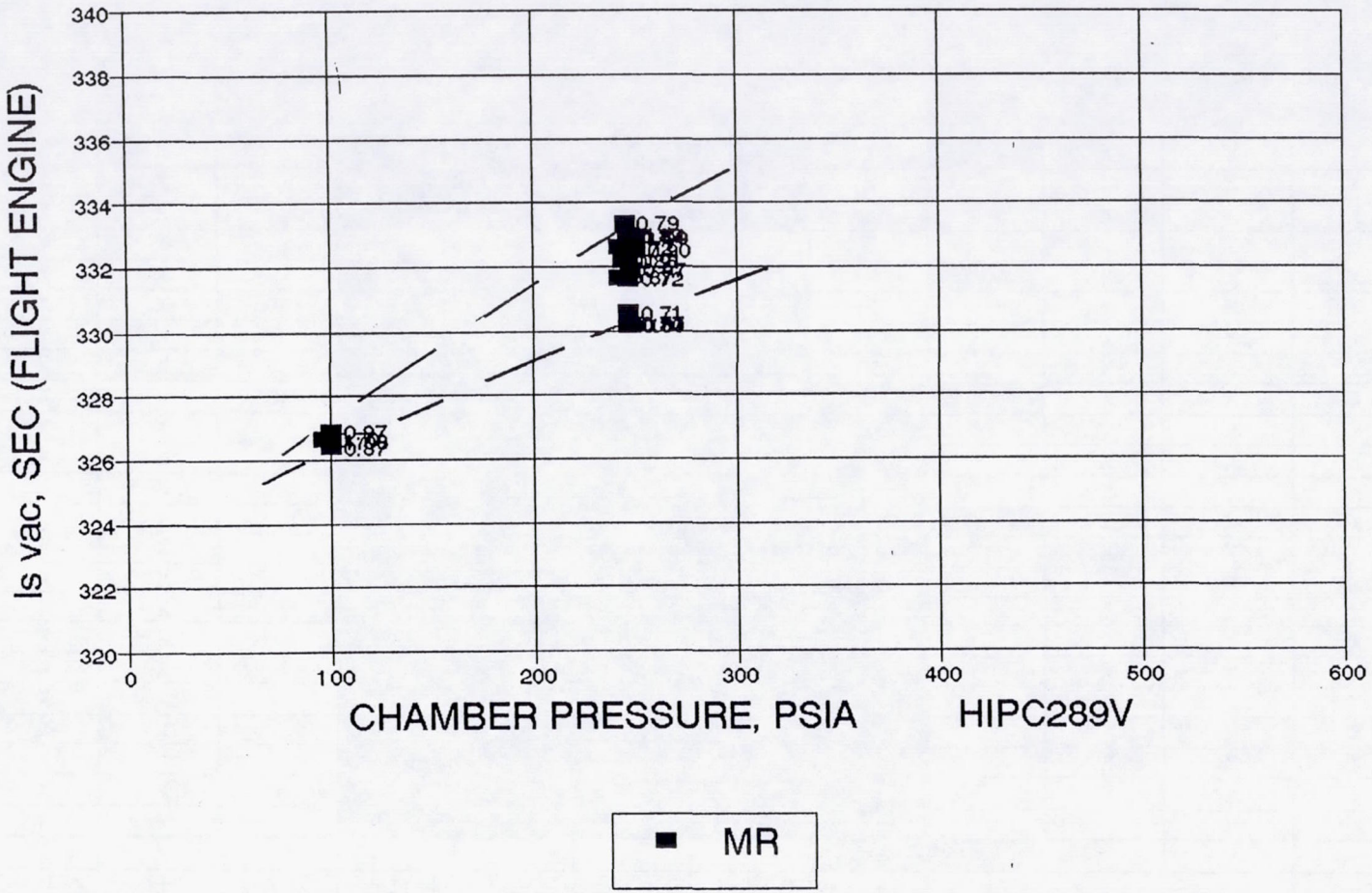

Figure 19. Flight Specific Impulse vs. Pc – e = 300:1, Tf 140 °F

Table 10. HIPC Task 4.0 Test – Data Status

HIPC285
10-27-94

X = AVAILABLE =COMPLETED =COPY TO NASA

TEST	A-AREA ENG UNIT	A-AREA PERF	A-AREA PLOTS	3308 ENG UNIT	3308 PERF	3308 PLOTS	3308 T-FILES	TEST VIDEO	PHOTOS	DATA CORRELLATION			
										STABIL.	COMB. EFF	THERMAL	PERFORM
101	X	X						X	X				
102	X	X		X	X	X	X	X			X	X	X
103	X	X	X	X	X	X	X	X		X	X	X	X
104	X	X		X	X	X	X	X		X	X	X	X
105	X	X		X	X	X	X	X		X	X	X	X
106	X	X		X	X	X	X	X		X	X	X	X
107	X	X		X	X	X	X	X		X	X	X	X
108	X	X		X	X	X	X	X			X	X	X
109	X	X		X	X	X	X	X			X	X	X
110	X	X		X	X	X	X	X			X	X	X
111	X	X		X	X	X	X	X		X	X	X	X
112	X	X		X	X	X	X	X	X		X	X	X
113	X	X		X	X	X	X	X		X	X	X	X
114	X	X		X	X	X	X	X		X	X	X	X
115	X	X		X	X	X	X	X		X	X	X	X
116	X	X	X	X	X	X	X	X	X	X	X	X	X
117	X	X		X	X	X	X	X		X	X	X	X
118	X	X		X	X	X	X	X		X	X	X	X
119	X	X		X	X	X	X	X		X	X	X	X
120	X	X		X	X	X	X	X	X	X	X	X	X
121	X	X											
122	X	X		X	X	X	X	X		X	X	X	X
123	X	X		X	X	X	X	X		X	X	X	X
124	X	X		X	X	X	X	X	X	X	X	X	X

Table 11. 100# Bay 2 Instrumentation List – HIPC Task 4

FUNCTION	PARAMETER	SYMBOL	RANGE	TRANSDUCER	DIGITAL	O-GR.	VIS.	FM TAPE
THRUSTER PERFORM.	THRUST A	FA	0-200 lbf	STRAIN GAGE	X	X	X	
	THRUST B	FB	0-200 lbf	STRAIN GAGE	X	X		
	THRUST CAL A	FCAL-A	0-200 lbf	STRAIN GAGE	X	X		
	THRUST CAL B	FCAL-B	0-200 lbf	STRAIN GAGE	X	X		
	CHAMB. PRESS 1 (RES. CAV.)	PC-1	0-750 psia	TABOR 206	X	X	X	X
	OXID FLOW 1	FMO-1	0.09-0.12 lbw/sec	TURBINE	X	X		
	OXID FLOW 2	FMO-2	0.09-0.12 lbw/sec	TURBINE	X	X		
	FUEL FLOW 1	FMF-1	0.12-0.16 lbw/sec	TURBINE	X	X		
	FUEL FLOW 2	FMF-2	0.12-0.16 lbw/sec	TURBINE	X	X		
	WATER FLOW 1 (TRIP FLNG.)	FMTW-1	0.20-0.30 lbw/sec	TURBINE	X	X		
	WATER FLOW 2 (TRIP FLNG.)	FMTW-2	0.20-0.30 lbw/sec	TURBINE	X	X		
	WATER FLOW 3 (Cu NOZZLE)	FMNW-1	0.20-0.30 lbw/sec	TURBINE	X	X		
	WATER FLOW 4 (Cu NOZZLE)	FMNW-2	0.20-0.30 lbw/sec	TURBINE	X	X		
	OXID PDFM POSITION	LOPDFM						
	FUEL PDFM POSITION	LFPDFM						
	OXID. VALVE INLET PRESS.	POVI	0-1000 psia	TABOR 206	X	X		
	FUEL VALVE INLET PRESS.	PFVI	0-1000 psia	TABOR 206	X	X		
	OXID INJ. INLET PRESS.	POJ	0-1000 psia	TABOR 206	X	X		X
	FUEL INJ. INLET PRESS.	PFJ	0-1000 psia	TABOR 206	X	X		X
	H2 ORIFICE UP	PHU	0-500 psia	TABOR 206	X	X		X
	CELL PRESSURE	PVAC-1,-2	0-1 psia	TABOR 206	X	X		X
	VALVE VOLTAGE	VTVC	0-30 Vdc		X	X		
THRUSTER TEMPERATURE	INJECTOR BODY	TJB-1,-2,-3	0-500oF	TYPE K	X			
	TRIP FLANGE BODY	TTFB-1,-2,-3	0-500oF	TYPE K	X			
	TRIP HOUSING	TH-1 THRU -6	0-2500oF	TYPE K 0.020 dia				
	COPPER NOZZLE TEMP.	TCN-1	0-200oF	TYPE K	X			
	COOLANT INLET TEMP (Cu N	TNWI	0-100oF	TYPE K	X			
	COOLANT OUTLET TEMP (Cu	TNWO	0-200oF	TYPE K	X			
	Re CHAMBER WALL T1	TC-1	40-4200oF	TYPE C (W5/Re	X		X	
	Re CHAMBER WALL T2	TC-2	40-4200oF	TYPE C (W5/Re	X		X	
	Re CHAMBER WALL T3	TC-3	40-4200oF	TYPE C (W5/Re	X		X	
	Re CHAMBER WALL T4	TC-4	40-4200oF	TYPE C (W5/Re	X			
	Re CHAMBER WALL T5	TC-5	40-4200oF	TYPE C (W5/Re	X			
	Re CHAMBER WALL T6	TC-6	40-4200oF	TYPE C (W5/Re	X			
	OXID INLET TEMP	TOV	40-100oF	TYPE K	X			
	FUEL INLET TEMP	TFV	40-250oF	TYPE K	X			
	TRIP FLANGE INLET WATER	TTWI	40-100oF	TYPE K	X		X	
	TRIP FLANGE OUTLET WATE	TTWO	40-250oF	TYPE K	X		X	
	Re CHAMBER HOT SPOT	PYROHI	to 4200F					
OPTICAL	OPTICAL MULTICH. ANAL.	EOMA	NOT USED					
STABILITY	CAVITY HIGH FREQ.	PHF-1	500-15000Hz	KISTLER		X		X
	CHAMBER HIGH FREQ.	PHF-2	500-15000Hz	PCB 122A		X		X
FACILITY PRESSURES	OXID TANK	POTS	0-1000 psia	TABOR 206	X		X	
	FUEL TANK	PFTS	0-1000 psia	TABOR 206	X		X	
	OXID LINE	POL-1	0-1000 psia	TABOR 206	X		X	
	FUEL LINE	PFL-1	0-1000 psia	TABOR 206	X		X	
	He BLEED ORIF.	PHE	0-1500 psia	TABOR 206	X		X	
	He VALVE ACT. +A/R	PVHE	0-1500 psia	TABOR 206	X		X	
FACILITY TEMPERATURES	OXID LINE	TOFM	40-100oF	TYPE K	X		X	
	FUEL LINE	TFFM	40-100oF	TYPE K	X		X	
	TEST CELL	TCELL	0-250oF	TYPE K	X		X	
	VALVE BODY TEMP. +A/R	TVB	40-500oF	TYPE K	X			

Table 12. Definition of Performance Summary Tabulations

The performance summaries (Job #14) are measured and calculated test parameters averaged over a stated time interval.
The heading provides comments on configuration and any special data processing applied.
The file under which the data are archived is listed, as are the test number, test date, clock time (24 hour) and test duration.
The date and time of printing of the computer output are listed in the upper right corner.
Data for two half-sec tests (-101 and -120) are omitted.

LINE No.	PARAMETER	UNITS	DEFINITION
	RUN.DATA-PT		This column heading has as its first three digits the test number; the last digits are the time interval sequence
0	START TIME	SEC	Time for start of data average
1	STOP TIME	SEC	Time for end of data average
2	TIME OF DAY	HR.SEC	Clock time (24 hour)
4	FMO-1	LBM/SEC [W]	Oxidizer flow meter #1, water flow equivalent
5	FMO-2	LBM/SEC [W]	Oxidizer flow meter #2, water flow equivalent
6	FMF-1	LBM/SEC [W]	Fuel flow meter #1, water flow equivalent
7	FMF-2	LBM/SEC [W]	Fuel flow meter #2, water flow equivalent
8	FMNW-1	LBM/SEC [W]	Copper nozzle flow meter #1, water flow equivalent
9	POTR	PSIA	Oxidizer regulator pressure
10	PFTR	PSIA	Fuel regulator pressure
11	FMNW-2	LBM/SEC [W]	Copper nozzle flow meter #2, water flow equivalent
12	POVI	PSIA	Thruster valve oxidizer inlet static pressure
15	PC-1	PSIA	Chamber static pressure
16	PFVI	PSIA	Thruster valve fuel inlet static pressure
17	POJ	PSIA	Injector oxidizer manifold inlet static pressure
18	PFJ	PSIA	Injector fuel manifold inlet static pressure
19	FCAL-A	LBF	Force stand calibration load cell, "A" bridge output
20	FCAL-B	LBF	Force stand calibration load cell, "B" bridge output

Table 12. Definition of Performance Summary Tabulations (cont.)

21	FA	LBF	Force stand measurement load cell, "A" bridge output
22	FB	LBF	Force stand measurement load cell, "B" bridge output
27	POL-1	PSIA	Oxidizer line pressure
29	PHE	PSIA	Helium supply pressure to helium bleed PCB high frequency transducer (in chamber)
30	TJB-3	DEG F	Injector body (exterior) temperature
31	TCN-1	DEG F	Copper chamber/nozzle exterior temperature
35	TCELL	DEG F	Test chamber ambient temperature
38	TC-4	DEG F	TC-4 is a tungsten 5%Re/tungsten 26%Re thermocouple on rhenium chamber 0.5 in. upstream o
39	TC-5	DEG F	TC-5 is a tungsten 5%Re/tungsten 26%Re thermocouple on rhenium chamber at throat
40	TC-6	DEG F	TC-6 is a tungsten 5%Re/tungsten 26%Re thermocouple on rhenium chamber 0.5 in. downstrea
46	TC-1	DEG F	TC-1 is a tungsten 5%Re/tungsten 26%Re thermocouple on rhenium chamber 1.5 in. upstream o
47	TC-2	DEG F	TC-2 is a tungsten 5%Re/tungsten 26%Re thermocouple on rhenium chamber 1.0 in. upstream o
48	TC-3	DEG F	TC-3 is a tungsten 5%Re/tungsten 26%Re thermocouple on rhenium chamber 0.75 in. upstream
50	TOV	DEG F	Temperature of the oxidizer at the valve
52	WOPDFM	LBM/SEC [P]	Oxidizer propellant flow rate measured by Positive Displacement Flowmeter (PDFM)
53	WFPDFM	LBM/SEC [P]	Fuel propellant flow rate measured by Positive Displacement Flowmeter (PDFM)
54	POTS	PSIA	Oxidizer storage tank pressure
55	PFL	PSIA	Fuel line pressure
56	VTCV	VOLTS	Valve actuation voltage
57	TFVI	DEG F	Fuel temperature at valve inlet
58	WOPDFM	LBM [W]	Oxidizer PDFM total displacement, pounds of water
59	WFPDFM	LBM [W]	Fuel PDFM total displacement, pounds of water
68	TJB-1	DEG F	Injector body temperature at 0 deg
69	TJB-2	DEG F	Injector body temperature at 120 deg
73	FMTW-1	LBM/SEC [W]	Front end heat flux sensor water flow, meter #1
74	FMTW-2	LBM/SEC [W]	Front end heat flux sensor water flow, meter #2
75	PHU	PSIA	Hydrogen shroud metering orifice inlet pressure
76	PVHE	PSIA	MOOG propellant valve actuation helium pressure
77	TOFM	DEG F	Temperature of oxidizer at flowmeters
78	TFFM	DEG F	Temperature of fuel at flowmeters
79	TTFB-1	DEG F	Temperature of trip housing outer ring, at 0 deg
80	TNWI	DEG F	Inlet temperature of nozzle cooling water (copper chamber)

Table 12. Definition of Performance Summary Tabulations (cont.)

81	TNWO	DEG F	Outlet temperature of nozzle cooling water (copper chamber)
82	TTWI	DEG F	Front end heat flux sensor water temperature in
83	TTWO	DEG F	Front end heat flux sensor water temperature out
84	TH-1	DEG F	Trip sleeve temperature, throat end, 0 deg
85	TH-2	DEG F	Trip sleeve temperature, injector end, 0 deg
86	TH-3	DEG F	Trip sleeve temperature, throat end, 120 deg
87	TH-4	DEG F	Trip sleeve temperature, injector end, 120 deg
88	TH-5	DEG F	Trip sleeve temperature, throat end, 240 deg
89	TH-6	DEG F	Trip sleeve temperature, injector end, 240 deg
90	WO TURB FM	LBM/SEC [P]	Oxidizer flow rate based on turbine FM, propellant [instantaneous parameters, averaged]
91	WF TURB FM	LBM/SEC [P]	Fuel flow rate based on turbine FM, propellant [instantaneous parameters, averaged]
92	MR TURB FM	--	Mixture ratio, oxidizer flow rate/fuel flow rate [instantaneous MR, averaged]
93	FADJ	LBF	Thrust adjustment for thermal offset [run -102 only]
94	PVAC-2	PSIA	Test cell ambient pressure
95	PVAC-2	PSIA	Test cell ambient pressure
96	PYROHI	deg f	Two-color pyrometer reading 0.5 in. upstream of throat [set to grey body; min.=2563oF]
97	TTFB-2	DEG F	Temperature of trip housing outer ring, at 120 deg
98	TTFB-3	DEG F	Temperature of trip housing outer ring, at 240 deg
99	MIDPT	SEC	Midpoint of time interval over which data are averaged
100	AT	IN^2	Measured nozzle throat area [cold]
101	AE	IN^2	Measured nozzle exit area
102	PA	PSIA	Ambient test cell pressure
103	NO CONTENT	PERCENT	Nitric oxide concentration of oxidizer, percent [for SGO calcs.]
104	F ZERO	LBF	Pre-test zero offset of thrust measurement
105	WO	LBM/SEC [P]	Oxidizer flow rate based on turbine FM, propellant [calculated from averaged parameters]
106	WF	LBM/SEC [P]	Fuel flow rate based on turbine FM, propellant [calculated from averaged parameters]
107	WT	LBM/SEC [P]	Total propellant flow rate based on turbine FM, propellant [calculated from averaged parameters
108	MR	--	Mixture ratio, oxidizer flow rate/fuel flow rate [calculated from averaged parameters]
109	F SL	LBF	Measured thrust at cell conditions
110	F VAC	LBF	Vacuum thrust calculated for zero back pressure
111	ISP VAC	LBF-SEC/LBM	Vacuum specific impulse calculated from F vac, and total propellant flow, WT
112	C STAR	FT/SEC	Characteristic exhaust velocity, calculated from C*=(PC-1)*AT*g/WT

Table 12. Definition of Performance Summary Tabulations (cont.)

113	CF	--	Nozzle thrust coefficient, Cf=(ISP VAC)/C*
114	%DIFF F	PERCENT	Difference between redundant thrust load cell readings, FA-FB
115	%DIFF FMO	PERCENT	Difference between redundant oxidizer turbine flowmeter readings
116	%DIFF FMF	PERCENT	Difference between redundant fuel turbine flowmeter readings
119	%DIFF FMO PD	PERCENT	Difference between oxidizer PDFM and average of oxidizer turbine flowmeter readings
120	%DIFF FMF PD	PERCENT	Difference between fuel PDFM and average of fuel turbine flowmeter readings
121	SGO	GM/CM^3	Specific gravity of oxidizer at flowmeter temperature and pressure
122	SGF	GM/CM^3	Specific gravity of fuel at flowmeter temperature
123	SGOJ	GM/CM^3	Specific gravity of oxidizer at injector inlet temperature and pressure
124	SGFRI	GM/CM^3	Specific gravity of fuel at valve inlet temperature
125	SGFJ	GM/CM^3	Specific gravity of fuel at injector inlet temperature
126	AVSGF	GM/CM^3	Average specific gravity of fuel
127	AVSGO	GM/CM^3	Average specific gravity of oxidizer
129	ROVJ		Hydraulic resistance of oxidizer circuit, valve to injector
130	ROJ		Hydraulic resistance of oxidizer circuit, injector to chamber
132	RFRV		Hydraulic resistance of fuel circuit, system to valve
133	RFVJ		Hydraulic resistance of fuel circuit, valve to injector
134	RFJ		Hydraulic resistance of fuel circuit, injector to chamber
136	KOVJ		Hydraulic conductance of oxidizer circuit, valve to injector
137	KOJ		Hydraulic conductance of oxidizer circuit, injector to chamber
140	KFVJ		Hydraulic conductance of fuel circuit, valve to injector
141	KFJ		Hydraulic conductance of fuel circuit, injector to chamber
142	WO PD	LBM/SEC [P]	Oxidizer flow rate, based on PDFM
143	WF PD	LBM/SEC [P]	Fuel flow rate, based on PDFM
144	WT PD	LBM/SEC [P]	Total propellant flow rate, based on PDFM
145	MR PD	--	Mixture ratio, based on PDFM flows
146	ISP PD	LBF-SEC/LBM	Vacuum specific impulse, based on PDFM flows
147	CSTAR PD	FT/SEC	Characteristic exhaust velocity, based on PDFM flows
149	ROVJ PD		Hydraulic resistance of oxidizer circuit, valve to injector (PDFM)
150	ROJ PD		Hydraulic resistance of oxidizer circuit, injector to chamber(PDFM)
152	RFRV PD		Hydraulic resistance of fuel circuit, system to valve (PDFM)
153	RVFJ RD		Hydraulic resistance of fuel circuit, valve to injector (PDFM)

Table 12. Definition of Performance Summary Tabulations (cont.)

154	RFJ PD		Hydraulic resistance of fuel circuit, injector to chamber (PDFM)
156	KOVJ PD		Hydraulic conductance of oxidizer circuit, valve to injector (PDFM)
157	KOJ PD		Hydraulic conductance of oxidizer circuit, injector to chamber (PDFM)
160	KFVJ PD		Hydraulic conductance of fuel circuit, valve to injector (PDFM)
161	KFJ PD		Hydraulic conductance of fuel circuit, injector to chamber (PDFM)
162	POVIT	PSIA	Thruster valve oxidizer inlet static pressure
163	POJT	PSIA	Injector oxidizer manifold inlet static pressure
164	PFRIT	PSIA	
165	PFVIT	PSIA	Thruster valve fuel inlet static pressure
166	PFJT	PSIA	Injector fuel manifold inlet static pressure
173	WCOOL TRIP	LBM/SEC [W]	Front end heat flux sensor water flow rate
174	DT TRIP	DEG F	Front end heat flux sensor water temperature rise
175	QTW	BTU/SEC	Front end heat transfer
176	WCOOL NOZ	LBM/SEC [W]	Nozzle heat flux water flow rate
177	DT NOZ	DEG F	Nozzle heat flux water temperature rise
178	QNW	BTU/SEC	Nozzle heat transfer

Table 13. Tests Reduced for High Frequency Data

TEST	CONFIGURATION			FIRING										
	Ht	Lt		TIME	MR	Pc	FREQ	AMPLITUDE,	AMPLITUDE,	PERCENT				
	in.	in.	Matl.	sec	O/F	psia	CAVITY	VOLT	PSIA	Pc	CHAMBER			
101	0.25	0.75	Cu	0.51										
102	0.25	0.75	Cu	15.0	0.84	248								
103	0.25	0.75	Cu	14.8	0.79	245	13400	0.00177	0.354	0.144313	14600	0.0014	0.28	0.114146
104	0.25	0.75	Cu	15.0	0.91	247	14100	0.00182	0.364	0.147428				
105	0.25	0.75	Cu	15.0	0.72	246	12100	0.00171	0.342	0.138799				
106	0.25	0.75	Cu	15.0	1.00	249	12800	0.0017	0.34	0.136711				
107	0.40	0.75	Cu	15.0	0.80	247	12800	0.00188	0.376	0.152288	2830			
108	0.40	0.75	Cu	15.0	0.90	250	10900	0.00155	0.31	0.124				
109	0.40	0.75	Cu	15.0	0.71	247	13000	0.00163	0.326	0.132252				
110	0.40	0.75	Cu	15.0	0.77	247	12300	0.00177	0.354	0.14332				
111	0.25	0.30	Cu	15.0	0.81	248	13200	0.00197	0.394	0.158615				
112	0.25	0.30	Cu	15.0	0.97	248	13800	0.00204	0.408	0.164649				
113	0.25	0.75	Re	15.0	0.72	242	13500	0.00151	0.302	0.124639				
114	0.25	0.75	Re	15.0	0.83	247	11900	0.00145	0.29	0.117552				
115	0.25	0.75	Re	15.0	0.87	242	14400	0.00141	0.282	0.116529				
116	0.25	0.75	Re	@14 sec	0.85	245	13800	0.0018	0.36	0.147239				
117	0.25	0.75	Ir-Re	15.0	0.70	97	1100	0.00114	0.228	0.235124				
118	0.25	0.75	Ir-Re	15.0	0.87	100	2000	0.00137	0.274	0.272936				
119	0.25	0.75	Ir-Re	15.0	0.97	101	1100	0.0012	0.24	0.238806				
120	0.25	0.75	Ir-Re	15.0	1.08	100	2000	0.0014	0.28	0.279441				
122	0.25	0.75	Cu	15.0	0.76	505	14200	0.00258	0.516	0.102118	17100	0.00207	0.414	0.081932
123	0.25	0.75	Cu	15.0	0.84	501	29000	0.00316	0.632	0.126047	2000	0.0019	0.38	0.075788
124	0.25	0.75	Cu	15.0	1.01	509	17100	0.00207	0.414	0.081352	2100	0.00111	0.222	0.043624

3.4.3 Analysis

The major areas of analysis which supported the Basic program were:

- Combustion efficiency/performance prediction
- Heat transfer
- Compatibility
- Stability
- Spacecraft integration.

These analyses are described here. In each case the analysis results are tabulated for the individual tests along with the measured parameters pertinent to the analysis. The basic source for the measurements are the data given in Appendix C.

3.4.3.1 Combustion Efficiency/Performance

Combustion efficiency and thruster performance were obtained by direct thrust measurements. These performance data are shown in Table 14. C* data are also shown here although they depend upon estimating the total pressure loss in the chamber and the hot nozzle throat and are therefore subject to error. Use of C* to predict specific impulse is subject to further error in nozzle C_F, which is not an inherent property of the nozzle but is dependent on the conditions of the gas flow into and through it as well.

The measured thrust has been corrected to vacuum conditions. A simplified JANNAF performance analysis methodology was used to extrapolate the low area ratio measured thrust data to the 300:1 area ratio flight conditions. The performance losses (kinetics, divergence, boundary layer, mixing, and vaporization) and the maximum theoretical performance (ODE, or one dimensional equilibrium) were defined for both the test and flight conditions for each test point in order to generate this extrapolation. The kinetics, divergence and boundary layer losses can be analytically determined accurately and then used with the measured test specific impulse (Isp) to determine the combined mixing and vaporization loss for the test condition. The combined mixing and vaporization loss, or injector loss, was assumed to be independent of the nozzle area ratio, e.g., low area ratio test or high area ratio flight. Consequently, the injector

Table 14. High Pc Task 4 Final Test Data

UPDATE 10-27-94

TESTBED DATA: CONFIGURATION AND PERFORMANCE MEASUREMENTS

C* CORRECTED FOR TOTAL PRESSURE AND HOT THROAT DIAMETER

TEST No.	TESTBED CONFIGURATION Ht in.	Lt in.	Matl.	COLD Dt IN.	AREA RATIO, e Ae/At	FIRING TIME sec	DATA TIME sec	MR O/F	PC-1 psia	Pt psia	Wt lbm/sec	TESTED NOZZLE Is vac sec	AEROJET PROJECTED AT TEST MR (95% Bell, 140F fuel) (e=300:1) Is vac sec	AEROJET PROJECTED AT OPTIM. MR (e=300:1) Is vac sec	AEROJET PROJECTED AT TEST MR COMBUST. EFFIC.	C* ft/sec	TESTED NOZZLE Cf vac –	COMMENT
101	0.25	0.75	Cu	0.519	1.68	0.5												
102	0.25	0.75	Cu	0.519	1.68	15.0	14.4	0.84	248	246	0.298	241	329	333	0.959	5656	1.371	Corr. for F offset at FS-2
103	0.25	0.75	Cu	0.519	1.68	14.8	14.3	0.79	245	243	0.298	241	327	333	0.963	5593	1.385	
104	0.25	0.75	Cu	0.519	1.68	15.0	14.4	0.91	247	245	0.300	241	330	332	0.952	5604	1.383	
105	0.25	0.75	Cu	0.519	1.68	15.0	14.4	0.72	246	244	0.302	238	322	332	0.961	5547	1.382	
106	0.25	0.75	Cu	0.519	1.68	15.0	14.4	1.00	249	246	0.300	241	332	333	0.946	5631	1.378	
107	0.40	0.75	Cu	0.520	1.67	15.0	14.4	0.80	247	245	0.297	239	324	330	0.954	5613	1.367	
108	0.40	0.75	Cu	0.520	1.67	15.0	14.4	0.90	250	248	0.301	241	330	333	0.954	5678	1.365	Valve leak: ignition pop
109	0.40	0.75	Cu	0.521	1.66	15.0	14.4	0.71	247	244	0.302	237	320	331	0.958	5594	1.364	
110	0.40	0.75	Cu	0.521	1.66	15.0	14.4	0.77	247	245	0.300	238	323	330	0.955	5636	1.359	
111	0.25	0.30	Cu	0.521	1.66	15.0	14.4	0.81	248	246	0.303	239	325	330	0.953	5616	1.367	
112	0.25	0.30	Cu	0.521	1.66	15.0	14.4	0.97	248	246	0.299	241	331	332	0.946	5668	1.366	
113	0.25	0.75	Re	0.521	3.11	15.0	14.4	0.72	242	240	0.301	266	323	333	0.964	5626	1.521	
114	0.25	0.75	Re	0.522	3.10	15.0	14.4	0.83	247	244	0.304	269	329	333	0.960	5707	1.514	
115	0.25	0.75	Re	0.522	3.10	15.0	14.4	0.87	242	240	0.299	268	328	332	0.953	5691	1.515	
116	0.25	0.75	Re	0.522	3.10	46.8	14.5	0.85	245	242	0.302	268	328	332	0.956	5694	1.515	F offset, POJ leak, PFJ line break
117	0.25	0.75	Ir-Re	0.833	18.3	15.0	14.4	0.70	97.0	90.5	0.291	290	318	327	0.953	5594	1.669	Miniskit chamber
118	0.25	0.75	Ir-Re	0.833	18.3	15.0	14.4	0.87	100	93.7	0.299	295	324	326	0.942	5649	1.677	
119	0.25	0.75	Ir-Re	0.833	18.3	15.0	14.4	0.97	101	93.8	0.298	296	326	327	0.933	5677	1.676	
120	0.25	0.75	Ir-Re	0.833	18.3	15.0	14.4	1.08	100	93.6	0.300	295	326	327	0.921	5643	1.680	
121	0.25	0.75	Cu	0.367	1.68	0.5												
122	0.25	0.75	Cu	0.367	1.68	15.0	14.4	0.76	505	504	0.304							Not corrected for leakage
123	0.25	0.75	Cu	0.367	1.68	15.0	14.4	0.84	501	500	0.302							Not corrected for leakage
124	0.25	0.75	Cu	0.367	1.68	15.0	14.4	1.01	509	508	0.304							Not corrected for leakage

TOTAL FIRING TIME= 383 sec

loss determined from the low area ratio test data (adjusted for heated fuel) was then applied with the predicted kinetics, divergence and boundary layer losses for the high area ratio flight engine to the appropriate maximum theoretical performance to extrapolate to the flight conditions.

All of the test data were obtained with ambient temperature propellants, whereas an optimum flight engine could include preheating the fuel to aid its vaporization. Consequently, the injector loss for the optimum flight performance was adjusted to account for increased fuel vaporization with fuel heated to 140°F.

The trend of the extrapolated performance with mixture ratio suggested that the optimum mixture ratio for the 250 psia chamber pressure engine was higher than that observed through the test data. In order to determine this optimum point, the injector efficiencies determined from all the test data were correlated with mixture ratio in order to extrapolate the 250 psia chamber pressure injector efficiency to higher mixture ratios. The trends with mixture ratio for all the tested low area ratio engines were similar, suggesting that the extrapolation could be validly made. This extrapolated injector efficiency was then determined, together with the ODE Isp to predict the high area ratio flight performance at the higher mixture ratios.

Vacuum I_S at 300:1 is plotted versus chamber pressure in Figure 19. I_S increases 2% as chamber pressure is increased from 100 to 250 psia. This system's performance is very flat over the mixture ratio range studied, 0.7 to 1.08:1, as shown in Figure 20.

The measured performance is compared to theoretical performance as a function of Pc and MR in Figure 21, which shows ODE and ODK specific impulse. The loss terms involved in the steps from ODE to delivered performance are listed in Table 15; the effects of pressure on the loss mechanisms is summarized in Table 16. Overall Isp efficiency defined as (delivered I_S)/(ODE I_S), is plotted as a function of chamber pressure in Figure 22 and as a function of MR in Figure 23.

Trip height was varied in the early tests; two heights were tested, 0.25 and 0.40 inches. As shown in Figure 24, heights in this range did not appear to influence performance. Trip length was viewed as well, at 0.3 and 0.75 in. An increment of about 1% was measured over this range of trip length increase, as shown in Figure 25.

Characteristic exhaust velocity increased less than 1% in going from 100 to 250 psia Pc, as shown in Figure 26.

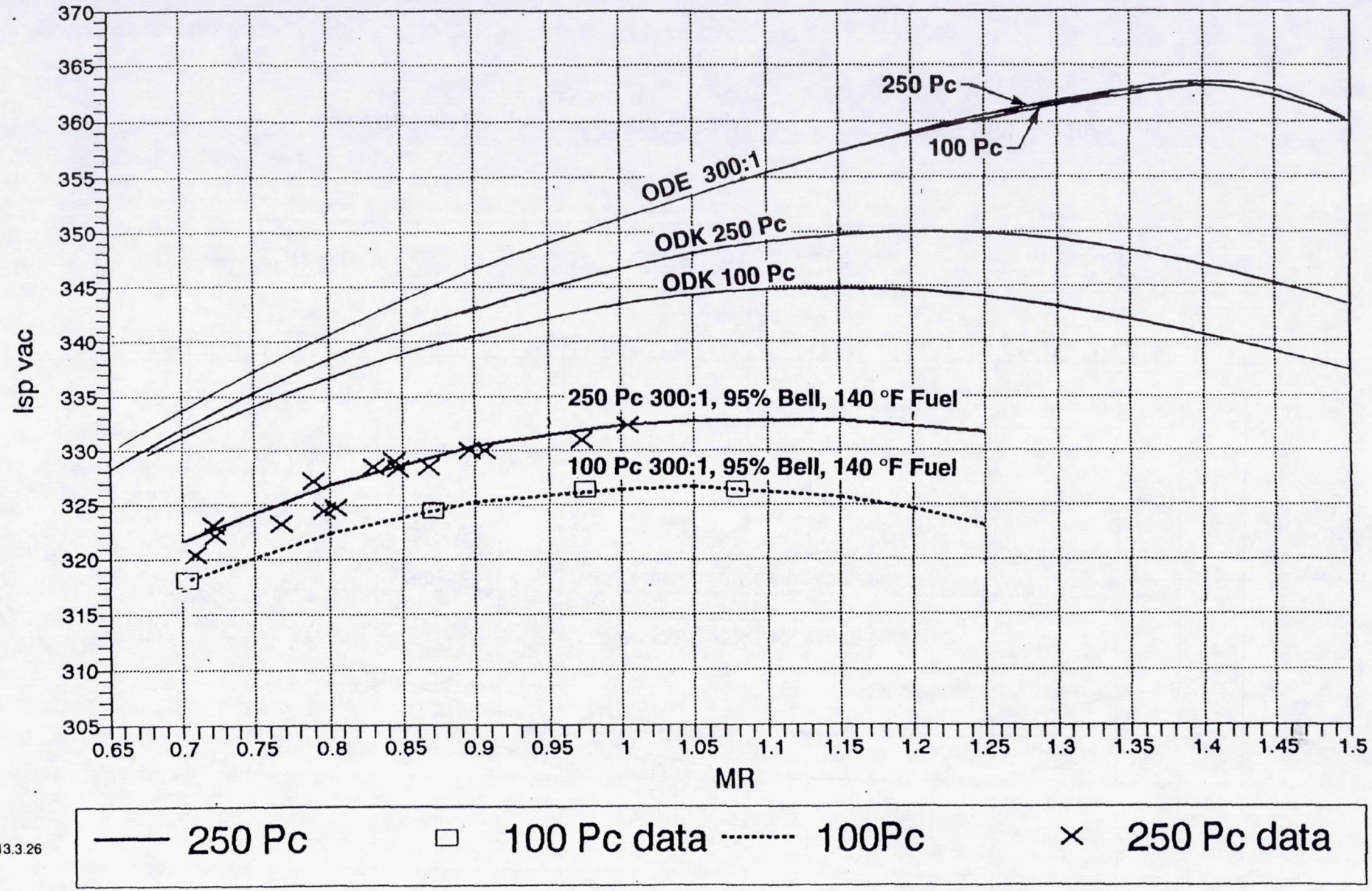

1.13.3.26

Figure 20. Cu and Re Chamber Data Extrapolated to 300:1, 95% Bell Nozzle, 140 °F Fuel Temperature

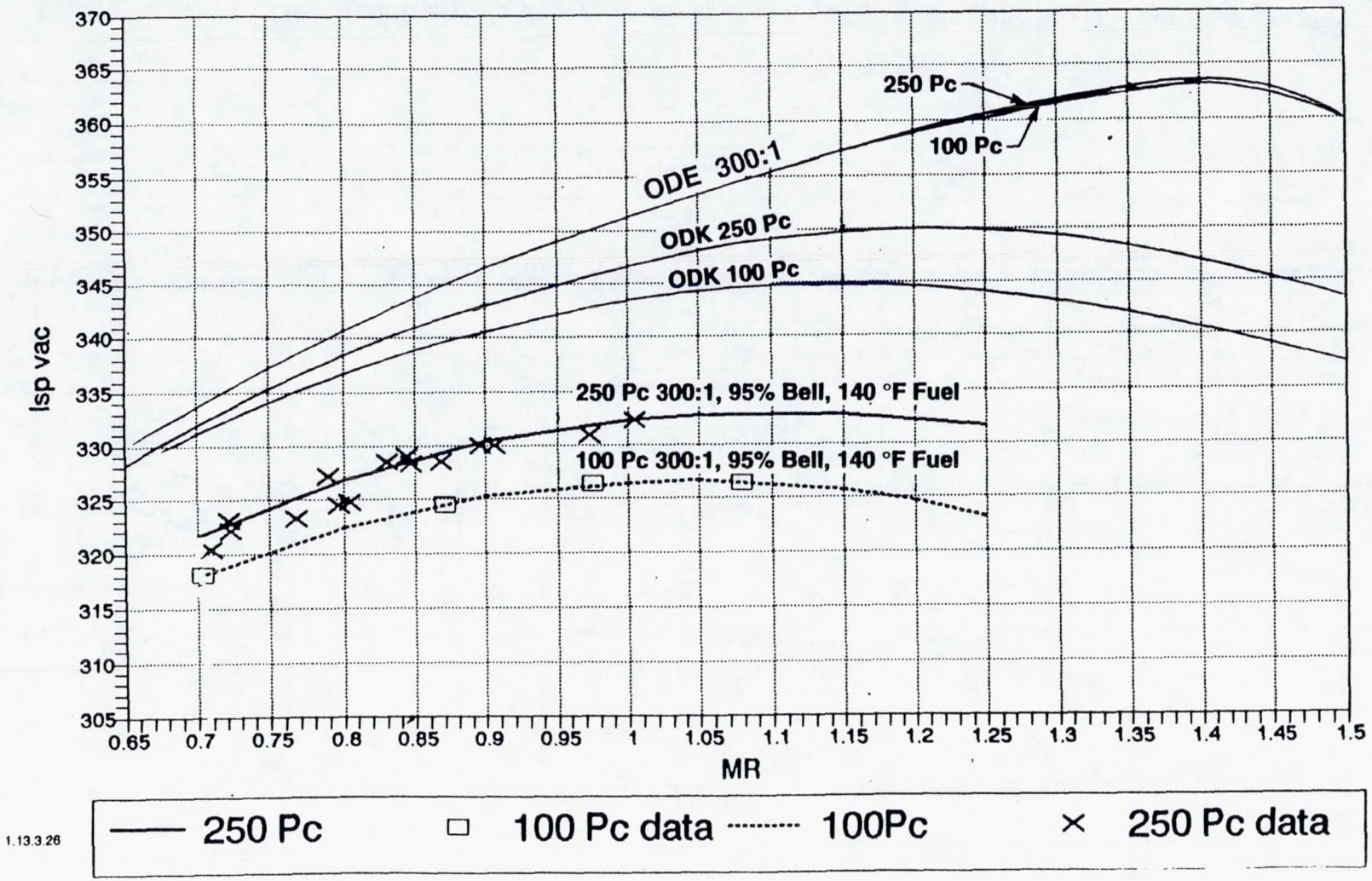

Figure 21. Cu and Re Chamber Data Extrapolated to 300:1, 95% Bell Nozzle, 140°F Fuel Temperature

Table 15. Extrapolation of Ir-Re Chamber Data to 300:1 Area Ratio and Heated Fuel

	Data Pt	Extrapolation to 300:1			Data Pt	Extrapolation to 300:1		
		Nominal	Added Lnz	Heated fuel + Added Lnz		Nominal	Added Lnz	Heated fuel + Added Lnz
Test Number	120	N/A	N/A	N/A	116	N/A	N/A	N/A
Pc (psia)	100	100	100	100	250	250	250	250
MR (ox/fuel)	1.08	1.05	1.05	1.05	0.85	1.15	1.15	1.15
Tox (deg F)	61	77	77	77		77	77	77
Tfuel (deg F)	66	77	77	140		77	77	140
%FFC	~20	~20	~20	~20	~20	~20	~20	~20
Area Ratio	18.3:1	300:1	300:1	300:1	3.1:1	300:1	300:1	300:1
Nozzle %bell	(20 deg conical exit)	83	95	95	(15 deg cone)	83	95	95
Isp ODE vacuum	325.7	353.3	353.3	353.3	279.5	357.3	357.3	357.3
Kinetics loss	8.1	9.3	9.3	9.3	1.4	7.7	7.7	7.7
Divergence loss	11.8	4.3	2.7	2.7	4.4	4.4	2.7	2.7
Boundary layer loss	3.0	9.3	9.4	9.4	1.5	7.4	7.9	7.9
Injector loss (mixing and vap)	0.974	0.975	0.975	0.983	0.985	0.976	0.976	0.982
Isp efficiency (Isp del / Isp ODE)	0.906	0.912	0.916	0.923	0.959	0.923	0.926	0.932
Isp delivered vacuum	294.9	322.1	323.6	326.3	268.1	329.7	330.9	332.9

Table 16. Increasing Chamber Increases Performance Efficiency

• Equilibrium	• Small Shift In Composition Towards More Complete Reaction That Slightly Increases Maximum Theoretical Performance
• Kinetics	• Increase In Reaction Rates Reduces Recombination Lag During Expansion Process Thus Increasing Performance Efficiency
• Divergence Loss	• Secondary Effect Only
• Boundary Layer Loss	• Loss Decreases Due to Reduced Nozzle Surface Area (With Constant Thrust) Which Over Powers the Effect of the Increase In Shear Drag and Heat Transfer
• Vaporization Loss	• Increase In Vaporization Rate Due to Increased Drag On Droplets and Increased Heat Flux
• Mixing Loss	• Shift In Optimum Mixture Ratio for Kinetics Limited Isp Reduces Mixing Loss for Specific Ranges of Injected Mixture Ratio

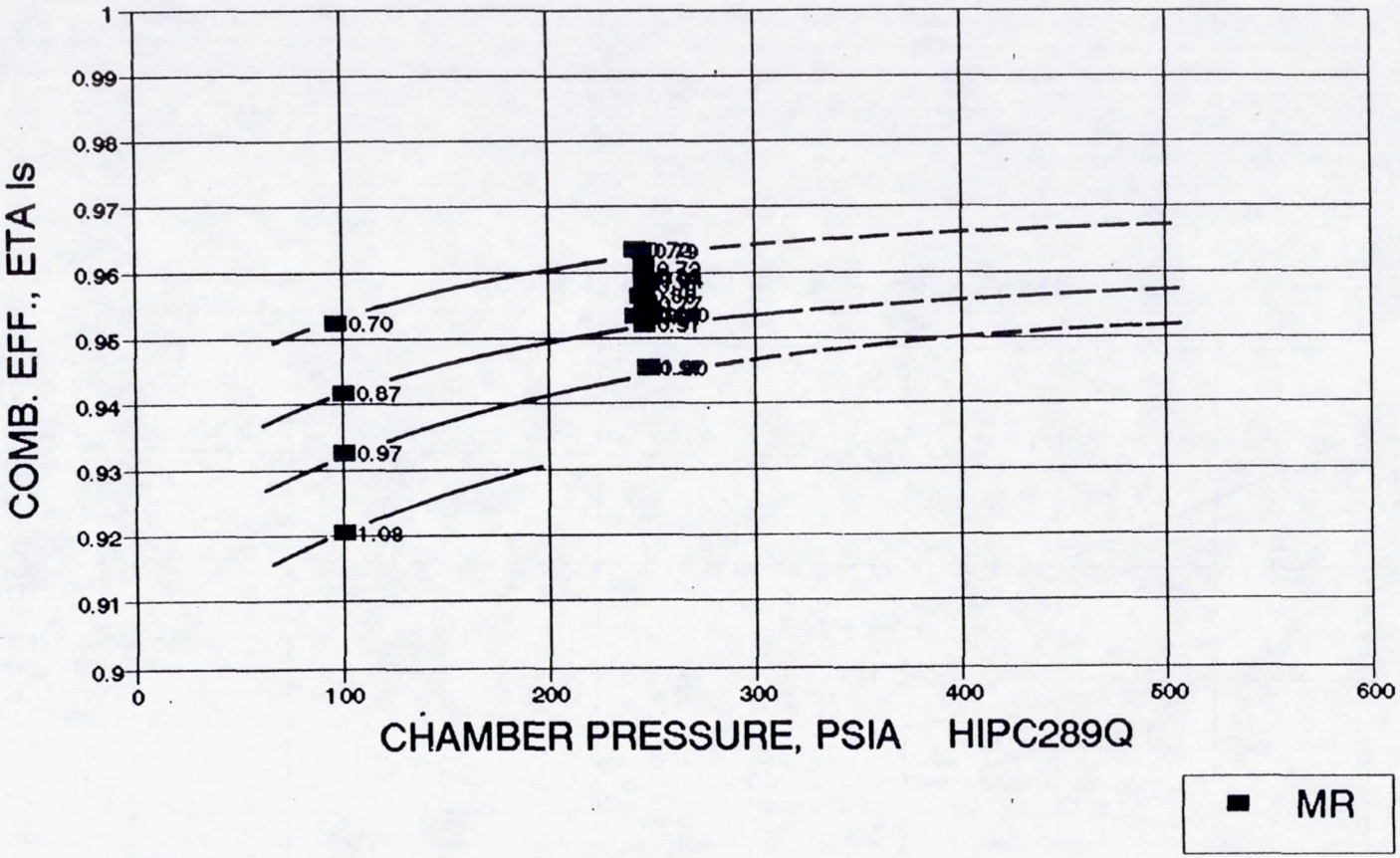

1.13.3.25

Figure 22. Combustion Efficiency vs Pc HIPC Task 4.0, All Data

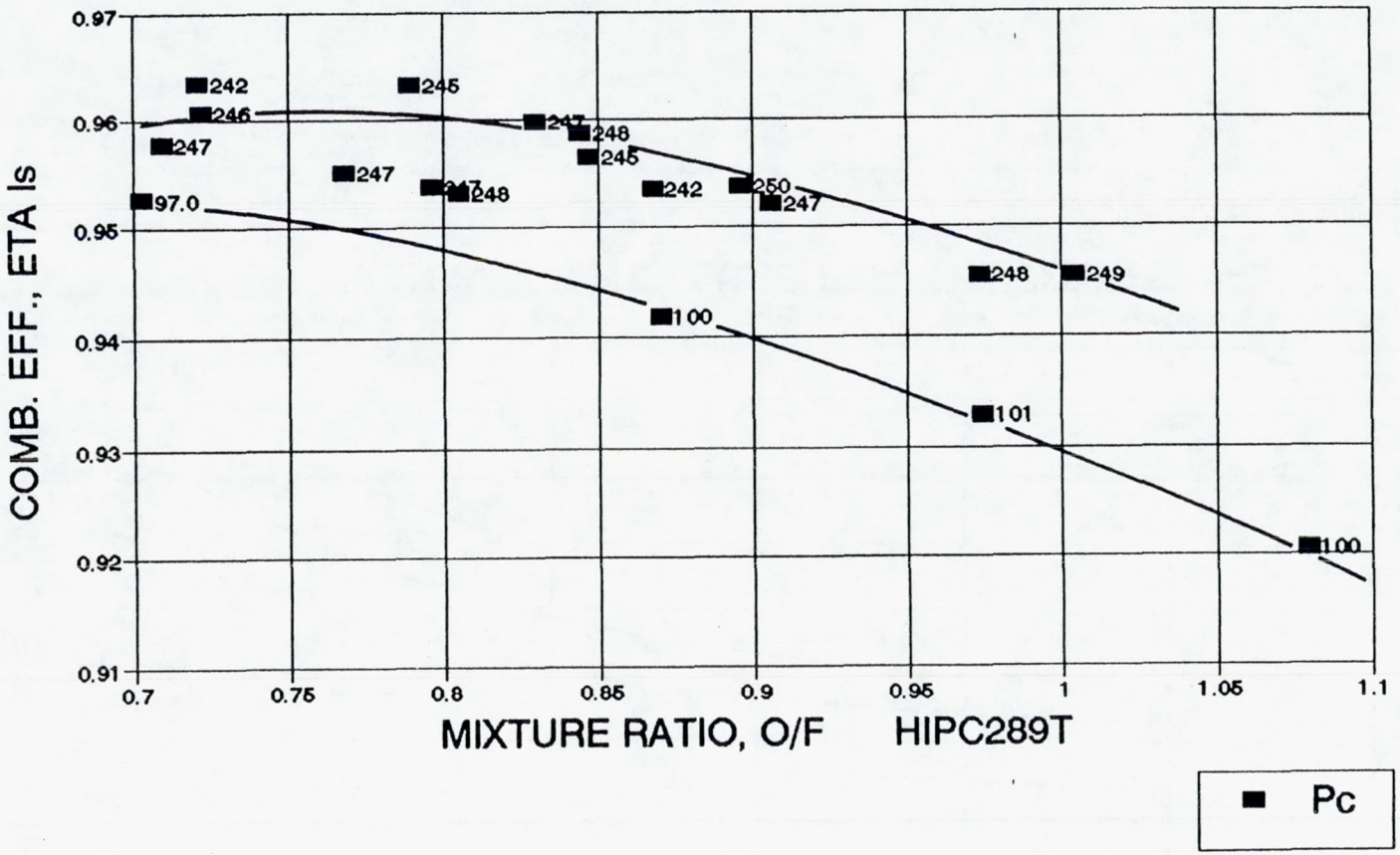

1.13.3.25

Figure 23. Combustion Efficiency vs MR HIPC Task 4.0, All Data

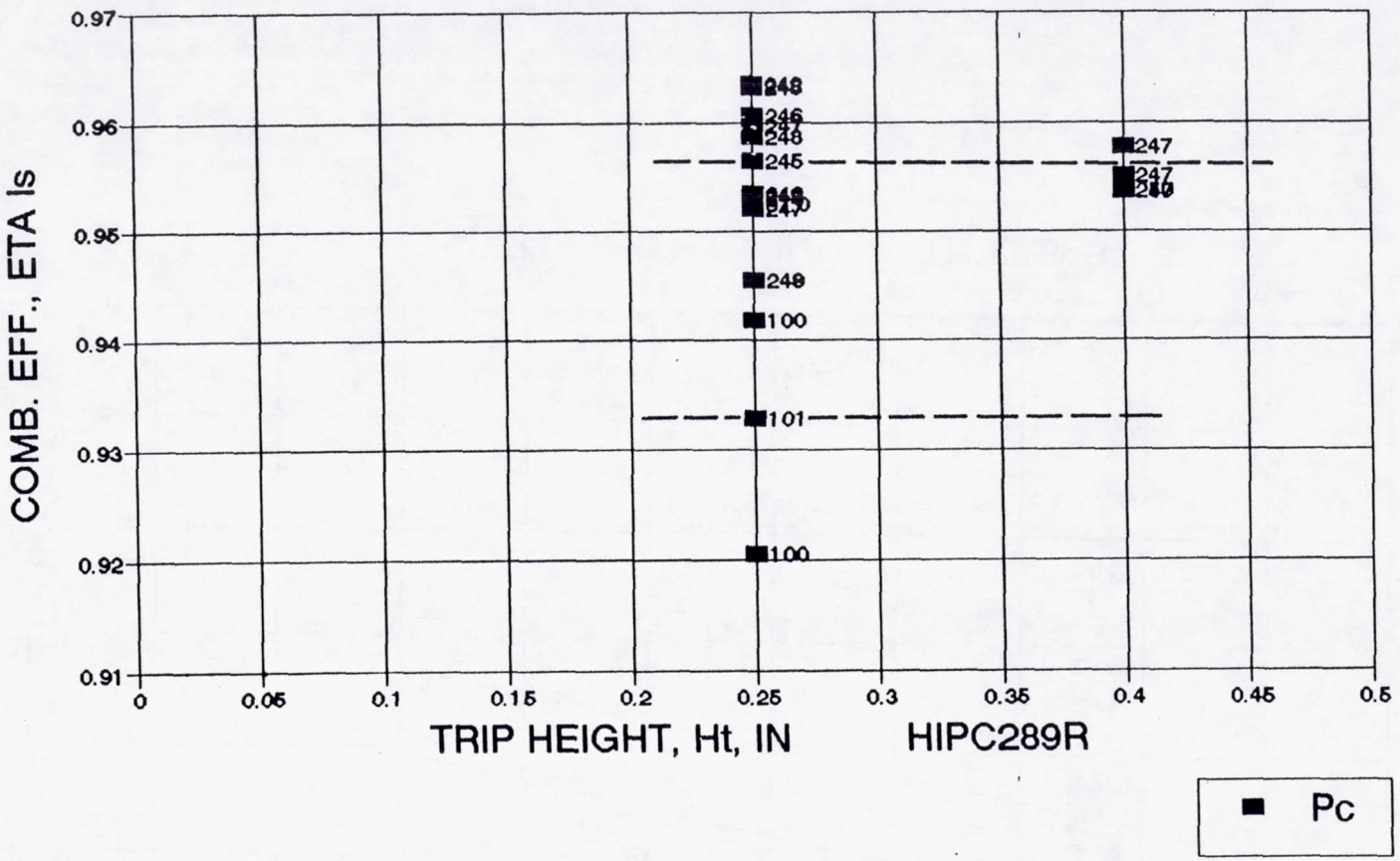

Figure 24. Combustion Efficiency vs Ht HIPC Task 4.0, All Data

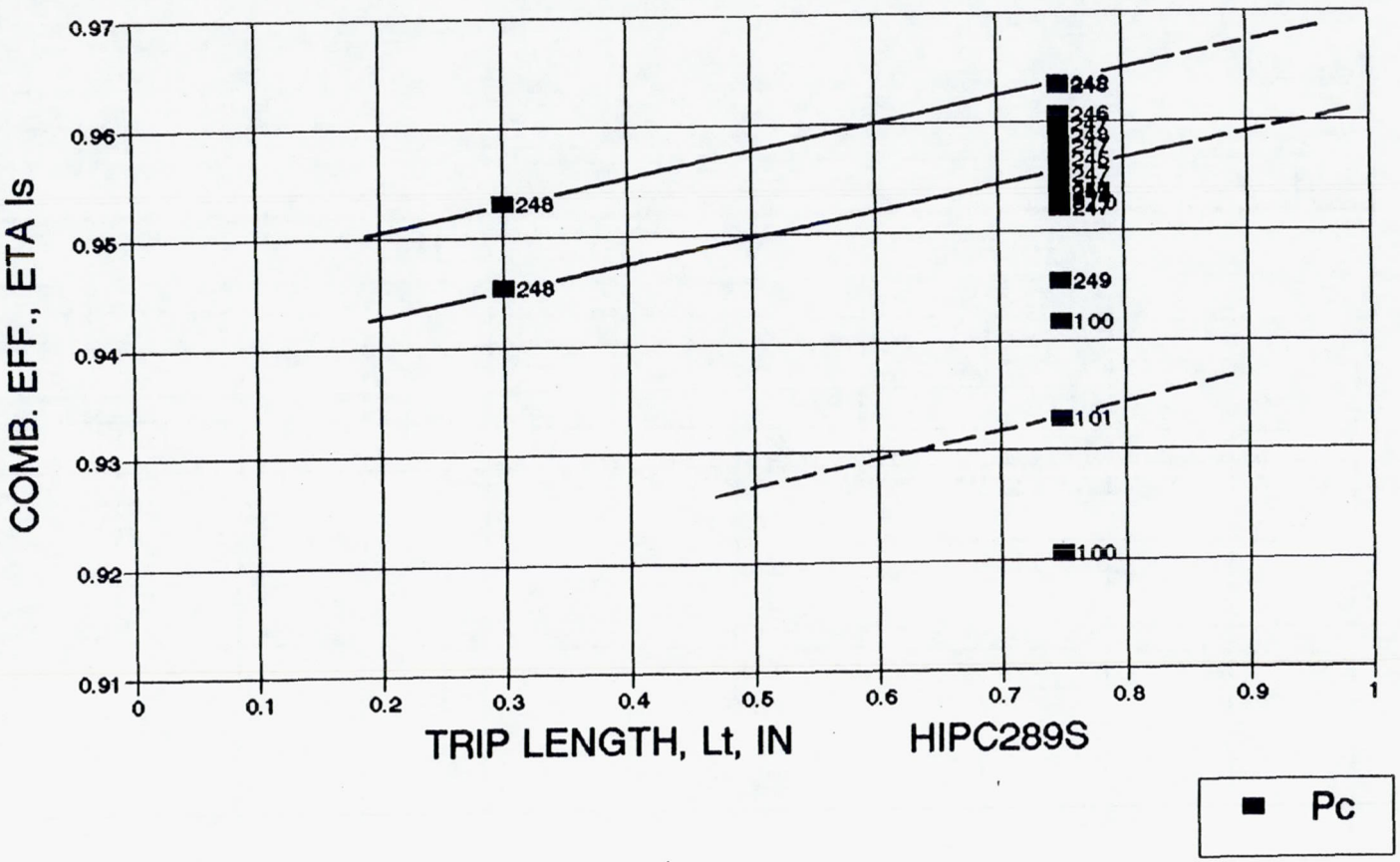

Figure 25. Combustion Efficiency vs Lt HIPC Task 4.0, All Data

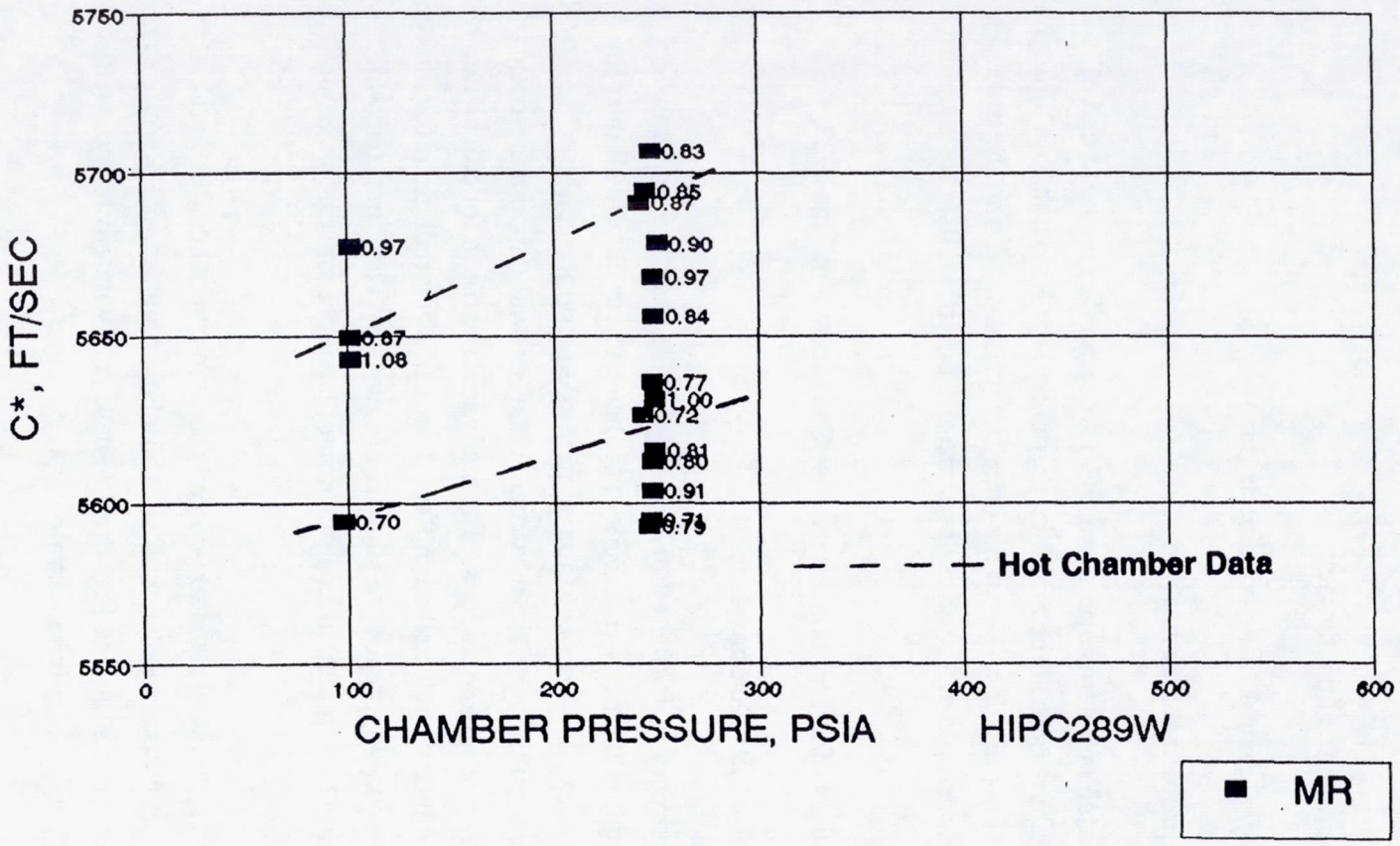

Figure 26. C* vs. Chamber Pressure Hot Throat, P Total

$$C^* = \frac{P_t A_t g_o}{\dot{W}_t}, \text{ ft/sec and}$$

P_t = total pressure at the throat

A_t = the throat area at firing conditions (hot)

$\dot{W}_t$ = total propellant flowrate.

The value of chamber pressure, PC-1, measured at the head end of the chamber, is corrected to total pressure at the throat by accounting for Rayleigh loss through the combustion zone and estimating the flow loss in the chamber (primarily due to the trip). Throat area is calculated based on measured chamber temperature and published data for rhenium thermal expansion.

The slight effect of mixture ratio on C* is shown in Figure 27.

3.4.3.2 Heat Transfer Determination

The primary method used in this program for chamber heat transfer determination was by measuring the transient response of the chamber outer wall over the length of the chamber. The measurements were concentrated in the converging section of the nozzle where the heat flux reaches a maximum. The maximum chamber wall temperature occurs in this region and sets the limit on operating conditions. The analytical approach for calculating heat transfer in the rocket engine has been described in Refs. 1 and 2. The predictions for throat heat transfer made in Task 2 using this approach are shown in Figure 28. The measured wall temperatures, shown in Table 17 and plotted as a function of chamber pressure in Figure 29 agree well with the prediction.

The two thin wall radiation-cooled rhenium chambers (100 and 250 psia chamber pressure) were in each instrumented with six 15 mil dia tungsten -5% Re/tungsten -25% Re thermocouples at the locations shown in Figure 30. These bare wires were spot welded to the chamber and supported with high temperature strain gage connectors.

The temperature-time responses were analytically modeled with an explicit step-wise thermal response solver which provided the best combination of heat transfer

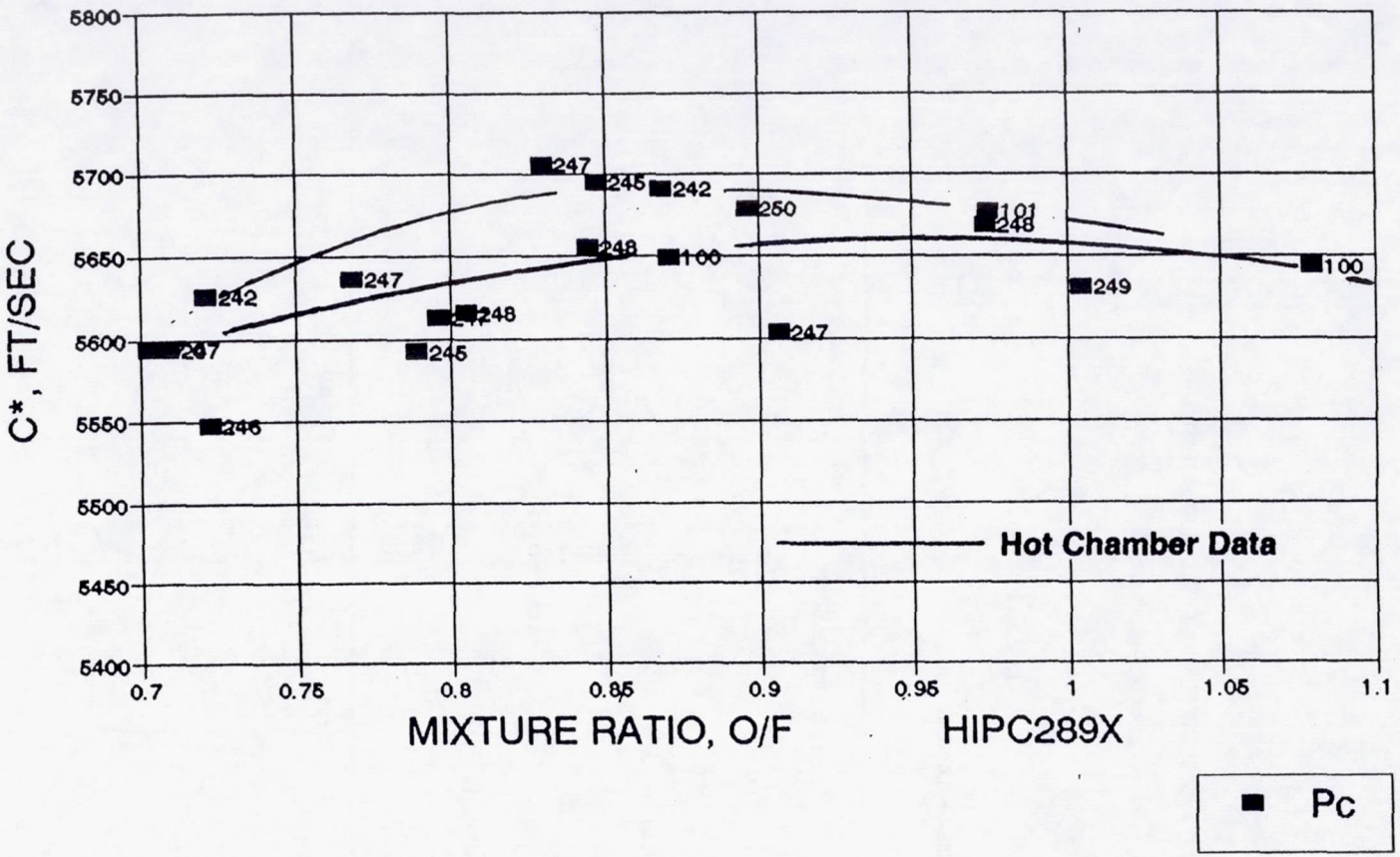

Figure 27. C* vs. Mixture Ratio Hot Throat, P Total

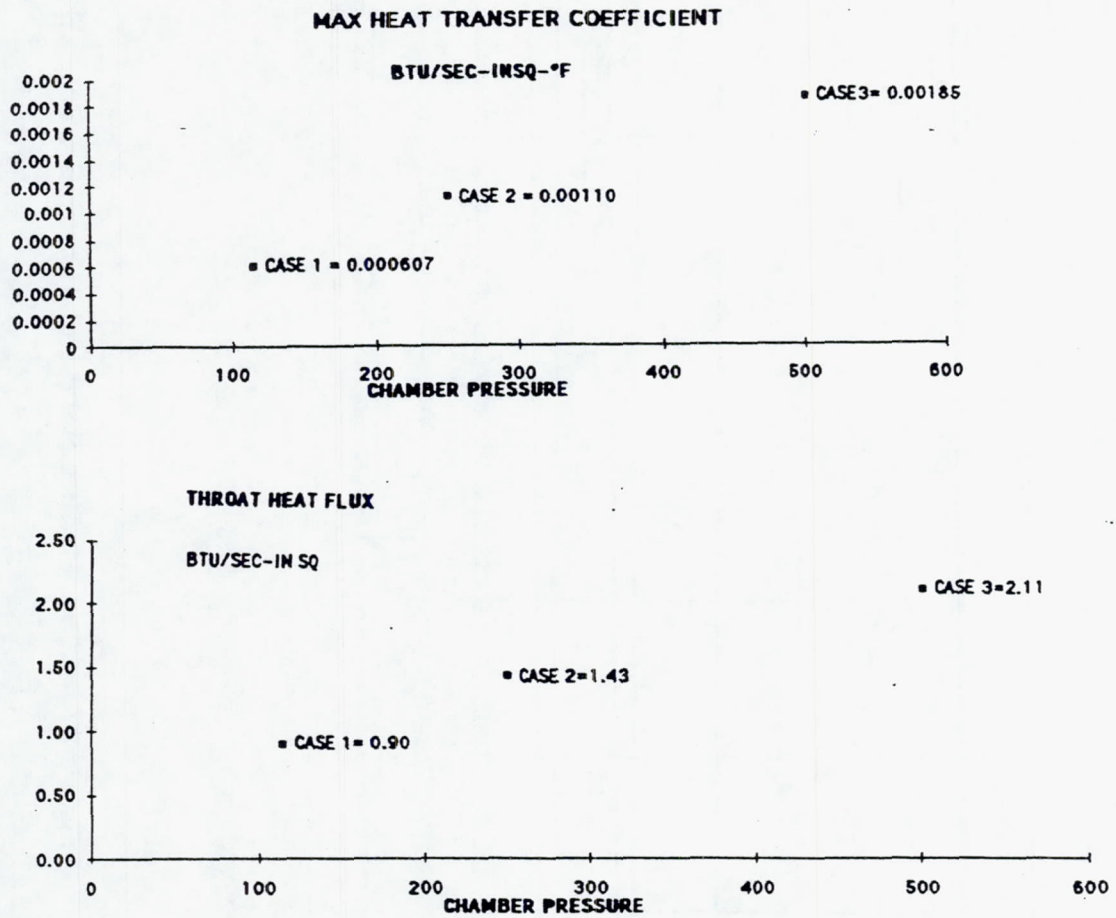

Figure 28. Thruster Heat Transfer vs. Chamber Pressure

Table 17. High Pc Task 4 – Testbed Data: Thermal Data

TEST No.	TESTBED CONFIGURATION Ht in.	Lt in.	Matl.	HOT Dt IN.	AREA RATIO, e Ae/At	FIRING TIME sec	DATA TIME sec	MR O/F	PC-1 psia	Wt lbm/sec	MAX TH-1 oF	TCN MAX oF	MAX VALUE AT 15 SEC TC-1 15	TC-2	TC-3	TC-4	TC-5	TC-6	PYROHI
101	0.25	0.75	Cu	0.519	1.68	0.5													
102	0.25	0.75	Cu	0.521	1.68	15.0	14.4	0.84	248	0.298	1979	411							
103	0.25	0.75	Cu	0.521	1.68	14.8	14.3	0.79	245	0.298	1952	420							
104	0.25	0.75	Cu	0.521	1.68	15.0	14.4	0.91	247	0.300	1952	462							
105	0.25	0.75	Cu	0.521	1.68	15.0	14.4	0.72	246	0.302	1544	462							
106	0.25	0.75	Cu	0.521	1.68	15.0	14.4	1.00	249	0.300	1947	475							
107	0.40	0.75	Cu	0.520	1.67	15.0	14.4	0.80	247	0.297	1769	>500							
108	0.40	0.75	Cu	0.523	1.67	15.0	14.4	0.90	250	0.301	1412	609							
109	0.40	0.75	Cu	0.523	1.66	15.0	14.4	0.71	247	0.302	1436	421							
110	0.40	0.75	Cu	0.523	1.66	15.0	14.4	0.77	247	0.300	1579	437							
111	0.25	0.30	Cu	0.523	1.66	15.0	14.4	0.81	248	0.303	1509	407							
112	0.25	0.30	Cu	0.523	1.66	15.0	14.4	0.97	248	0.299	1697	420							
113	0.25	0.75	Re	0.521	3.11	15.0	14.4	0.72	242	0.301	--	--	2896	2756	1542	3331	3410	3066	3557
114	0.25	0.75	Re	0.522	3.10	15.0	14.4	0.83	247	0.304	--	--	3050	2883	3624	3637	3603	3215	3709
115	0.25	0.75	Re	0.522	3.10	15.0	14.4	0.87	242	0.299	--	--	3163	3018	3820	3831	3680	2739	3797
116	0.25	0.75	Re	0.522	3.10	46.8	14.5	0.85	245	0.302	--	--	3101	2968	3882	3826	3664	2717	3782
117	0.25	0.75	Ir-Re	0.833	18.3	15.0	14.4	0.70	97.0	0.291		--				*	*	2292	3253
118	0.25	0.75	Ir-Re	0.833	18.3	15.0	14.4	0.87	100	0.299		--	3424	3607		*	*	2468	3495
119	0.25	0.75	Ir-Re	0.833	18.3	15.0	14.4	0.97	101	0.298		--	3593	3769		*	*	2563	3601
120	0.25	0.75	Ir-Re	0.833	18.3	15.0	14.4	1.08	100	0.300		--	3819	3788		*	*	2641	3774
121	0.25	0.75	Cu	0.367	1.68	0.5													
122	0.25	0.75	Cu	0.370	1.68	15.0	14.4	0.76	505	0.304		769							
123	0.25	0.75	Cu	0.370	1.68	15.0	14.4	0.84	501	0.302		842							
124	0.25	0.75	Cu	0.369	1.68	15.0	14.4	1.01	509	0.304		650							

TOTAL FIRING TIME= 363 sec

*Initial response appears correct; reads low at 15 sec

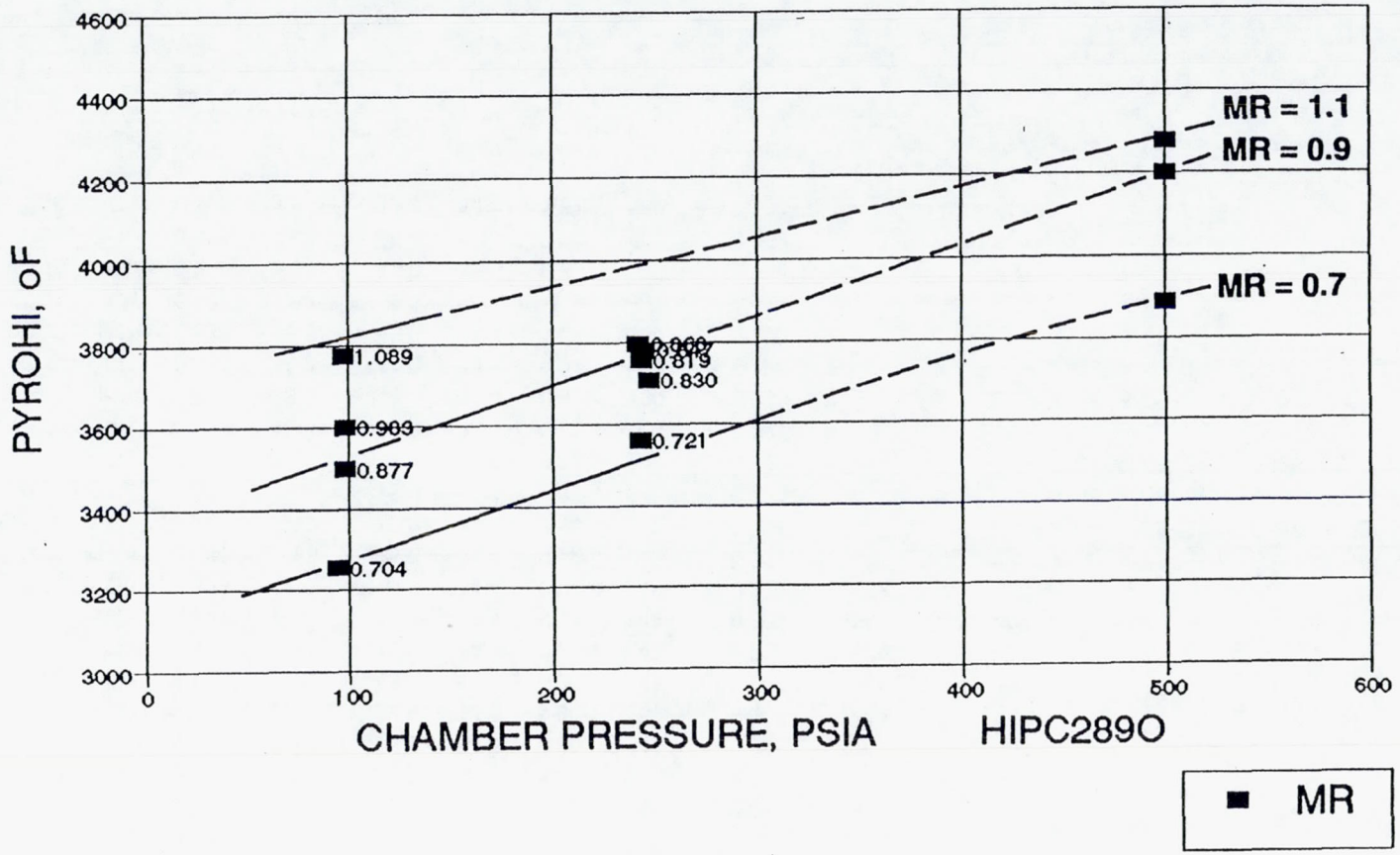

Figure 29. Chamber Temperature vs. Pressure – HIPC Task 4, Rhenium Chambers

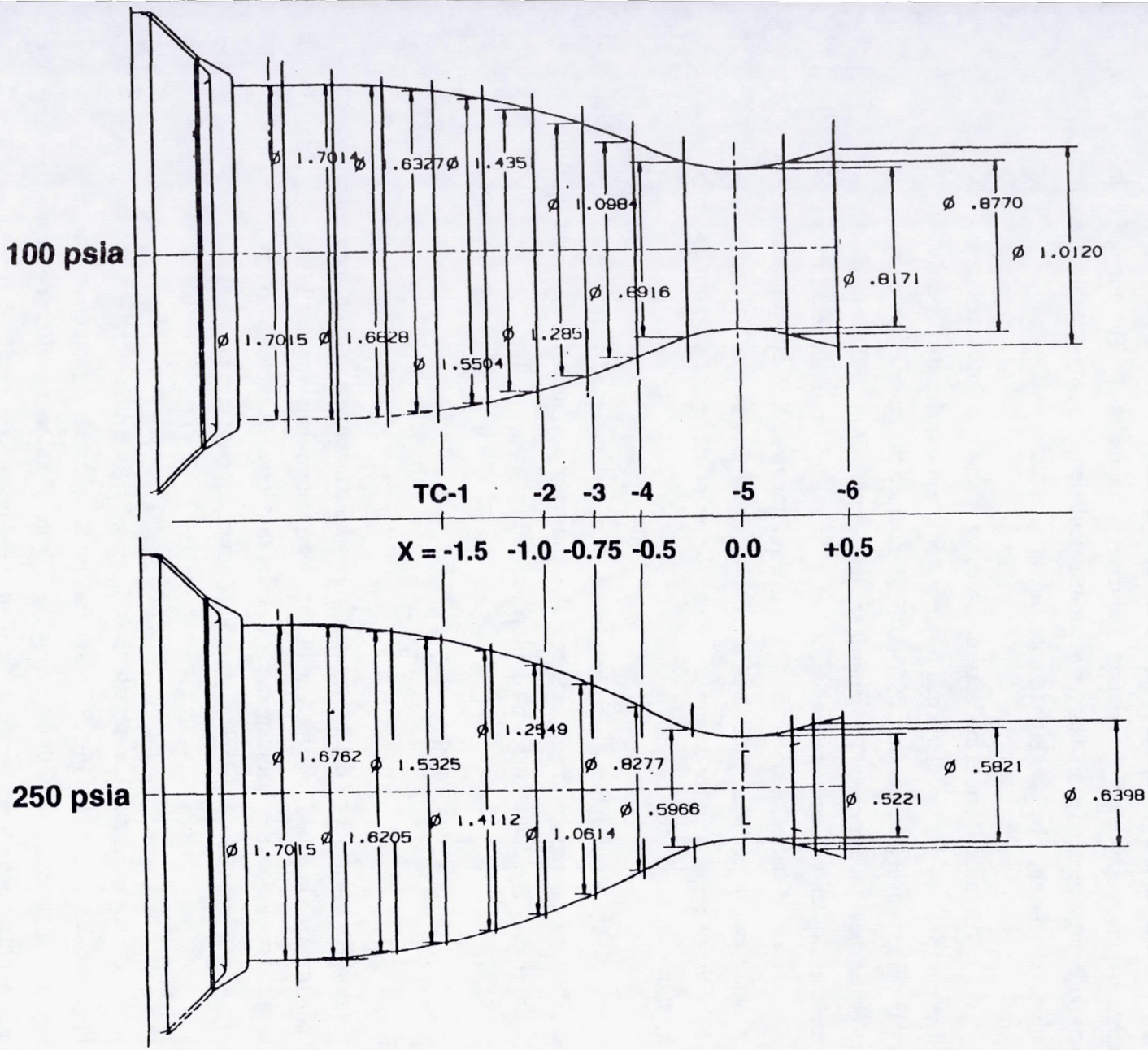

Figure 30. Chamber Heat Transfer Measurement Locations

coefficient and gas side recovery temperature to match the response. This model incorporates the temperature varying properties of the rhenium and the external radiation. The purpose of the model is to provide engineering design data for accurate calculation of steady-state wall temperature at any location in the chamber and high temperature portion of the nozzle exit.

A typical thermal model response curve is matched with test data in Figure 31. The curve shows the model thermal response for a heat transfer coefficient of 0.001 Btu/in.^{2}-sec-°F and a recovery temperature of 3300°F. Plotted are the outer and inner wall temperatures of the rhenium chamber. The latter is the temperature of the iridium protective layer. The measured outer wall temperature for the hot test zone, 0.5 in. ahead of the throat, for test -113 is also shown. It can be seen that the full transient through steady state response of the chamber is very accurately produced. This enables accurate prediction of transient and steady-state response of the chamber wall for design purposes. Response curves for all thermocouples in all tests are shown in Appendix D.

The test duration of 15 sec was chosen to give essentially steady state wall temperatures. Plotted on the graph are gas side heat flux and outer wall radiation loss. At equilibrium these are equal. The deviation from equilibrium, defined as

$$100 * \frac{(q_{hg} - q_{rad})}{2 * q_{cw}}$$

is plotted in Figure 32, which shows that most cases were within much less than one percent of equilibrium conditions. Outer wall radiation conditions were determined empirically by matching the initial cooldown thermal response at thruster shutdown. A typical cooldown response is shown in Figure 33. A complete set of cool down response curves is given in Appendix D.

The measured heat transfer coefficients, h_g, in Btu/in.^{2}-sec°F at the six measurement locations are plotted in Figure 34 as a function of chamber pressure. As can be seen there may be a slight decrease with increasing Pc. Figure 35 shows the effect of location on h_g. The corresponding recovery temperatures are plotted in Figure 36.

This method for determining H_g and T_r has the advantage that it does not rely solely on the slope of the temperature time curve; differentiation of experimental data is

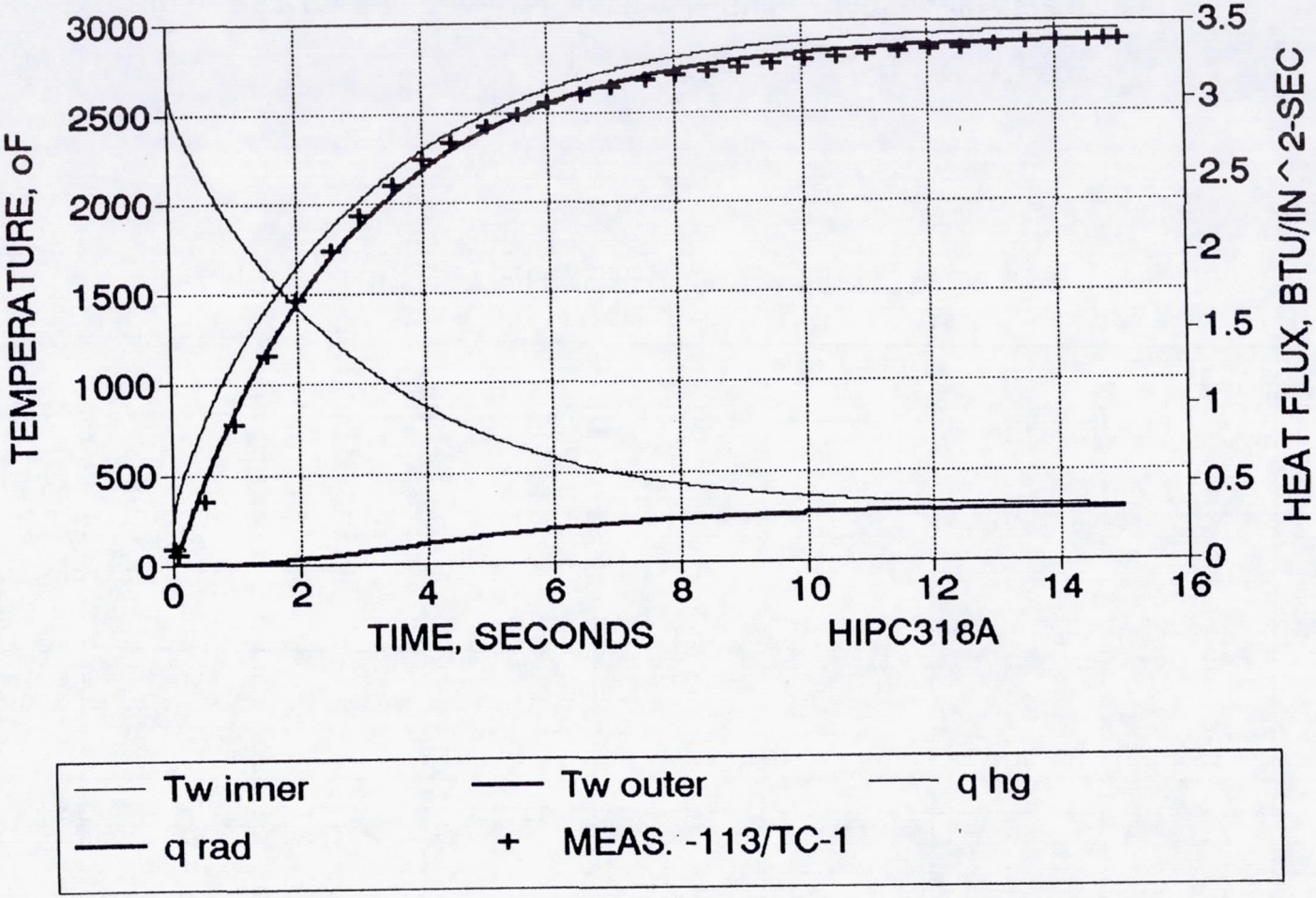

Figure 31. Chamber Thermal Response Tr=3300°F/hg=0.0010/PC=242/MR=0.72

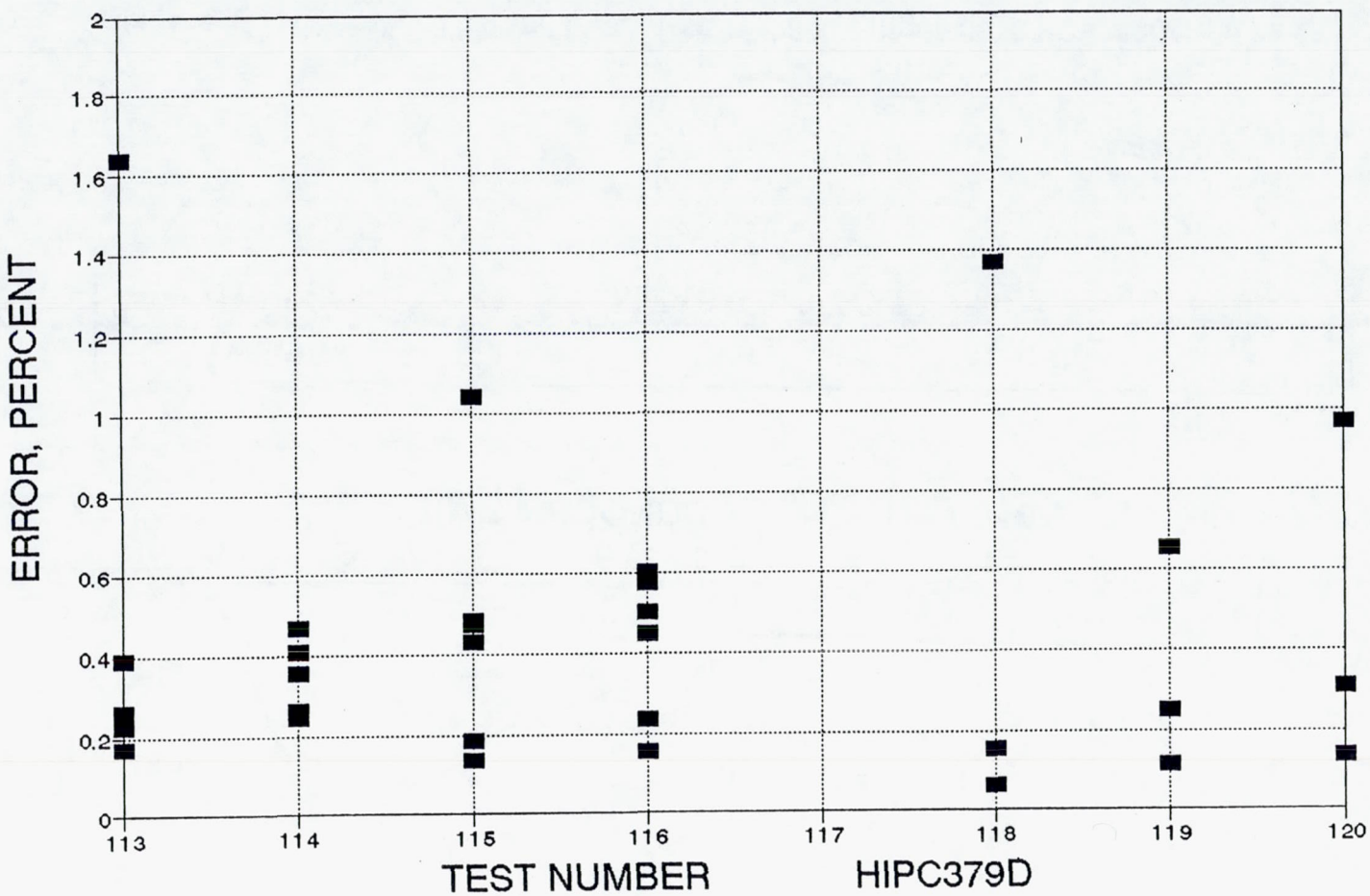

Figure 32. Error in Approaching Steady-State – 100*(qg-qrad)/(2*q cw)

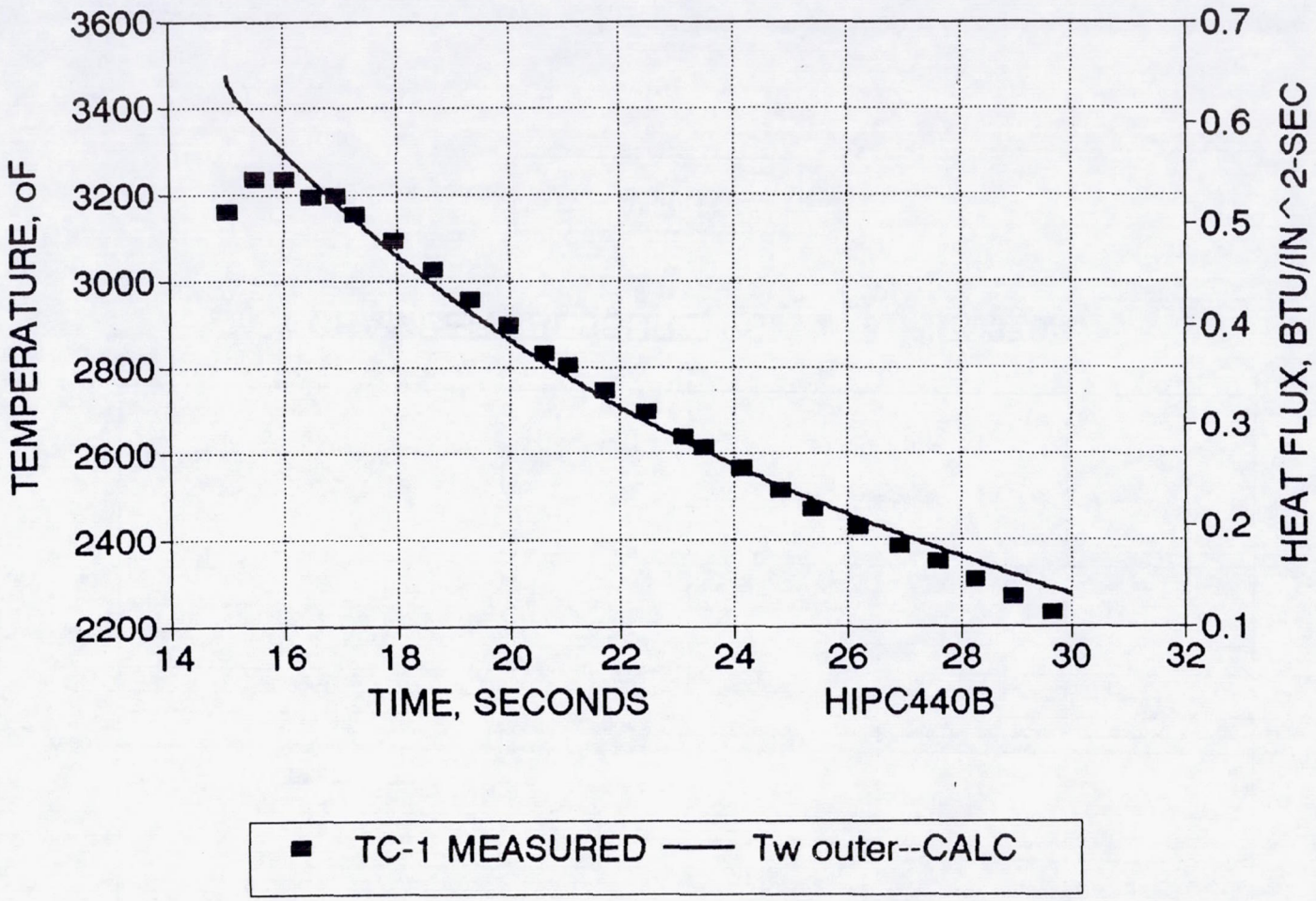

Figure 33. Chamber Thermal Response Test-115 Post Cooling, TC-1. e=0.80

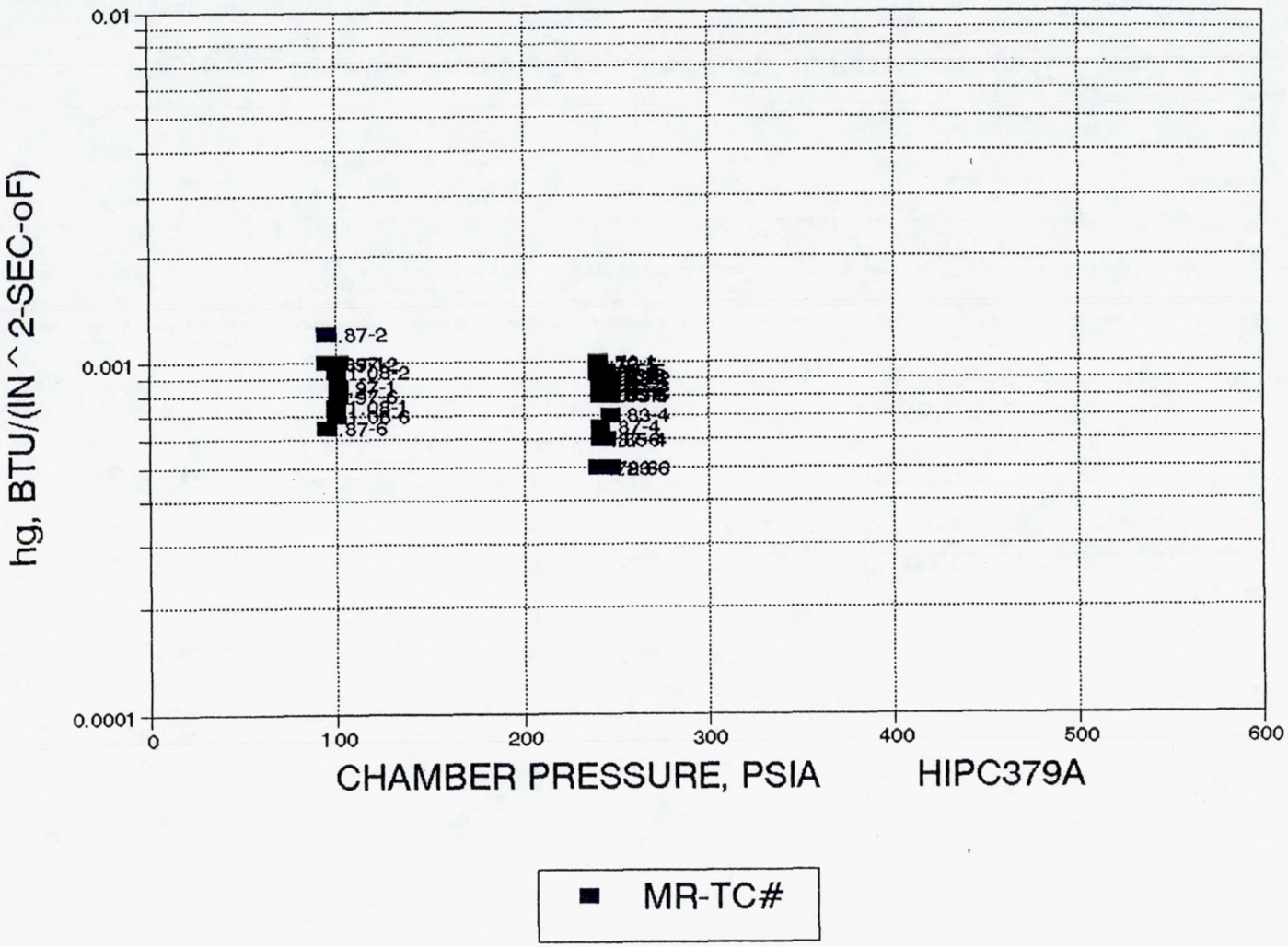

Figure 34. Heat Transfer Coefficient vs. Pc

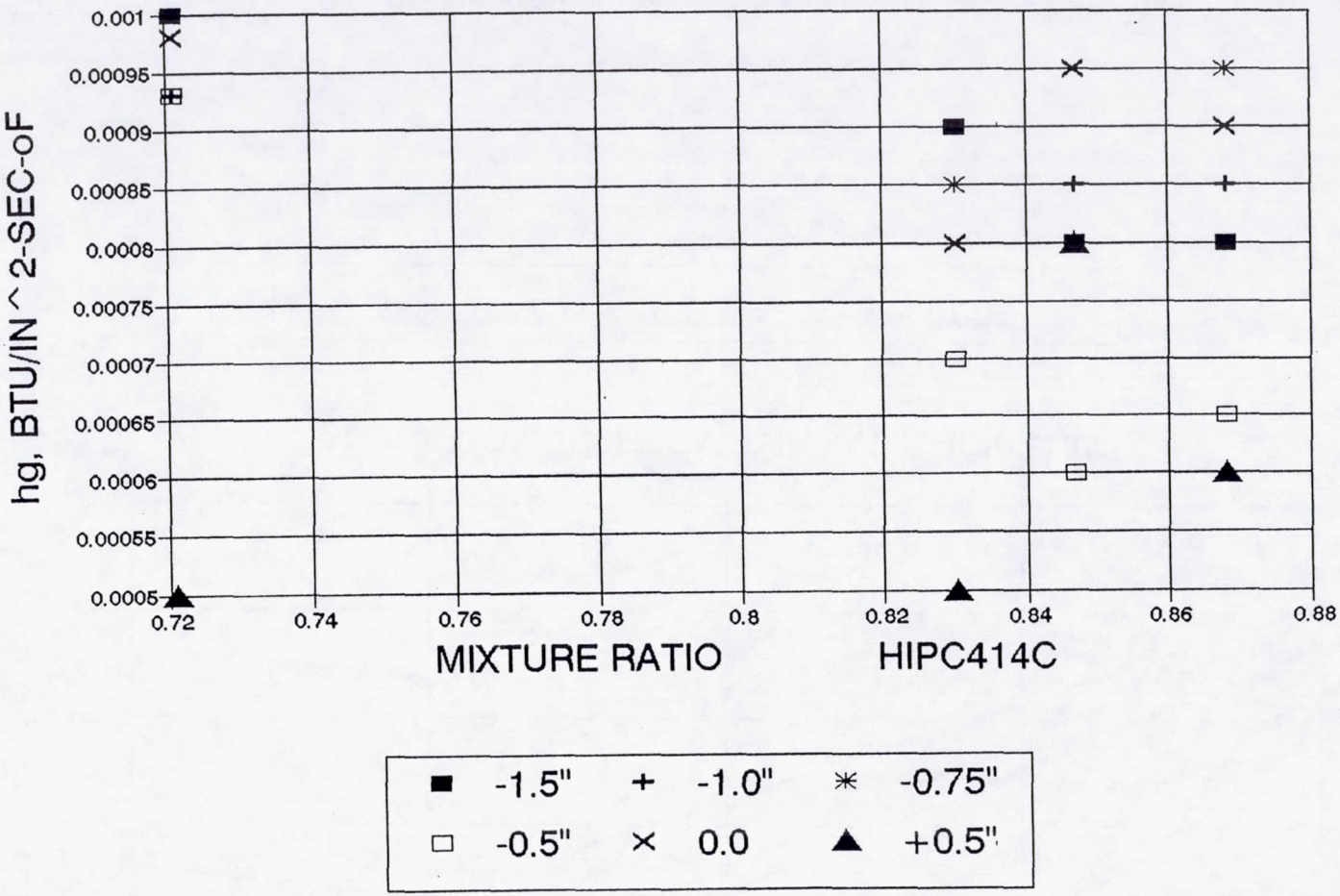

Figure 35. Heat Transfer Coefficient – Measured Data - Pc = 250 psia

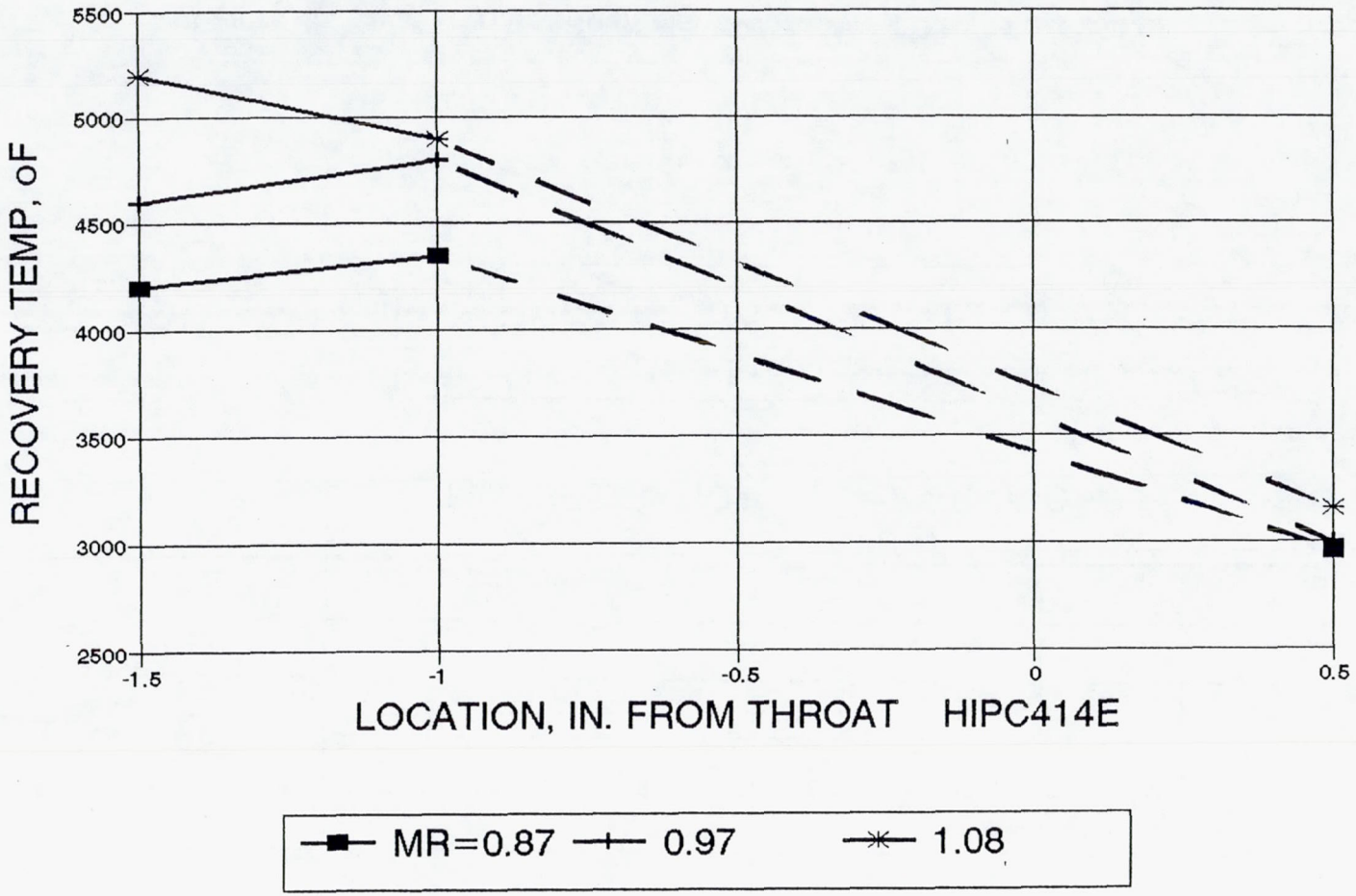

Figure 36. Gas Recovery Temperature – Measured Data - Pc = 100 psia

inherently error-prone. In the end, the present method gives, by definition, a result which closely matches the actual response. Any mismatch with the experimental data is the result of either non-constant h_g (e.g., because of changing operating point or unstable heat transfer conditions), or because of thermocouple error (e.g., unbonding from the surface). Note that the wall temperature measurement does not depend on surface emissivity.

The expected correlation of heat transfer with operating conditions is shown in Figure 37 from Ref. 1, which shows the Bartz correlation and a previously determined empirical correlation as a function of throat Reynolds number.

The calculated heat transfer coefficients measured in this program have been correlated at a function of Stanton number, Prandtl number, and Reynolds number, as shown in Figure 38. Shown on the curve are all the hot chamber heat transfer data in terms of $N_{st}*N_{pr}^{0.6}$ as a function of throat Reynolds number. Also shown are the Bartz equations, which greatly over predicts the hg for these small chambers with gradually contoured inlet sections which result in laminar flow to high Reynolds numbers. Shown as well is a correlation which has proven to closely match previous data for lower temperature chambers (Ref. 1). This agrees with the data only at very low Re and overpredicts at higher values. In this coordinate system the 100 psia and 250 psia data clearly fall on two distinct curves, with the 250 psi values being about one-sixth the 100 psi values.

These data are well-fit by the expression

$$N_{ST} * N_{Pr}^{2/3} = C_1 R_{e_{dt}}^{(C_2)}$$

where

$C_1 = 600$ at 100 Pc and 300 at 250 Pc

and $C_2 = -1.1$.

These expressions derived from the test data are plotted in Figure 39. The experimental range of the data is $10^4 \leq R_{e_{dt}} \leq 2 \times 10^5$. In the previous work this upper value of Re was the point at which transition to higher levels of heat transfer occurred. In that work, this

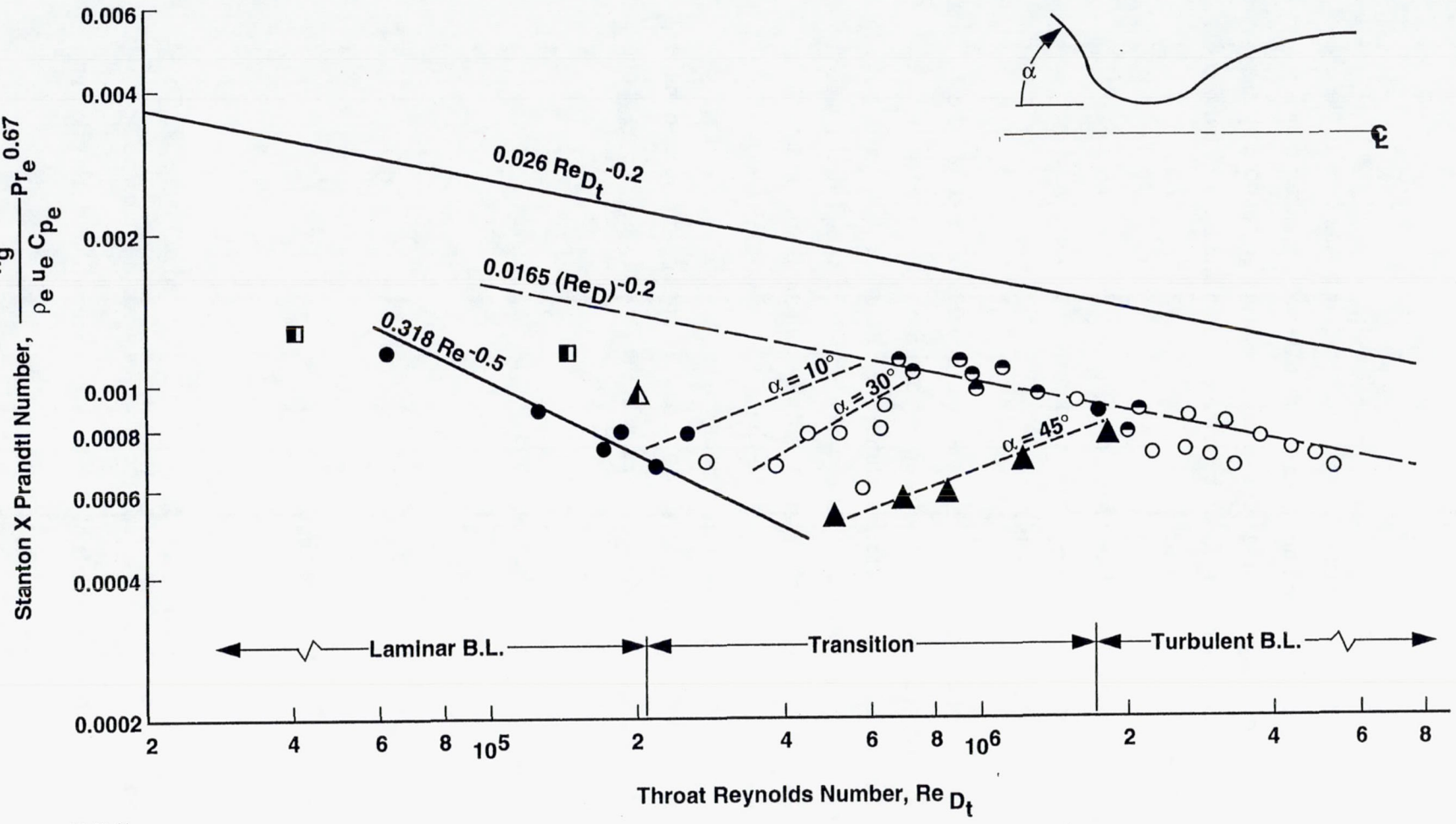

Figure 37. Correlation of Heat Transfer With Operating Conditions (From Ref. 1)

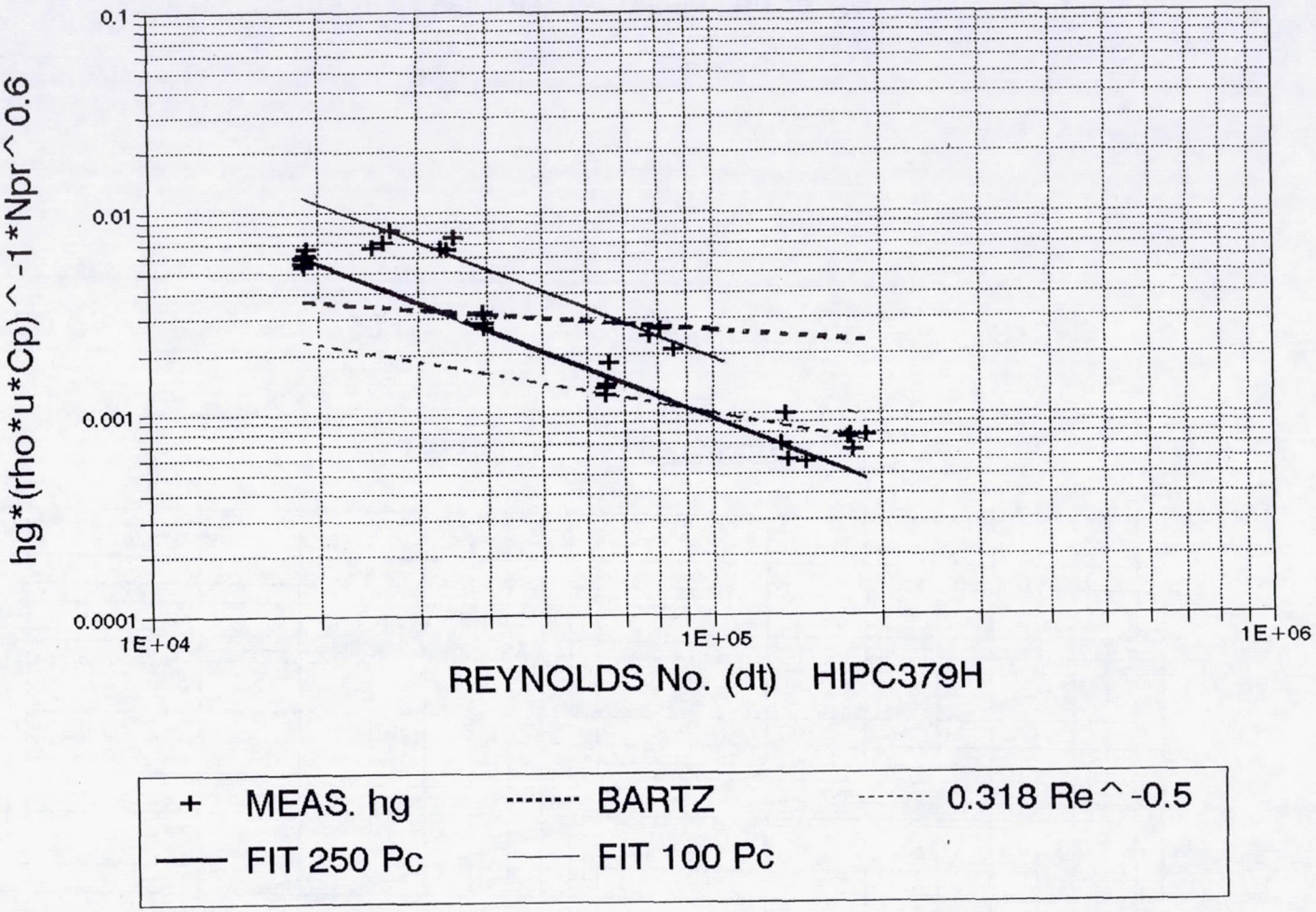

Figure 38. Heat Transfer Correlation With Operating Conditions – FIT 100 and 250 Pc Data

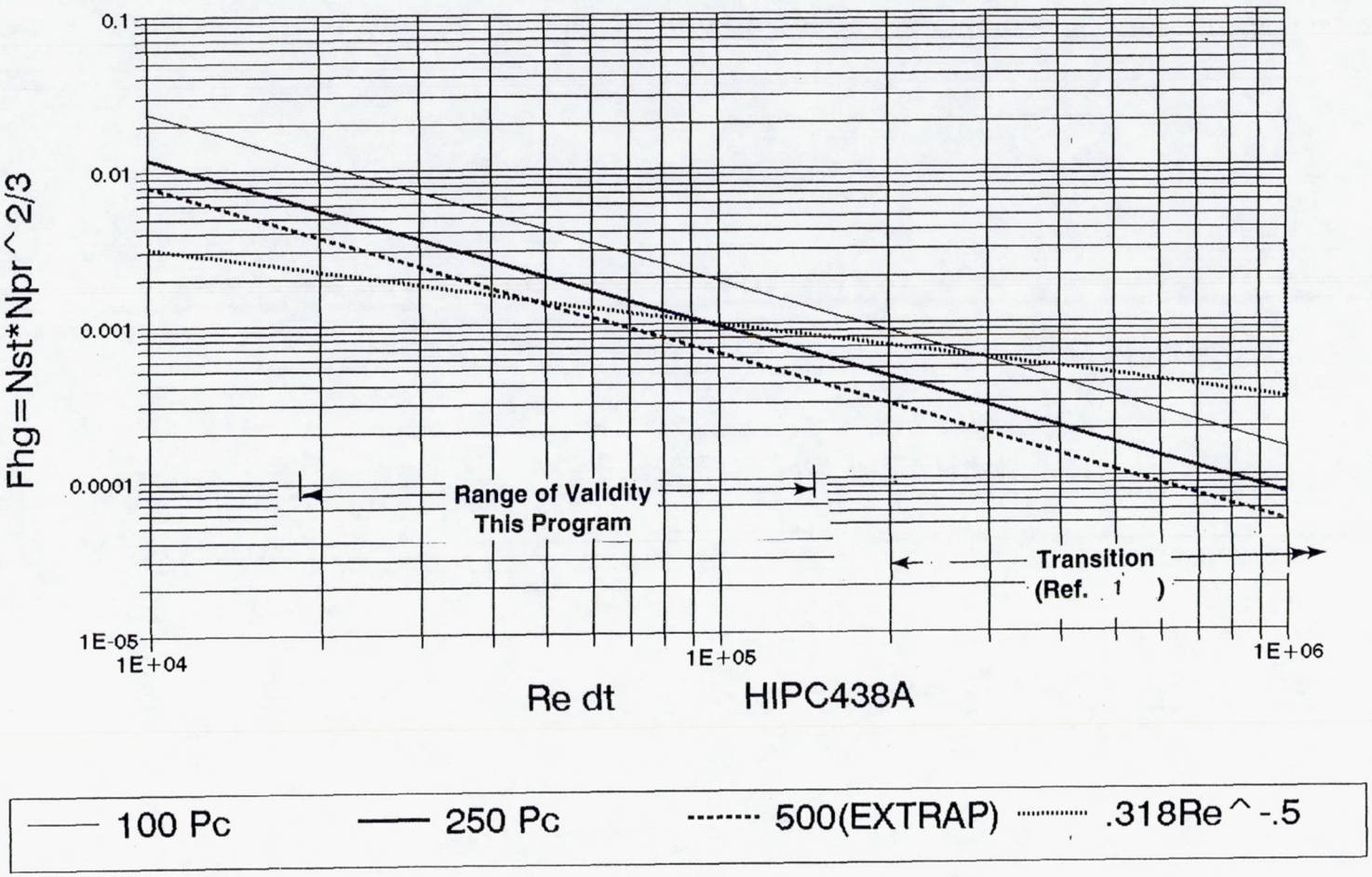

Figure 39. Correllate Fhg vs. Re

new, higher level was best matched by 0.0165 $R_{e_{dt}}^{-0.2}$ (Figure 37), while the laminar regime was best fit by 0.318 $R_e^{-0.5}$. At higher Reynolds numbers than reached in this program (greater than 200,000), we expect the data to make a transition to this curve.

The variation of measured heat transfer coefficient with location and mixture ratio at 250 psia Pc is shown in Figure 40. The data for all but the lowest MR (0.72) show a general fall to a minimum as the station 0.5 in. ahead of the throat is approached, with a rise at the throat and then a fall in the nozzle.

The corresponding variations in recovery temperature are plotted in Figure 41. The corresponding set of data for 100 psia Pc are included in Appendix D.

The initial recovery temperatures are somewhat under the well-mixed reaction temperature, indicating that the trip has not completely mixed the fuel rich film cooling layer with the core. This is confirmed with the general rise in recovery temperature as the throat is approached indicating that the incompleted mixed core flow is approaching the wall. Generally the recovery temperature then falls significantly, in part because of further mixing and in part because of the reduction in recovery temperature with Mach number.

Note that some of the recovery temperatures derived from the heat transfer data represent unrealistically high recovery temperatures, i.e., higher than could be reasonably expected at core mixture ratio. Since no evidence of streaking (high mixture ratio flow striations) has been seen with this injector, two possible explanations remain. The first possibility would be inaccurate temperature measurements caused by faulty thermocouples; since these are not redundant measurements this possibility cannot be ruled out. The second relates to chemical reaction which releases energy at the wall when oxidizer rich core flow encounters the fuel rich boundary. Perhaps under these conditions total enthalpy would be a better heat transfer parameter than recovery temperature.

Although this program did not investigate different trip heights and lengths in combination with hot wall thermal measurements, it is clear that this can be an excellent indicator of degree of mixing introduced by the trip. This is very important to obtaining long life for the Ir-Re chamber material system. It is evident that hot wall transient response measurements made in (short) 15 sec tests can show if the trip is high enough to give good compatibility at the wall (and, incidentally, increased performance through better mixing).

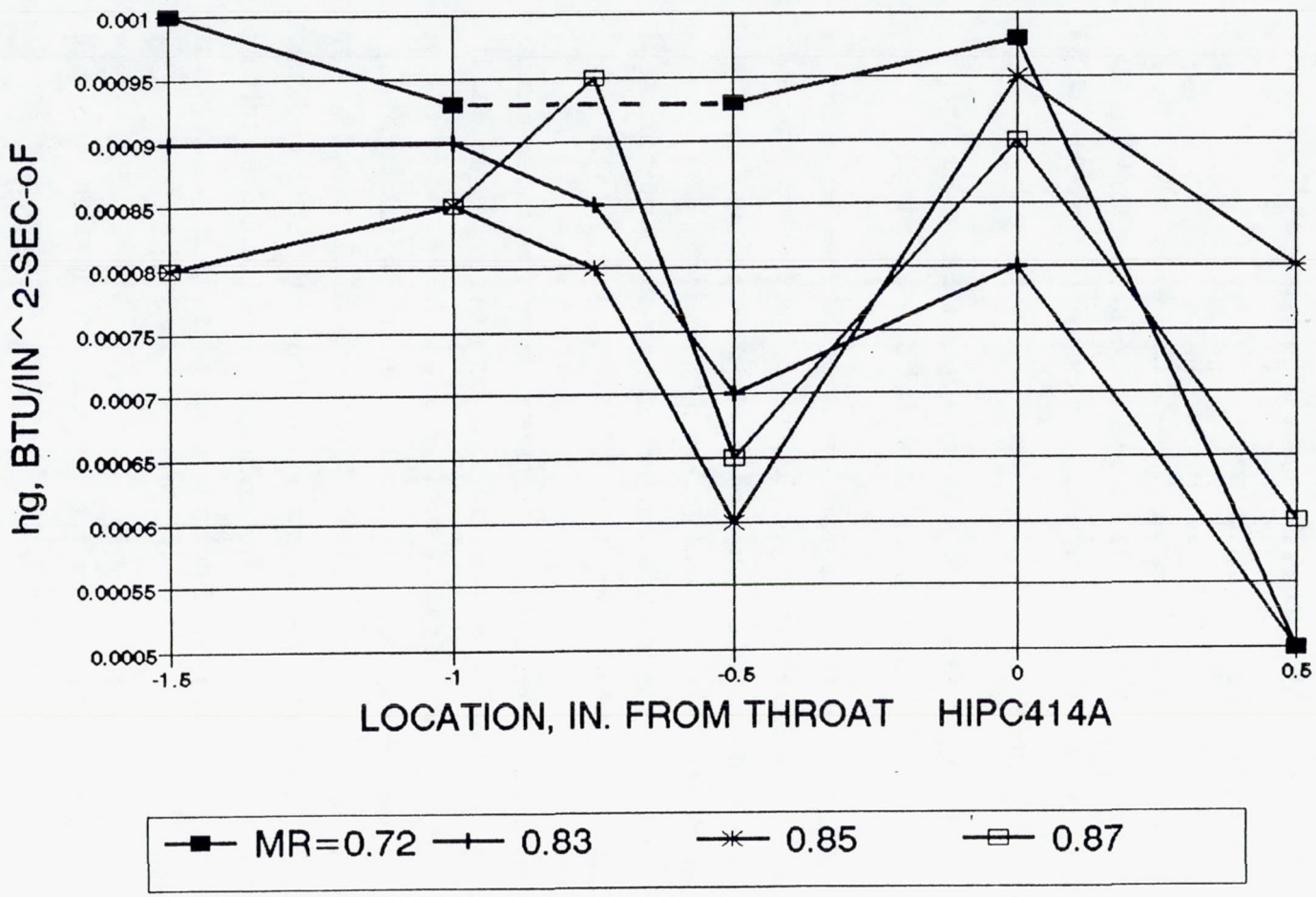

Figure 40. Heat Transfer Coefficient Measured Data - Pc=250 psia

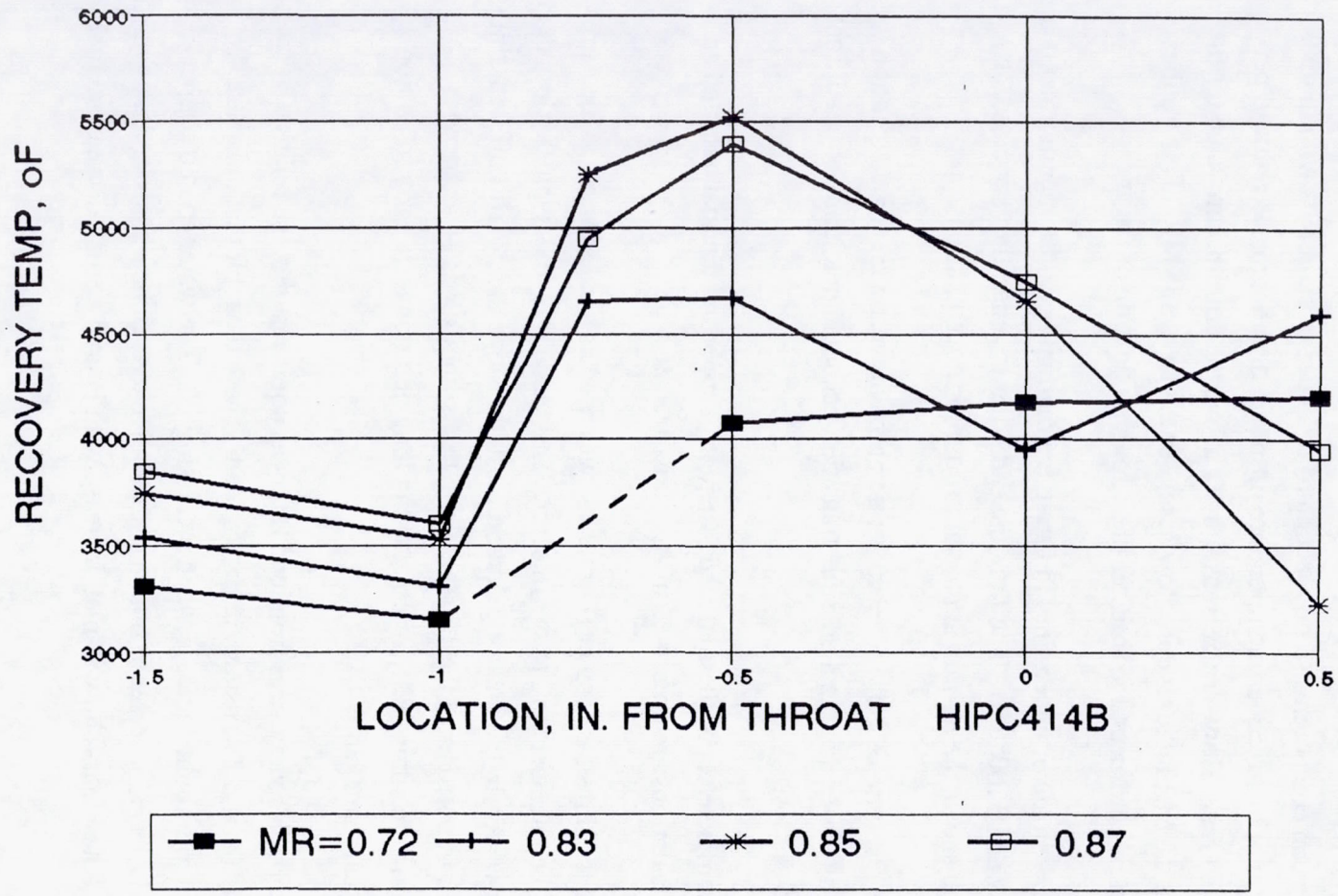

Figure 41. Gas Recovery Temperature Measured Data - Pc=250 psia

For the NTO/hydrazine propellant system, there is no life penalty for excess fuel at the wall (i.e., no carbon compounds so no reaction of cyanides or carbonyls with the Ir). So the only penalty implicit in low recovery temperature upstream of the throat is reduced performance through unreacted fuel. However, increases in Tr above the equilibrium value for the well-mixed reaction at engine MR indicate core flow at higher than average MR. This implies excess oxidizer which can be detrimental to thruster life through oxidation of the Ir.

The estimate of uncertainty in fitting the thermal response measurements is approximately ±5% for hg and ±100°F Tr. The fit at the end point is generally very close, as shown in Figure 42, which shows the error in approach to equilibrium conditions.

The response of the wall temperature at the downstream nozzle location is best fit with two pairs of hg-Tr, indicating a possible transition occurs in heat transfer conditions at this point during the 15 sec test.

A complete set of thermal response plots, supporting thermal data and an example of the model calculations are presented in Appendix D.

The trip-injector adapter (Figure 43) was used as a calorimeter to measure the heat conducted from the chamber wall to the injector. This value was low, typically less than 0.5 Btu/sec at 15 sec. However, in the one long duration test, the slope did not roll off with time, as shown in Figure 44. Extrapolation of these data to long times (thousands of seconds) is clearly uncertain, indicating the advisability of conducting long duration tests early in Option 1 to address front end thermal management.

Although steady state front end flux was not measured, the relative magnitudes of the flux at 100 and 250 psia were determined. These data, plotted in Figure 45, show overall little change to a slight decrease when increasing Pc. The water cooled copper chamber/nozzle was used as a calorimeter to obtain comparative overall heat transfer data, which are plotted in Figure 46. These data show a small increase with Pc and a small decrease at high MR.

3.4.3.3 Compatibility

A rhenium witness foil was the primary source of compatibility data for these tests. The foil, 3 mil in thickness, and 0.7 in. long, lined the inner surface of the chamber

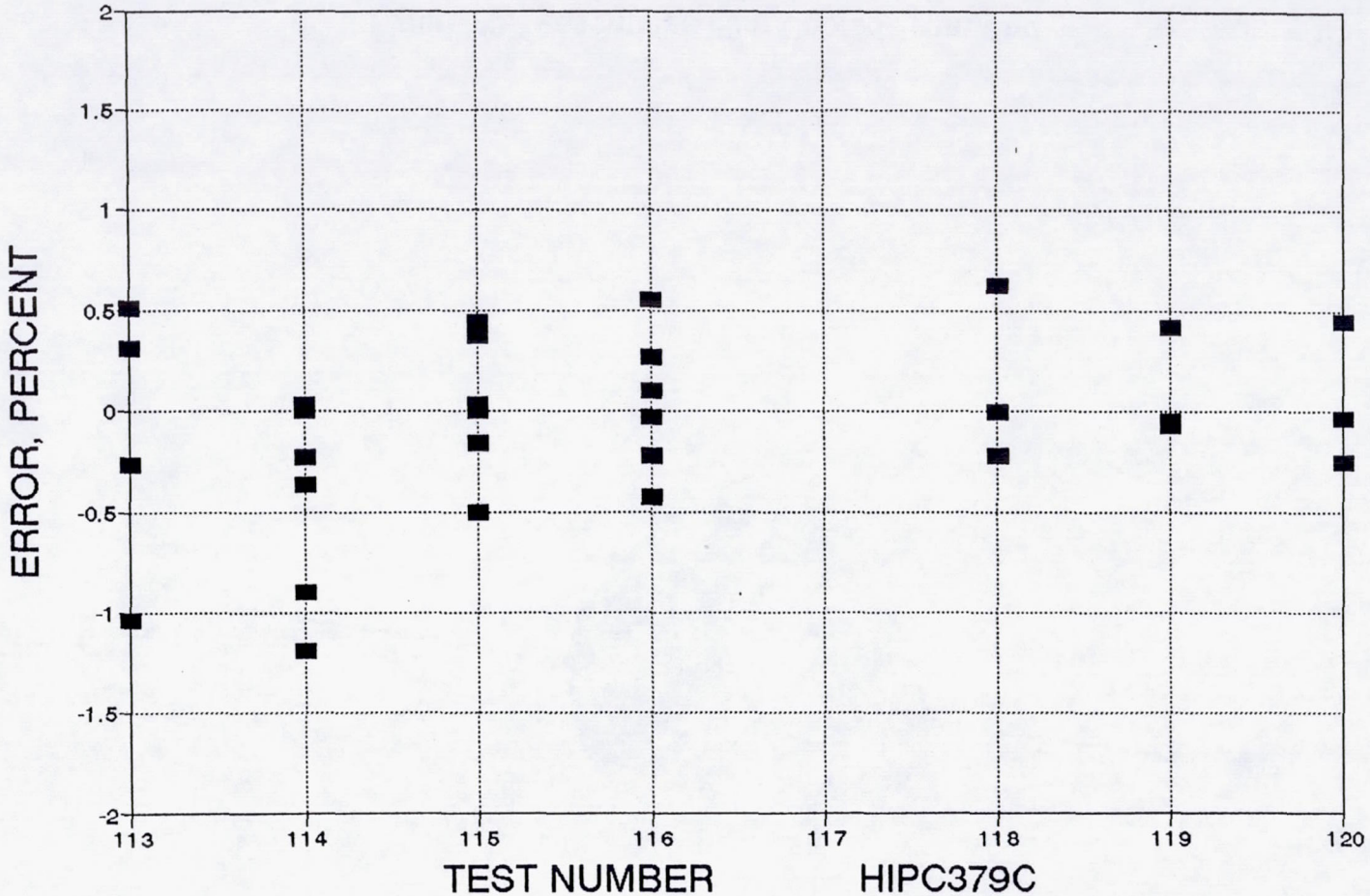

Figure 42. Error in Matching Measurement Tw – 1008(Tcalc-Tmeas)/Tmeas

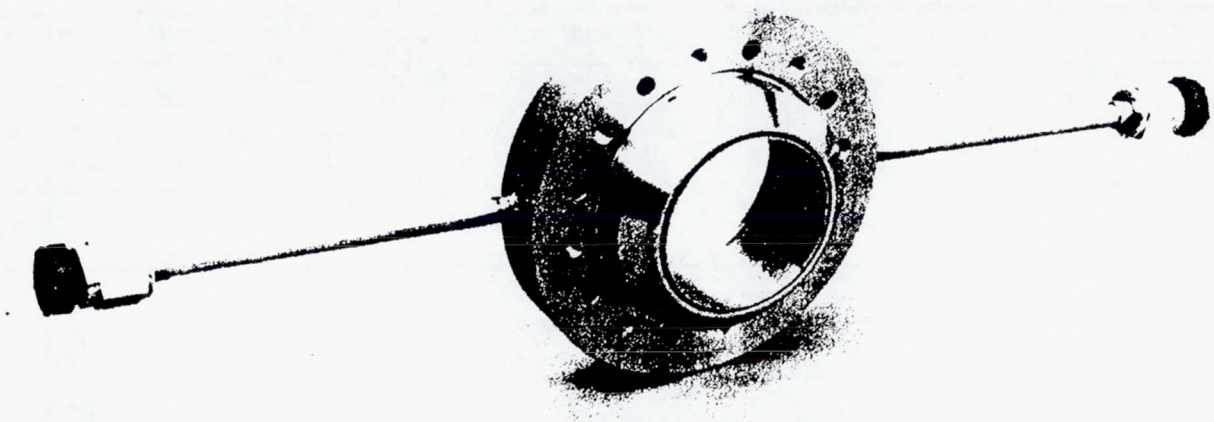

Figure 43. Assembled Film Cooled Front End

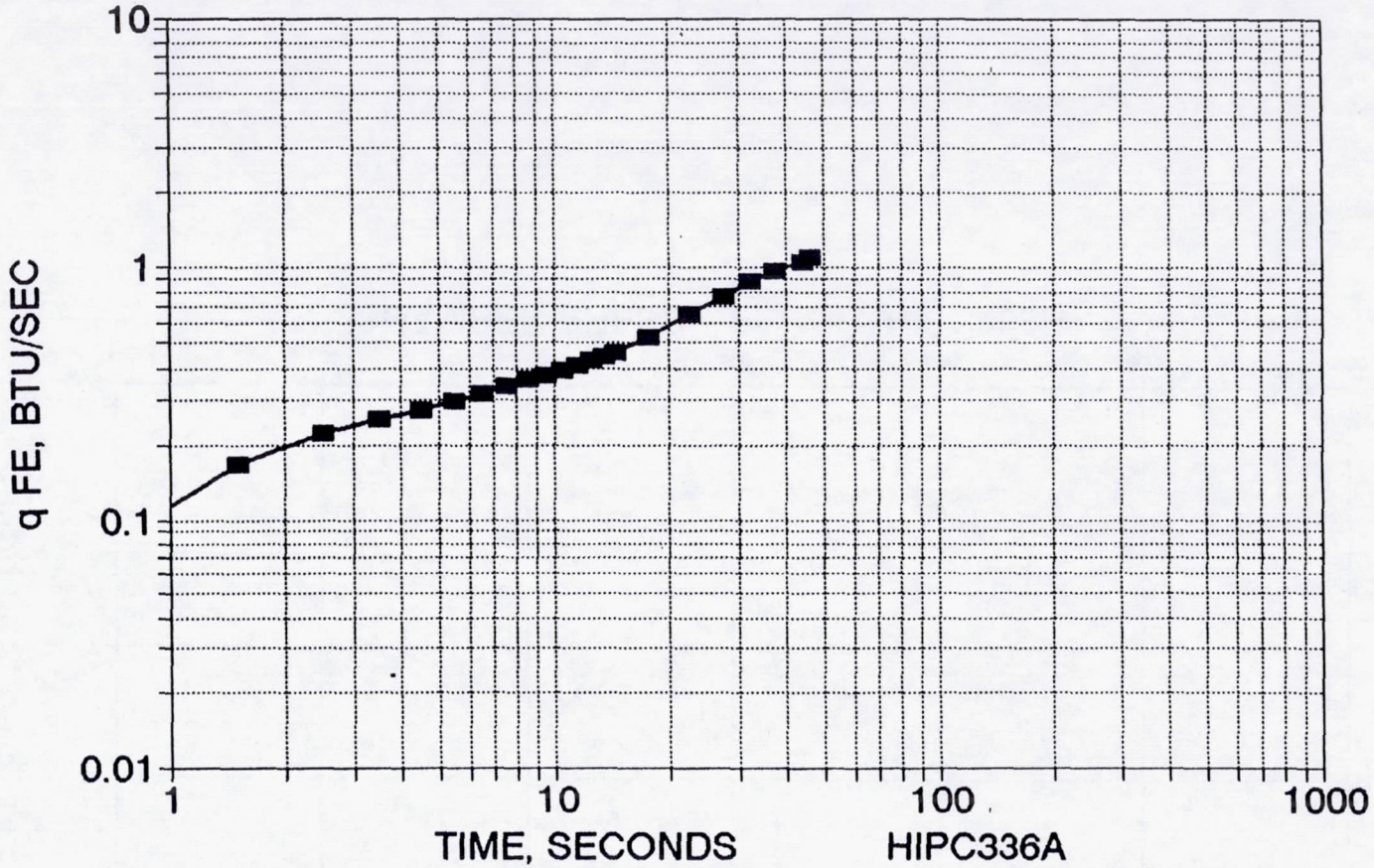

Figure 44. Front End Heat Transfer Versus Time Test-116

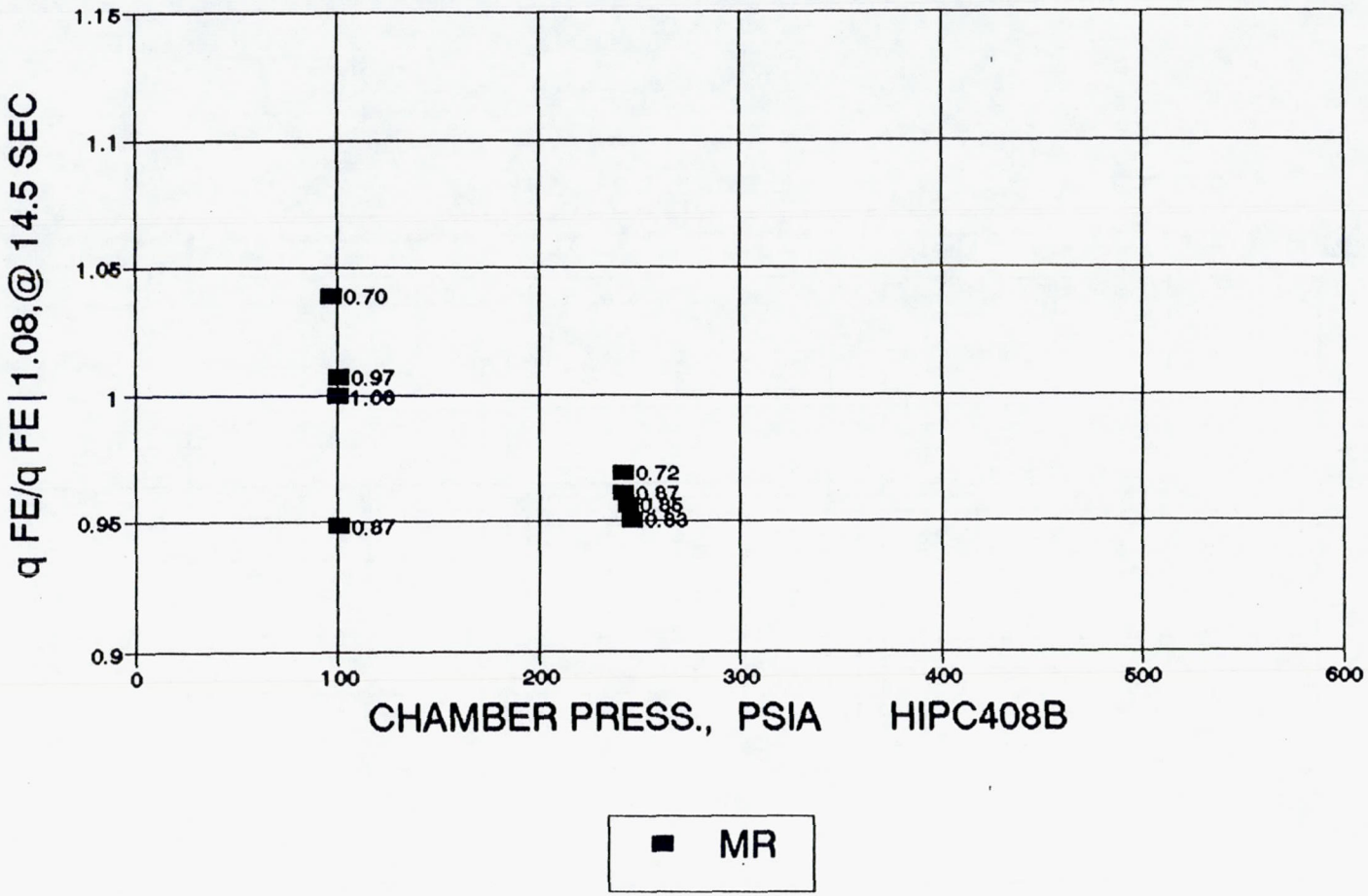

Figure 45. Normalized Front End Heat Transfer; 1.0=100 Pc at MR=1.08

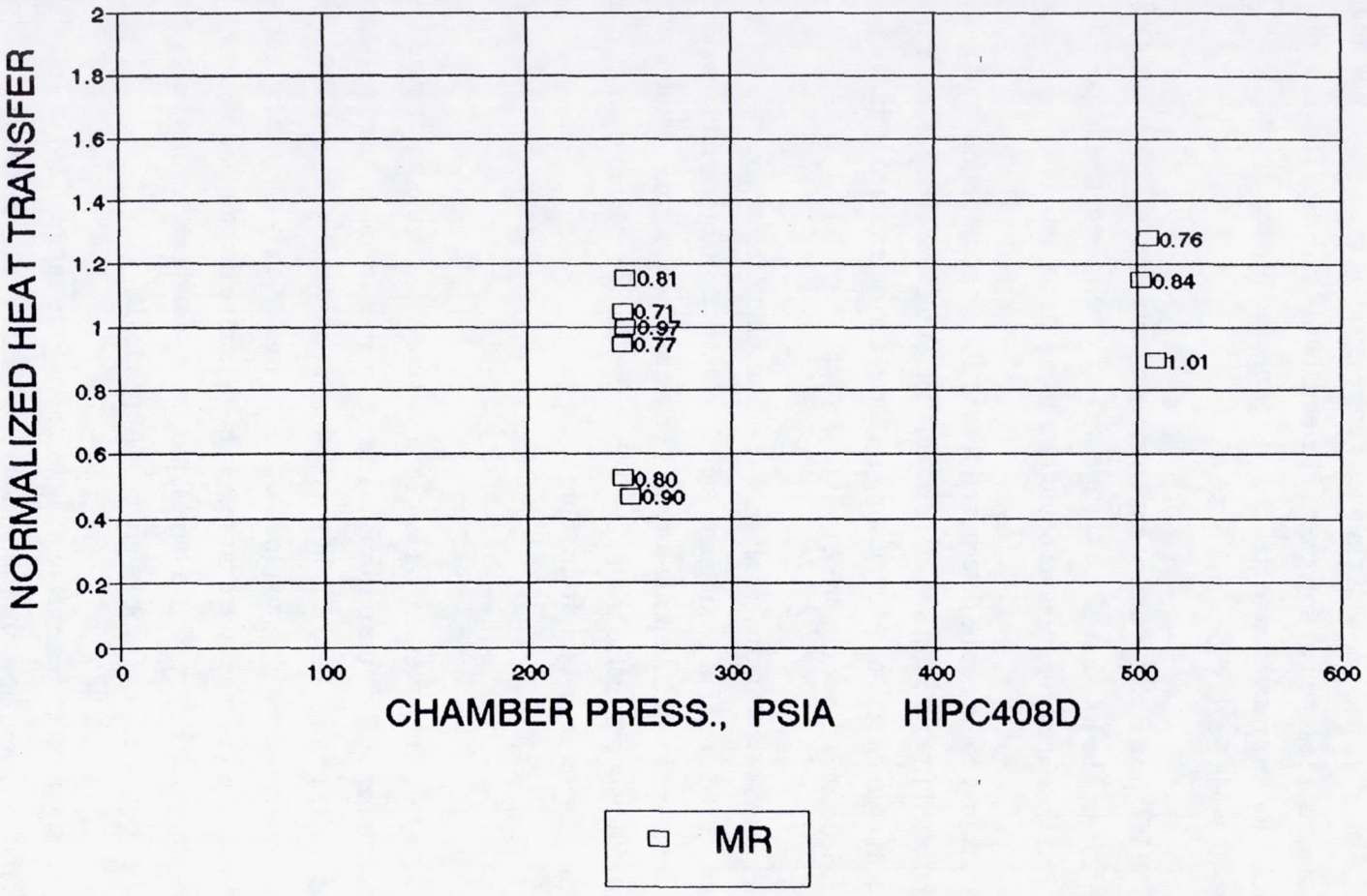

Figure 46. Nozzle/Chamber Heating Water-Cooled Copper

downstream of the trip. The measured mass loss in 6 tests corresponding to a total exposure time of 75 sec corresponds to a mass loss rate of unprotected Re equal to 14 mils/hr. This is in the same range of unprotected Re loss measured in Ref. 3). The projected life for an unprotected Re chamber, based on 10% decay in Pc, is shown in Figure 47.

The 250 psia Pc Re chamber experienced a mass loss of 1.35 gm (out of 682.9 gm) in 92 sec of firing. The location of the change was not determined; the throat did not erode. Bake out of residual surface contaminants could be a factor in the loss.

Mass loss could not be determined for the 100 Pc chamber due to deposits from the Pt/Haynes 25 melted from the trip. Visual examination of the electrodeposited Ir layer shows removal in the converging section. More testing is required to determined if this is a deficiency in the electrodeposited Ir coating process.

As noted in the thermal analysis discussion, calculated recovery temperature is a measure of the extent of mixing and therefore the potential for iridium oxidation. Future tests should be conducted with all up flight-type Re chambers whose inner contour has been accurately determined by a repeatable technique such as the Cordax machine, which can locate coordinates to much better than 1 mil from setup to setup.

3.4.3.4 Stability

High frequency pressure measurements were made in the injector resonator cavity and, for copper chamber tests, in the chamber. The cavity measurements used a Kistler transducer; the chamber measurement used a PCB helium bleed transducer. The transducer outputs were displayed on high-speed oscillograph for monitoring immediately after a test and were also recorded on FM tape. The FM tapes were processed to yield time domain and PSD frequency domain plots of the data. Figure 48 is a typical plot of amplitude versus frequency from the spectral analysis; the complete set of plots is given in Appendix D.

The set of measurements relating to stability are summarized in Table 18, which shows thruster configuration, operating conditions and injector pressure drop.

In all cases the spectral analysis showed extremely low amplitude pressure fluctuations of the order of ±0.3 psia at 100 and 250 Pc and ±0.6 psia at 500 Pc. These values

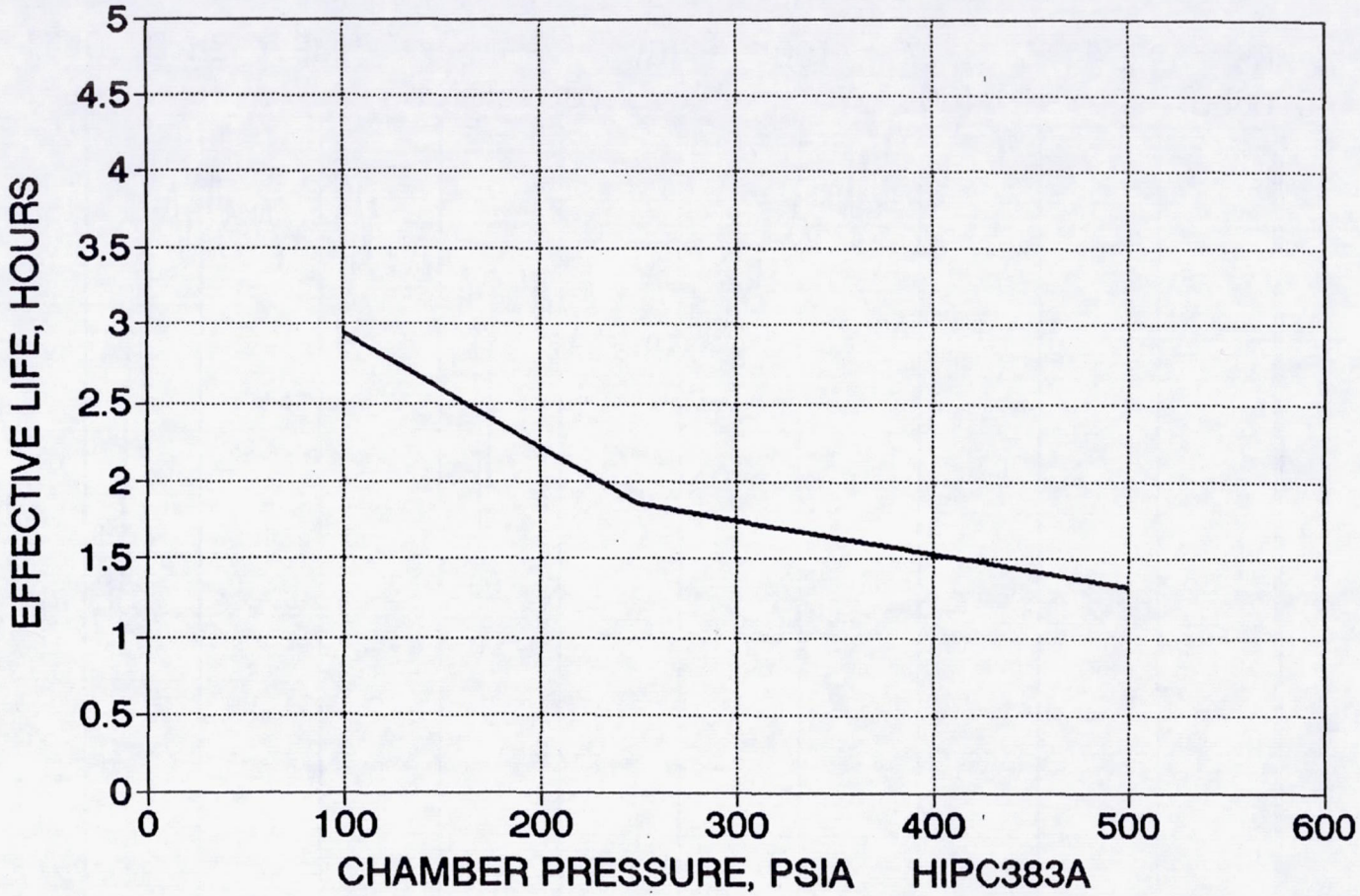

Figure 47. Uncoated Rhenium Chamber Life NTO/Hydrazine

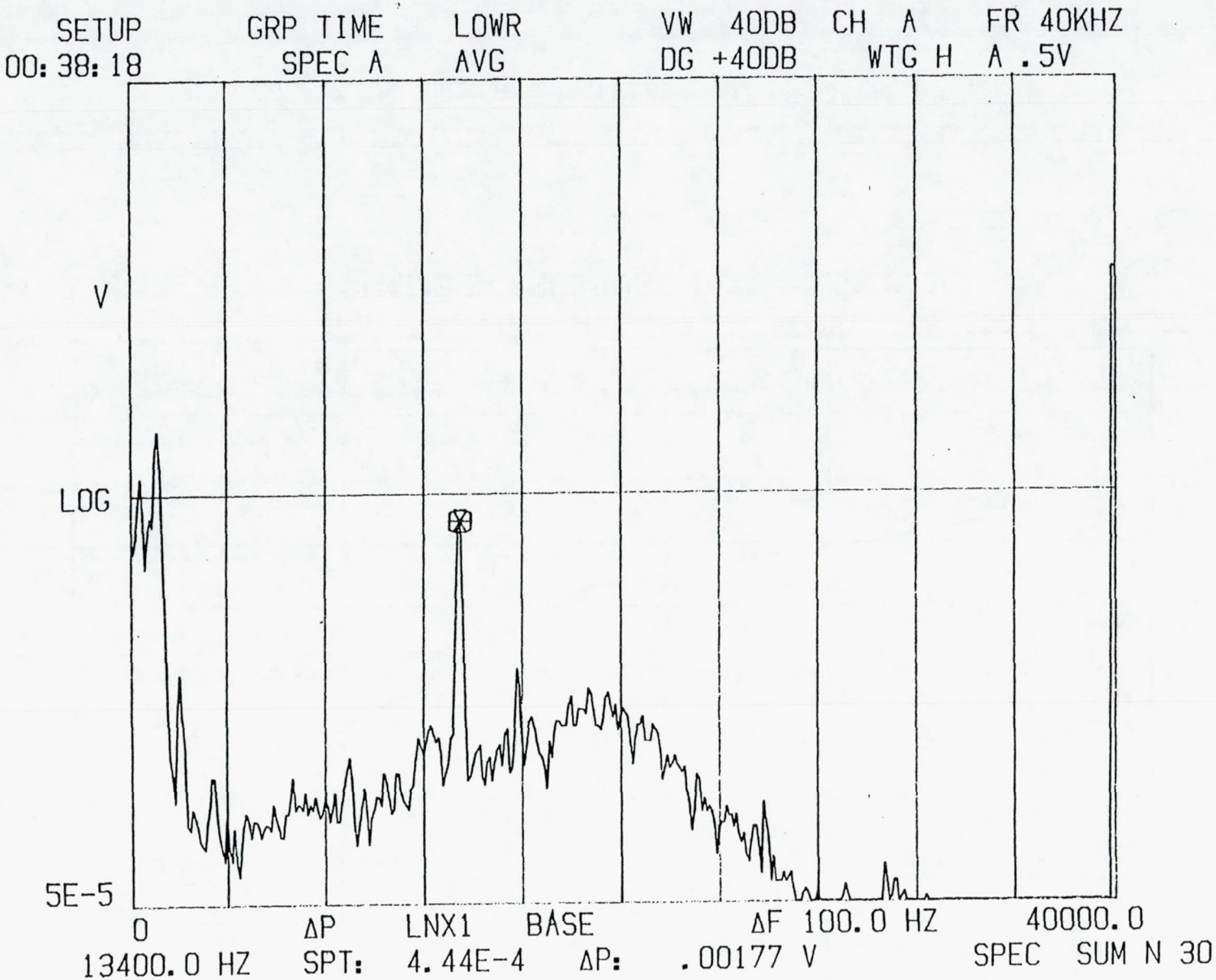

Figure 48. 0.005 HIPC Task 4 – Cavity Kistler Test 103

Table 18. Testbed Data: Stability Data

HIPC410
9-27-94

UPDATE 10-27-94

FINAL TEST DATA

HIGH Pc TASK 4 TESTING

TEST No.	TESTBED CONFIG. Ht In.	Lt In.	FIRING TIME sec	MR O/F	PC-1 psia	Wt lbm/sec	INJECTOR DELTA P OXID psi	FUEL psi	INJECTOR DELTA P/Pc OXID	FUEL	CAVITY FREQ Hz	AMPLITUDE, PSIA	PERCENT Pc	CHAMBER FREQ Hz	AMPLITUDE, PSIA	PERCENT Pc
101	0.25	0.75	0.5													
102	0.25	0.75	15.0	0.84	248	0.298	58.3	93.9	0.235	0.379						
103	0.25	0.75	14.8	0.79	245	0.298	54.8	99.4	0.223	0.405	13400	0.35	0.14	14600	0.28	0.11
104	0.25	0.75	15.0	0.91	247	0.300	65.1	89.7	0.264	0.363	14100	0.36	0.15			
105	0.25	0.75	15.0	0.72	246	0.302	51.5	110.6	0.209	0.449	12100	0.34	0.14			
106	0.25	0.75	15.0	1.00	249	0.300	71.3	81.3	0.287	0.327	12800	0.34	0.14			
107	0.40	0.75	15.0	0.80	247	0.297	55.2	98.9	0.224	0.401	12800	0.38	0.15	2830		
108	0.40	0.75	15.0	0.90	250	0.301	63.9	91.1	0.256	0.364	10900	0.31	0.12			
109	0.40	0.75	15.0	0.71	247	0.302	49.8	112.3	0.202	0.456	13000	0.33	0.13			
110	0.40	0.75	15.0	0.77	247	0.300	50.8	104.8	0.206	0.424	12300	0.35	0.14			
111	0.25	0.30	15.0	0.81	248	0.303	57.4	101.4	0.231	0.408	13200	0.39	0.16			
112	0.25	0.30	15.0	0.97	248	0.299	64.3	80.0	0.259	0.323	13800	0.41	0.16			
113	0.25	0.75	15.0	0.72	242	0.301	56.0	111.8	0.231	0.461	13500	0.30	0.12			
114	0.25	0.75	15.0	0.83	247	0.304	65.7	101.9	0.266	0.413	11900	0.29	0.12			
115	0.25	0.75	15.0	0.87	242	0.299	67.7	93.9	0.280	0.388	14400	0.28	0.12			
116	0.25	0.75	46.8	0.85	245	0.302	65.8	97.7	0.269	0.400	13800	0.36	0.15			
117	0.25	0.75	15.0	0.70	97.0	0.291	51.2	105.0	0.528	1.083	1100	0.23	0.24			
118	0.25	0.75	15.0	0.87	100	0.299	61.2	91.4	0.610	0.911	2000	0.27	0.27			
119	0.25	0.75	15.0	0.97	101	0.298	65.4	82.1	0.651	0.817	1100	0.24	0.24			
120	0.25	0.75	15.0	1.08	100	0.300	74.5	74.8	0.744	0.747	2000	0.28	0.28			
121	0.25	0.75	0.5													
122	0.25	0.75	15.0	0.76	505	0.304	46.8	110.1	0.093	0.218	14200	0.52	0.10	17100	0.41	0.08
123	0.25	0.75	15.0	0.84	501	0.302	55.2	97.2	0.110	0.194	29000	0.63	0.13	2000	0.38	0.08
124	0.25	0.75	15.0	1.01	509	0.304	65.9	83.2	0.129	0.163	17100	0.41	0.08	2100	0.22	0.04

were always less than ±0.3 percent of chamber pressure and represent very quiet operation of the thruster.

The low amplitude fluctuation visible in the PSD plots is an organized frequency in the 12,000 to 14,000 Hz range which is the expected range for the 1T-1L combustion resonance, which is highly damped indicating stable operation.

The effect of chamber pressure on the dominant frequency of this very low amplitude signal is shown in Figure 49. The effect of chamber pressure on the amplitude of the signal is shown in Figure 50. Figure 51 shows that the measured frequency was independent of mixture ratio.

As shown in Table 18 the injector showed very stable operating even at very low ratios of $\Delta P/Pc$, down to as low as 0.1 for the oxidizer circuit and 0.2 for the fuel circuit at 500 Pc. This high stability has been characteristic of injectors with splashplate elements, enhanced by a resonator cavity.

Stable operation at low injector ΔP is crucial to early use of high pressure thrusters on spacecraft.

3.4.3.5 Spacecraft Integration

Application of high pressure, high performance thrusters to spacecraft introduces two new issues which must be addressed. The first is the practical upper limit on thruster inlet pressure at the interface with the spacecraft. The second is the increased radiation heat transfer from the thruster resulting from its higher operating temperature (3600-3900°F for the high pressure Ir-Re engine versus 2500-2600°F for columbium thrusters).

The hydraulic characteristics measured for the testbed thruster are summarized for all tests in Table 19. The measured inlet pressure conditions for the oxidizer and fuel, POVI and PFVI respectively, are shown, along with the required tank pressures for typical spacecraft propellant delivery systems (30 psi ΔP at nominal flow rates). These data are plotted in Figure 52 for the full test program, from 100 to 500 psia, over the range of MR from 0.7 to 1.1. Typical existing spacecraft and flight-qualified tanks have safe working pressures of 325 to 400 psia. Clearly the 500 Pc engine will greatly exceed this (over 600 psia P_T required). The 250 psia Pc thruster tank pressure requirements are plotted in Figure 53; here the required

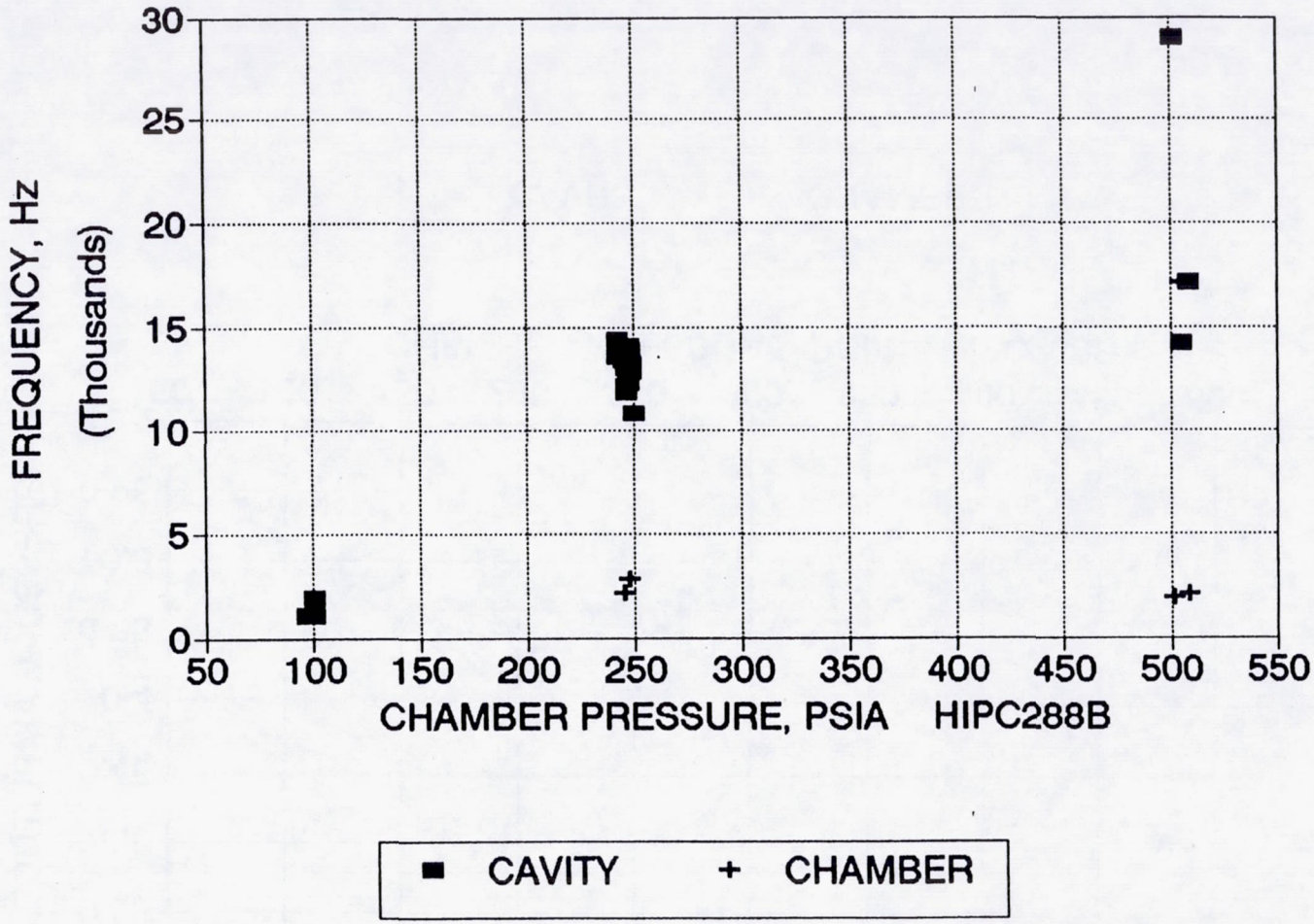

Figure 49. Spectral Analysis – Task 4 Testing Cavity=Kistler; Chamber=He Bleed PCB

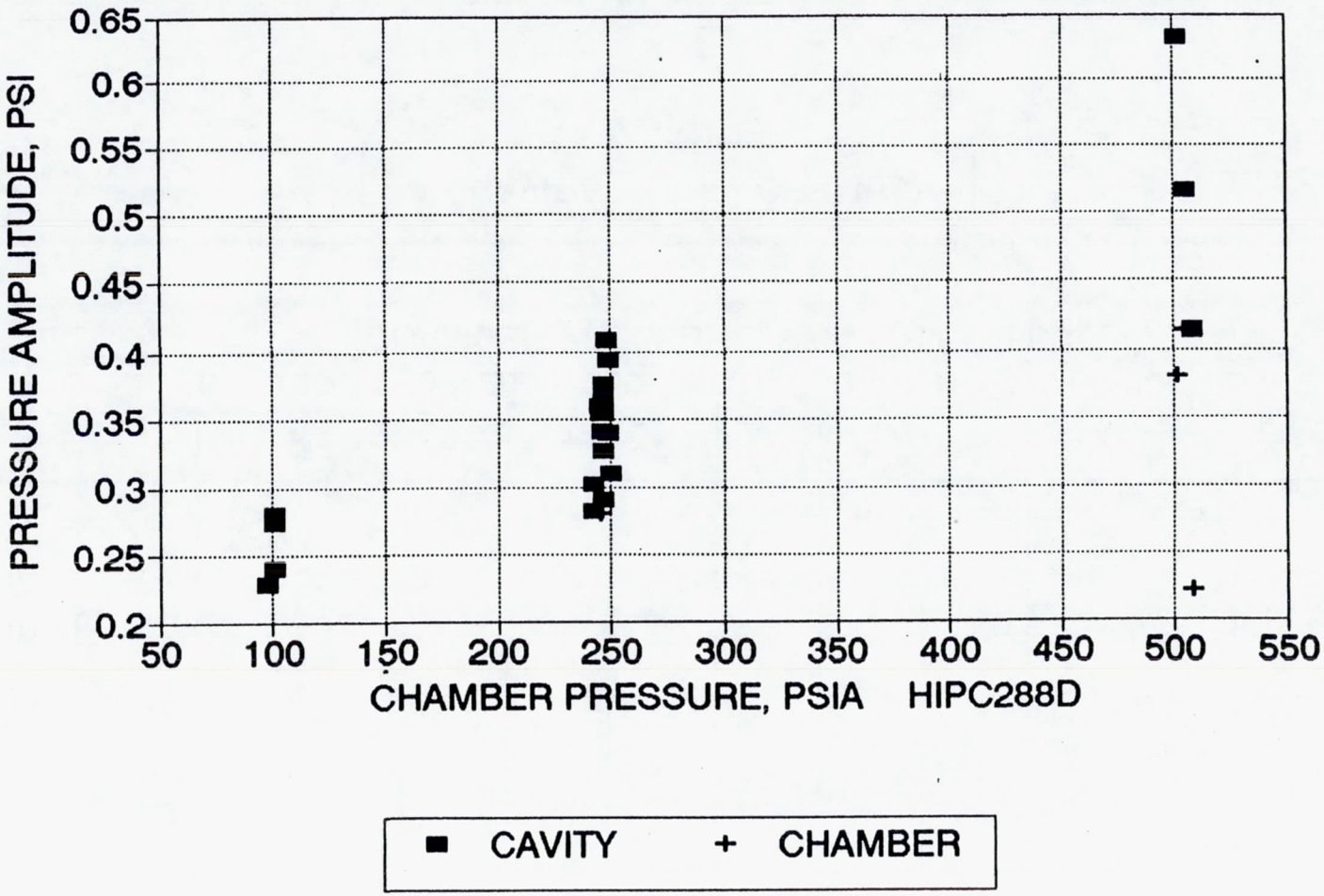

Figure 50. Spectral Analysis – Task 4 Testing Cavity=Kistler; Chamber=He Bleed PCB

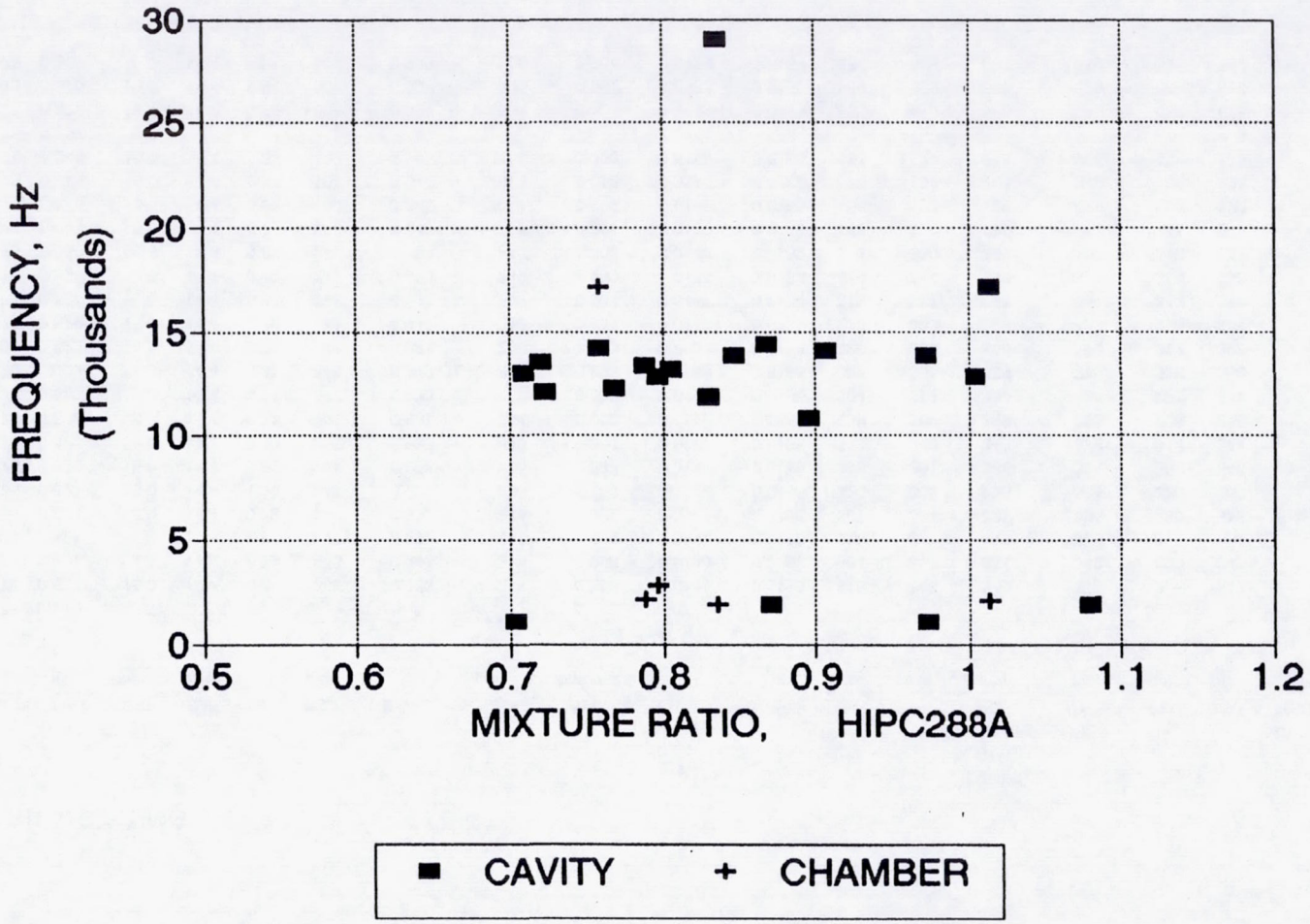

Figure 51. Spectral Analysis – Task 4 Testing Cavity=Kistler; Chamber=He Bleed PCB

Table 19. Testbed Data: Hydraulic Balance Data

HIPC409
9-27-94

UPDATE 10-27-94

FINAL TEST DATA
HIGH Pc TASK 4 TESTING

TEST No.	TESTBED CONFIG. Ht in.	Lt in.	HOT Dt IN.	FIRING TIME sec	DATA TIME sec	MR O/F	PC-1 psia	1-DP/Pc	Pt psia	Wt lbm/sec	Kwoj	Kwfj	REQUIRED FLIGHT TANK PRESSURES POVI psia	PFVI psia	POT psia	PFT psia	POJ psia	PFJ psia	INJECTOR DELTA P OXID psi	FUEL psi
101	0.25	0.75	0.519	0.5																
102	0.25	0.75	0.521	15.0	14.4	0.84	248	0.993	246	0.298	0.0148	0.0166	310	348	340	378	306	342	58	94
103	0.25	0.75	0.521	14.8	14.3	0.79	245	0.993	243	0.298	0.0148	0.0166	304	352	334	382	300	345	55	99
104	0.25	0.75	0.521	15.0	14.4	0.91	247	0.993	245	0.300	0.0147	0.0165	316	343	346	373	312	337	65	90
105	0.25	0.75	0.521	15.0	14.4	0.72	246	0.993	244	0.302	0.0147	0.0166	301	364	331	394	298	357	51	111
106	0.25	0.75	0.521	15.0	14.4	1.00	249	0.993	246	0.300	0.0148	0.0165	325	335	355	365	320	330	71	81
107	0.40	0.75	0.520	15.0	14.4	0.80	247	0.993	245	0.297	0.0147	0.0165	306	351	336	381	302	346	55	99
108	0.40	0.75	0.523	15.0	14.4	0.90	250	0.993	248	0.301	0.0147	0.0165	318	346	348	376	314	341	64	91
109	0.40	0.75	0.523	15.0	14.4	0.71	247	0.993	244	0.302	0.0148	0.0165	299	366	329	396	296	359	50	112
110	0.40	0.75	0.523	15.0	14.4	0.77	247	0.993	245	0.300	0.0152	0.0165	304	357	334	387	298	352	51	105
111	0.25	0.30	0.523	15.0	14.4	0.81	248	0.993	246	0.303	0.0148	0.0165	309	355	339	385	306	350	57	101
112	0.25	0.30	0.523	15.0	14.4	0.97	248	0.993	246	0.299	0.0153	0.0168	320	335	350	365	312	328	64	80
113	0.25	0.75	0.529	15.0	14.4	0.72	242	0.993	240	0.301	0.0146	0.0165	298	363	328	393	298	354	56	112
114	0.25	0.75	0.530	15.0	14.4	0.83	247	0.993	244	0.304	0.0147	0.0164	313	357	343	387	312	349	66	102
115	0.25	0.75	0.530	15.0	14.4	0.87	242	0.993	240	0.299	0.0146	0.0164	310	344	340	374	310	336	68	94
116	0.25	0.75	0.530	46.8	14.5	0.85	245	0.993	242	0.302	0.0148	0.0162	311	350	341	380	310	342	66	98
117	0.25	0.75	0.844	15.0	14.4	0.70	97.0	0.945	90.5	0.291	0.0139	0.0165	149	203	179	233	148	202	51	105
118	0.25	0.75	0.845	15.0	14.4	0.87	100	0.945	93.7	0.299	0.0148	0.0166	166	193	196	223	162	192	61	91
119	0.25	0.75	0.845	15.0	14.4	0.97	101	0.945	93.8	0.298	0.0150	0.0165	175	182	205	212	166	183	65	82
120	0.25	0.75	0.846	15.0	14.4	1.08	100	0.945	93.6	0.300	0.0149	0.0165	185	174	215	204	175	175	74	75
121	0.25	0.75	0.367	0.5																
122	0.25	0.75	0.370	15.0	14.4	0.76	505	0.998	504	0.304	0.0159	0.0163	555	616	585	646	552	615	47	110
123	0.25	0.75	0.370	15.0	14.4	0.84	501	0.998	500	0.302	0.0153	0.0165	556	599	586	629	557	599	55	97
124	0.25	0.75	0.369	15.0	14.4	1.01	509	0.998	508	0.304	0.0156	0.0164	577	509	607	539	575	592	66	83

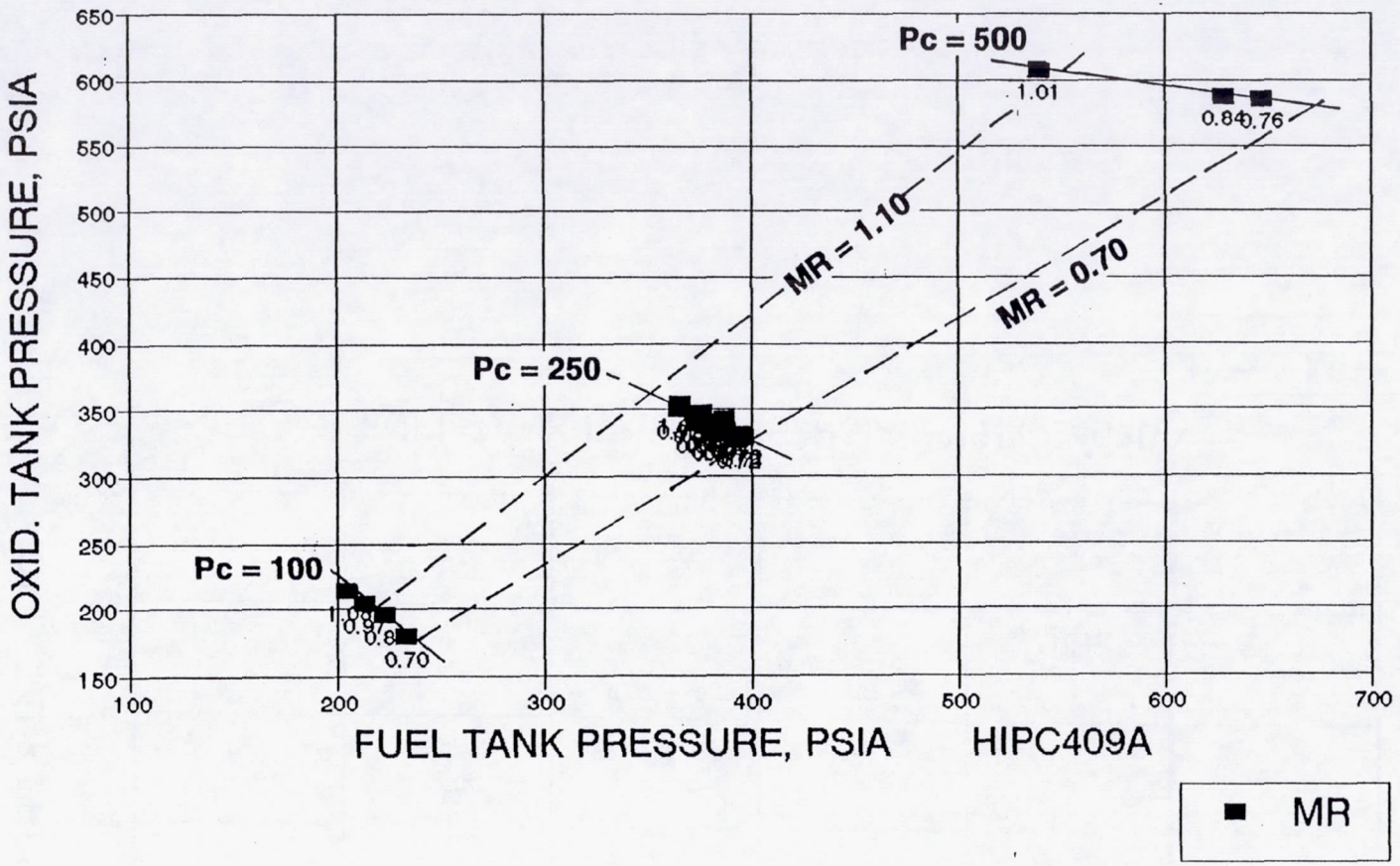

Figure 52. Flight Tank Pressures – HIPC Task 4.0, Testbed Engines

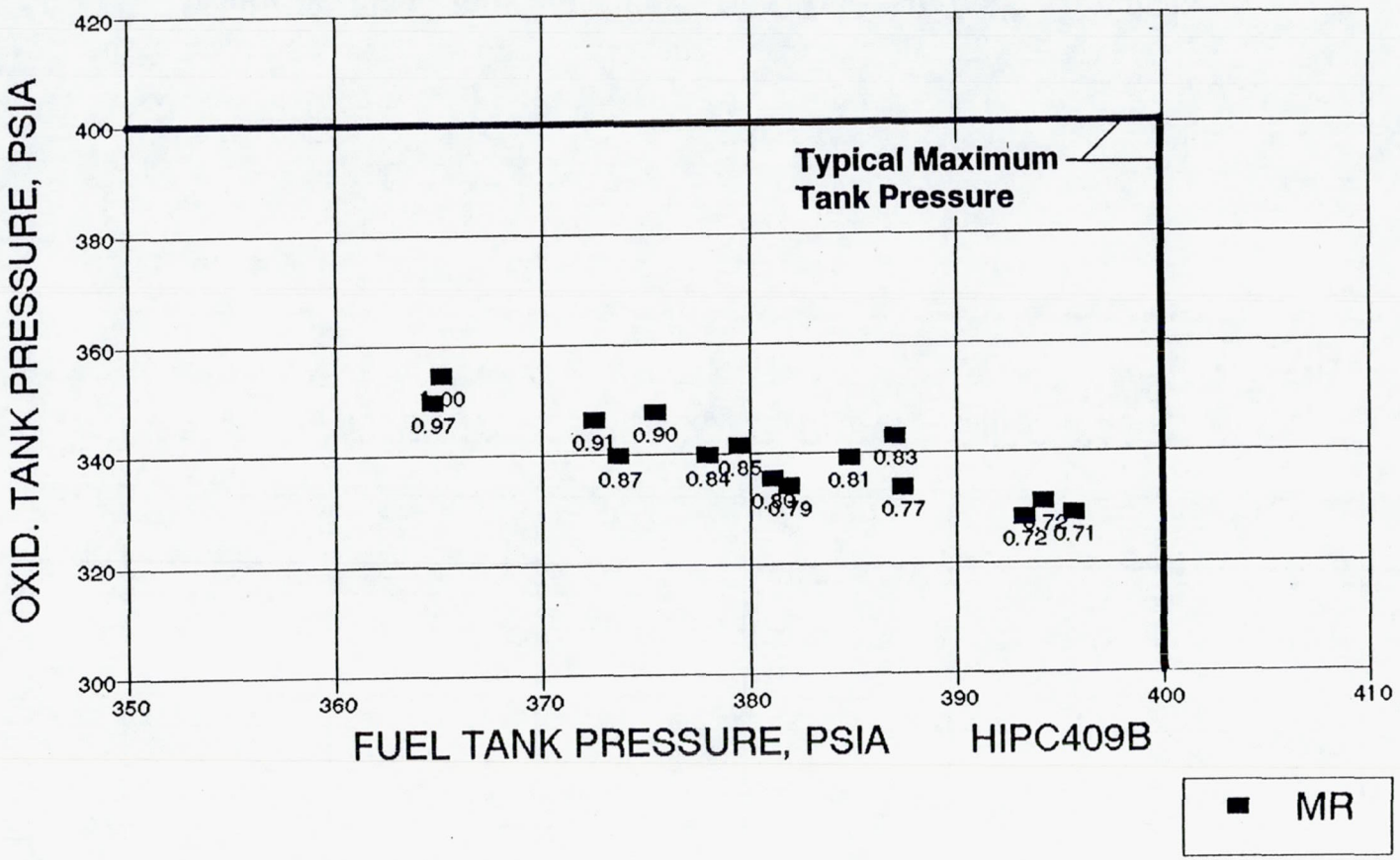

Figure 53. Flight Tank Pressures – HIPC Task 4.0, 250 Pc Testbed Engine

pressures are well below the 400 psia limit. At design operating mixture ratio (1.05), the tank pressure required is 360 psia for both oxidizer and fuel.

Although in principle this engine would operate at 250 Pc with existing tanks, in practice the spacecraft designers specify very wide ranges of inlet pressure, in part to accommodate failure modes (HS601) and in part because of operation in a blow down mode (BUS-1, Ref. 4). It is possible to design spacecraft propulsion systems to operate in a much tighter inlet pressure range (e.g., the NEAR propulsion system). This has the advantage of maximizing thruster life and performance. It will require a philosophy change on the part of the spacecraft primes, who appear to underestimate the risk they build into their systems by requiring thruster operation over a wide range of inlet pressure.

The increased radiation to the spacecraft is a matter of degree; the expected increase due to the higher operating temperature is a factor of three. Existing Cb thrusters use radiation shields; these must be upgraded to protect the spacecraft from the higher flux. Such a shield was tested successfully on a 3600F Ir-Re chamber (Ref. 5).

REFERENCES

1. Schoenman, L., and Block, P., "Laminar Boundary-Layer Heat Transfer in Low-Thrust Rocket Nozzles," J. Spacecraft, Volume 5, No. 9, Pages 1082-1089, September 1968.

2. Boldman, D. R., Schmidt, J. F., and Ehlers, R. C., "Effect of Uncooled Inlet Length and Nozzle Convergence Angle on the Turbulent Boundary Layer and Heat Transfer in Conical Nozzles Operating With Air," J. of Heat Transfer, November 1967, Pages 341-350.

3. Jassowski, D. M., and Gage, M.L., "Advanced Small Rocket Chambers Option 1 – 14 lbf Ir-Re Rocket," Final Report, NASA Contract Report 191014, August 1992.

4. Hern, H. C., "Design and Development of a Large Bipropellant Blowdown Propulsion System," AIAA 29th JPC, June 1993, AIAA 93-2118.

5. Jassowski, D. M., and Schoenman, L., "Advanced Small Rocket Chambers 110 lbf Ir-Re Flight-Type Thruster" Contract NAS 3-25646 Option 3 Final Report, in Preparation.

REPORT DOCUMENTATION PAGE

Form Approved
OMB No. 0704-0188

1. AGENCY USE ONLY (*Leave blank*)	2. REPORT DATE	3. REPORT TYPE AND DATES COVERED
	October 1997	Final Contractor Report

4. TITLE AND SUBTITLE

High Pressure, Earth-Storable Rocket Technology
Volume 1

5. FUNDING NUMBERS

WU–242–70–01
NAS3–27003

6. AUTHOR(S)

D.M. Jassowski

7. PERFORMING ORGANIZATION NAME(S) AND ADDRESS(ES)

Aerojet
P.O. Box 13222
Sacramento, CA 95813–6000

8. PERFORMING ORGANIZATION REPORT NUMBER

E–9400

9. SPONSORING/MONITORING AGENCY NAME(S) AND ADDRESS(ES)

National Aeronautics and Space Administration
Lewis Research Center
Cleveland, Ohio 44135–3191

10. SPONSORING/MONITORING AGENCY REPORT NUMBER

NASA CR–195427/VOL1

11. SUPPLEMENTARY NOTES

Project manager, Brian D. Reed, Space Propulsion Technology Division, NASA Lewis Research Center, organization code 5430, (216) 977–7489.

12a. DISTRIBUTION/AVAILABILITY STATEMENT

Unclassified - Unlimited
Subject Category: 20 Distribution: Nonstandard

This publication is available from the NASA Center for AeroSpace Information, (301) 621–0390.

12b. DISTRIBUTION CODE

13. ABSTRACT (*Maximum 200 words*)

The effect of elevated chamber pressure on combustion efficiency and heat transfer has been determined at the 100 lbf (445 N) thrust level for nitrogen tetroxide propellants. Measurements were made up to 500 psia (3.45 MPa) with testbed hardware; tests at 100 psia (0.690 MPa) and 250 psia (1.72 MPa) were made with radiation-cooled rhenium chambers. The first task of the program served to determine desirable thruster applications and operating conditions: high total impulse, i.e. communication satellite or spacecraft bus axial engines, at chamber pressures up to 250 psia (1.72 MPa) pressure-fed, or up to 500 psia (3.45 MPa) pump-fed. The hardware modifications and testing required to obtain the data were determined in Task 2, which included design-support hot fire tests; supplemental hardware, including a 250 psia (1.72 MPa) Pc rhenium chamber and a 20% fuel-film cooled platelet injector was fabricated in Task 3. Testing showed that satisfactory operation of Ir-Re radiation chambers is assured at pressures up to 250 psia and may be possible up to 500. The heat transfer data obtained show good correlation with throat Reynolds number and are generally under values given by the simplified Bartz equation; chambers equilibrium temperatures match predicted values. Preliminary optimization of trip configuration and mixture ratio were made; Isp performance from thrust measurements was within 1% of predicted values. Stability, compatibility, and front-end thermal management were determined to be satisfactory.

14. SUBJECT TERMS

Rockets; Satellite propulsion; High pressure; Heat transfer; Combustion efficiency; High performance rhenium thrusters; Iridium coatings; Radiation cooling

15. NUMBER OF PAGES

106

16. PRICE CODE

A06

17. SECURITY CLASSIFICATION OF REPORT	18. SECURITY CLASSIFICATION OF THIS PAGE	19. SECURITY CLASSIFICATION OF ABSTRACT	20. LIMITATION OF ABSTRACT
Unclassified	Unclassified	Unclassified	